

# **Crustal deformation in southern Tibet and the Higher Himalayan Crystalline –a palaeomagnetic approach**

Dissertation

zur Erlangung des Grades eines Doktors der Naturwissenschaften

der Geowissenschaftlichen Fakultät  
der Eberhard-Karls-Universität Tübingen

vorgelegt von  
Rachida El Bay  
aus Nador

2010

Tag der mündlichen Prüfung: 28. 01. 2009

Dekan: Prof. Dr. Peter Grathwohl

1. Berichterstatter: Prof. Dr. Erwin Appel

2. Berichterstatter: Prof. Dr. Eva Schill

## **Contents**

### **Summary (Zusammenfassung)**

#### **1. Introduction**

##### **1.1. Overview**

##### **1.2. Tectonic background**

##### **1.3. Main tectonic units and age constraints**

#### **2. Analytical Methods**

#### **3. Magneto-mineralogy and palaeomagnetic results**

##### **3.1. Tethyan Himalaya –southern Tibet**

###### **3.1.1. Nyalam section**

- 3.1.1.1. Results
- 3.1.1.2. Discussion

###### **3.1.2. Kharta valley**

- 3.1.2.1. Results
- 3.1.2.2. Discussion

###### **3.1.3. Dinggye extensional zone**

- 3.1.3.1. Results
- 3.1.3.2. Discussion

###### **3.1.4. Yadong/Pari area**

- 3.1.4.1. Results
- 3.1.4.2. Discussion

###### **3.1.5. Area between Tingri and Lhatse**

- 3.1.5.1. Results
- 3.1.5.2. Discussion

###### **3.1.6. Discussion with regard to west-east extent**

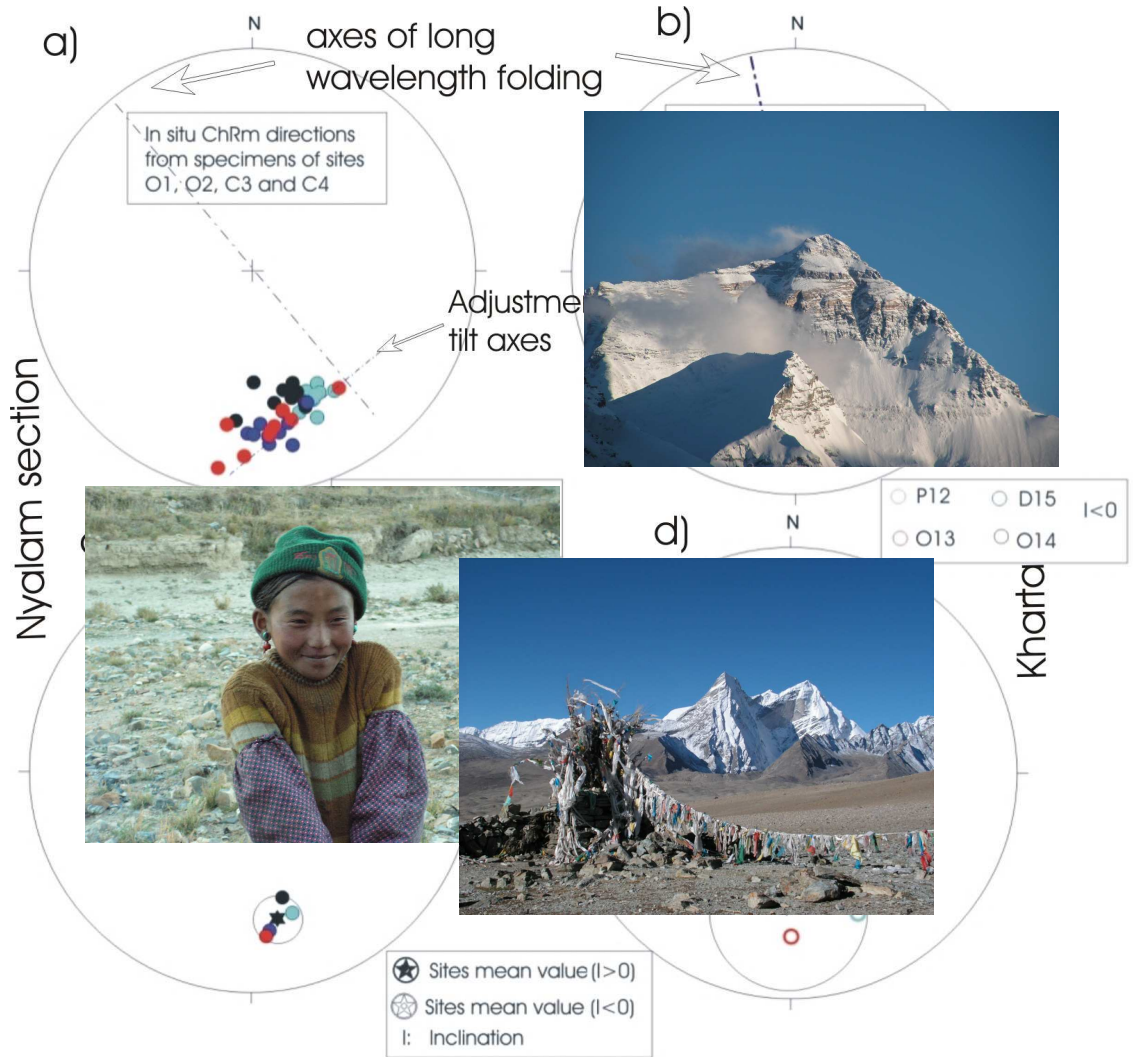
###### **3.1.7. Discussion with regard to south-north transect**

- 3. 2. Higher Himalayan Crystalline of Solu Khumbu**
- 3. 2. 1. Results of magneto-mineralogy**
- 3. 2. 2. Mechanism of remanence acquisition**
- 3. 2. 3. Palaeomagnetic results and tectono-metamorphic implication**

References

Appendix

*For the unknown Tibetan child near Shigaze*



## Summary

Remagnetization is a common process in the Himalayan Tibet orogen system. Stable secondary magnetic remanences acquired in pyrrhotite ( $ChRM^{pyr}$ ) can provide meaningful information on the thermo-tectonic evolution history of an orogen.

Significant stable  $ChRM^{pyr}$  have been isolated for all sampling areas within this study. On the basis of new findings the question of the occurrence of stable primary  $ChRM^{pyr}$  is also addressed.

In southern Tibet along a west-east traverse between  $86^\circ$  and  $89^\circ$ E the sampling area has been subdivided in 4 main sectors (A), (B), (C) and (D) corresponding to the Nyalam section, the Kharta valley, the Dinggye extensional zone and the Yadong/Pari area, respectively (s. Fig 2, 3). In order to separate local and regional tectonic effects manifesting in this region palaeomagnetic results have been analyzed for each sector, and are combined for evaluation within a regional tectonic frame.

Regardless the alternating directional arrangement of the  $ChRM^{pyr}$  being north-west in (A), north-east in (B), again north-west in (C), north-east between (C) and (D), and finally north-west in (D), a remarkable non Gaussian-, but systematic small circle distribution of the  $ChRM^{pyr}$  directions is revealed in nearly all sectors, likely as a consequence of tilting and/or vertical axes rotation. Since this behavior is not restricted to a small number of sites within a sector, it is expected that it reflects a regional trend linked to east-west extension (long wavelength tilting) and north-south compression (“periodic” doming) (s. Fig. 8B).

The resume of palaeomagnetic results (s. Fig. 27) confirms the observations pointing to the occurrence of a consistent systematic regional trend in the area between  $86^\circ$  and  $89^\circ$ E. A relationship is established, confirming the regional occurrence of this phenomenon. Toward separation and quantification of the palaeomagnetic results, a 2-case concept (visualized in Fig. 27) is suggested, and data is evaluated with regard to vector remanence directions, expected for Oligocene/Miocene time.

The ascertained regional trend is expressed as a dispersion of palaeomagnetic data from different sectors on a common mean small circle. Vertical axis rotation and tilting are determined by back tilting of measured inclinations to expected ones for this region. The proposed model enables the quantification of vertical and horizontal axis rotations, rotational shortening and oroclinal bending. A resultant mean clockwise rotation of  $16.5^\circ$  ( $\alpha_{95} = 11.5^\circ$ ) is regarded as the characteristic regional value for the whole studied area. Its coincidence with results reported from adjacent areas implies the occurrence of a uniform pattern of rotation on a large regional scale.

From the model reconstructed tilt axes are in agreement with GPS velocity data revealing broadly distributed contraction across the plateau (doming as a response to “channel flow”), oriented  $\sim$   $N30^\circ$ E, as well as orthogonal extension (long wavelength folding).

Regardless the complexity and variability in the remanence behavior between sampling localities and within specimens dominating stable  $ChRM^{pyr}$  directions have been isolated from the high-grade metamorphic gneisses of HHC. Pyrrhotite is assumed to be formed/re-equilibrated at the ductile/brittle deformation transition regime. The mechanism of its remanence acquisition is extensively discussed with regard to given metamorphic conditions. A TRM is likely acquired and its age will correspond to the age of the last metamorphic cooling event. Data evaluation reveal no significant (or a slight anti-clockwise rotation) versus India. Within the concept of the “channel flow” palaeomagnetic data suggest an episodic exhumation of the channel by continuous feeding of partially molten material. The youngest Miocene remanence age inferred from  $ChRM^{pyr}$  data would correspond to the last cooling event, and thus document the cessation of the channel flow. Ditto, a link to the North Himalayan gneiss domes is proposed.

In addition to the examination of a west-east trend in southern Tibet (parallel to the main tectonic unit of the Himalayan arc) a south-north section approximately perpendicular to the main strike of the Himalayan arc at ca. 87°E is surveyed. The latter comprises from the south to the north, the HHC of Solu Khumbu, the Kharta valley and the area between Tingri and Lhatse termed sector- (F), (B) and (E), respectively.

Despite differences on site scale, the calculated overall mean for 12 sites suggests that no rotation (or a slight apparent counter-clockwise rotation) has had happened in Solu Khumbu (F). To the north in the Tethyan sedimentary series, sector (B) subdivided in Kharta valley south and Kharta valley north as well as sector (E) indicate that a clockwise rotation slightly increasing toward the north has occurred on this transect.

Generally, with regard to results of this study, the top to the north sense of shear of the extensional structures (the South Tibetan Detachment System (STDS) and the Kangmar-Gyrong Thrust (KGT) included), and sigmoidal oblique dextral normal shear along the Indus Yarlong Suture Zone (IYSZ) would support the development of a clockwise rotation slightly increasing toward the IYSZ. Furthermore, it is not excluded that block rotation is triggered by motion transferred by accumulation and/or accommodation from the STDS in the south to the IYSZ in the north (both considered as interacting 1<sup>st</sup> order faults) via first order thrusts and numerous all kind of small sized 2<sup>nd</sup> order thrusts, oblique and parallel to the main strike normal faults. A general working model suggesting the interaction of the STDS and the IYSZ is presented (s. Fig. 28). On the other hand, however, not in contradiction with these assumptions, the calculated common intersecting declination  $D = 16.5 \pm 18.2^\circ$  for sector (E) coincident with the mean value  $16.5 \pm 11.5^\circ$  representing the regional trend between 86° and 89°E, might at first glance invoke a contradiction with these of an increasing clockwise rotation toward the IYSZ. However, a separation of local effects (manifesting as described above) from the regional trend characterized by the 16.5° declination renders again the assumption plausible.

With regard to the new findings the hypothesis of a uniform clockwise rotation increasing to the east can be yet not proved or rejected. A major effect, inferred from palaeomagnetic data, attributed to long wavelength folding, doming and associated low/high normal faults/thrust system became more evident.

In summary, palaeomagnetism is a potential applied method in deciphering deformation processes on local-, meso- and regional scale.

Various rock-magnetic measurements and experiments carried out within this study allow new semi-quantitative and qualitative insights in the magneto-mineralogy of low- and high-grade metamorphic rocks.

## Zusammenfassung

Remagnetisierung ist in der jüngeren Entwicklung des Himalaja-Tibet Orogens ein weit verbreitetes Phänomen. In Pyrrhotin erworbene sekundäre magnetische Remanenzen ( $ChRM^{Pyr}$ ) können bedeutende Informationen zur metamorphen und tektonischen Entwicklungsgeschichte eines Orogens liefern.

Für alle im Rahmen dieser Arbeit beprobten Gebiete wurden signifikante stabile  $ChRM^{Pyr}$  identifiziert. Anhand der neuen Befunde stellt sich zudem die Frage, ob auch primär erworbene Remanenzen in Pyrrhotin auftreten.

Das Beprobungsgebiet entlang einer West-Ost Traverse in Süd-Tibet, zwischen  $86^\circ$  und  $89^\circ E$ , wurde in 4 Hauptsektoren unterteilt, welche Nyalam Profil (A), Kharta Valley (B), Dinggye Extensionszone (C), und Yadong/Pari Gebiet (D) genannt werden (s. Abb. 2, 3). Zur Separation von lokalen und regionalen tektonischen Effekten wurden die paläomagnetischen Ergebnisse für die Gebiete einzeln analysiert und dann für die Evaluierung in einem regionalen geologischen Rahmen kombiniert.

Über eine alternierende Richtung der  $ChRM^{Pyr}$  (Nord-West in A, Nord-Ost in B, wiederum Nord-West in C, Nord-Ost zwischen C und D und anschließend Nord-West in D) fällt auf, dass in praktisch allen Sektoren keine Gauß-Verteilungen, sondern systematische Kleinkreis-Verteilungen vorliegen, welche vermutlich als Resultat von Faltung und/oder Rotation um vertikale Achsen entstanden sind. Da dieses Verhalten sich nicht auf eine geringe Anzahl von Beprobungsstellen innerhalb eines Sektors beschränkt, kann gefolgert werden, dass die Beobachtung einen regionalen Trend widerspiegelt, welcher in Verbindung mit der Ost-West Extension (langwellige Faltung) und der Nord-Süd Kompression („periodische“ Aufdomung) steht (s. Abb. 8B).

Die Gesamtbetrachtung der paläomagnetischen Ergebnisse (s. Abb. 27) bestätigt die Beobachtungen, welche auf die Existenz eines konsistenten regionalen Trends zwischen  $86^\circ$  und  $89^\circ E$  hindeuten. Es wird ein „Zwei-Phasen“-Modell zur Erklärung dieses Phänomens vorgeschlagen. Dieses Konzept (visualisiert in Abb. 27) erlaubt die Separation und Quantifizierung der paläomagnetischen Ergebnisse. Die Auswertung der Daten erfolgte im Hinblick auf erwartete Remanenzrichtungen während des Zeitraums von Oligozän-Miozän.

Der nachgewiesene Trend kommt durch die Verteilung der paläomagnetischen Daten auf einem, für alle Gebiete, gemittelten Kleinkreis, zum Ausdruck. Durch Rück-Rotation der gemessenen Inklinationen in die Erwartungslage wurden Rotationen um vertikale und horizontale Achsen bestimmt. Das vorgeschlagene Modell erlaubt die Quantifizierung von Rotationen um vertikale und horizontale Achsen, von „Rotational Shortening“ und „Oroclinal Bending“. Eine resultierende Rotation im Uhrzeigersinn von  $16.5^\circ$  ( $\alpha_{95} = 11.5^\circ$ ) wird als charakteristischer regionaler Wert für das gesamte Gebiet betrachtet. Die Übereinstimmung mit Ergebnissen aus benachbarten Gebieten führt zu der Annahme der Existenz eines einheitlichen Rotationsmusters auf regionaler Skala. Die anhand des Modells rekonstruierten Falteachsen sind in Übereinstimmung mit GPS-Geschwindigkeiten. Letztere offenbaren eine großräumige  $\sim N30^\circ E$  orientierte Verteilung der Kontraktion entlang des Plateaus (Aufdomung als resultierender Effekt durch „Channel Flow“) sowie auch der dazu senkrechten Extension (langwellige Faltung).

Aus den hochgradig metamorphen Gneissen des Hoch-Himalaya (HHC) wurden dominierende stabile  $ChRM^{Pyr}$  Richtungen isoliert, unabhängig von der Komplexität und Variabilität im Remanenz-Verhalten zwischen Beprobungslokalitäten und von Einzelproben. Eine Bildung bzw. Re-Equilibration des Pyrrhotin während des Übergangs vom duktilen zum spröden Verhalten wird angenommen. Der Mechanismus des Remanenzserwerbs wird im Hinblick auf gegebene

Rahmenbedingungen der Metamorphose ausführlich diskutiert. Die Auswertung der Daten zeigt keine signifikante Rotation relativ zu Indien (bzw. eine geringe Rotation gegen den Uhrzeigersinn). Die paläomagnetische Daten könnten auf eine episodische Exhumierung des „Channel Flow“ hindeuten, mit der Annahme einer kontinuierlichen Produktion von teilgeschmolzenem Krustenmaterial.

Ergänzend zur Analyse eines West-Ost Trends in Süd-Tibet parallel zur Streichrichtung der großtektonischen Einheiten des Himalaya wurde ein senkrecht dazu orientiertes Süd-Nord Profil getestet. Letzteres umfasst das HHC von Solu Khumbu(F), das Kharta Valley (B) und das Gebiet zwischen Tingri und Lhatse (E). Der berechnete Mittelwert aus 12 Beprobungslokalitäten zeigt keine signifikante Rotation versus Indien im Solu Khumbu Gebiet. Nach Norden hin, in den Tethyserien, deuten sowohl die Daten aus dem Sektor (B), unterteilt in Kharta Valley Nord und Süd, als auch aus dem Sektor (E), darauf hin, dass eine Rotation im Uhrzeigersinn stattgefunden hat, welche nach Norden hin zunimmt.

Die nach Norden ausgerichteten Extensionsstrukturen und die abgestufte dextrale Scherung entlang der Indus-Yarlung Suturezone (IYSZ) stützen die aus den Ergebnissen dieser Arbeit interpretierten nach Norden zunehmenden Rotation im Uhrzeigersinn. Zudem wäre vorstellbar, dass Blockrotationen durch Bewegungen entstanden, welche durch Akkumulation und/oder Akkommodation, bedingt durch die Interaktion des South Tibetan Detachment Systems (STDS) und IYSZ, verursacht wurden. Die ermittelte Deklination  $D=16.5\pm 18.2^\circ$  für Sektor (E) stimmt mit dem generellen Mittelwert von  $16.5\pm 11.5^\circ$  überein, welcher wiederum den regionalen Trend zwischen  $86$  und  $89^\circ\text{E}$  repräsentiert. Dies könnte den Anschein eines Widerspruchs mit dieser Annahme erwecken. Die Annahme ist aber plausibel, wenn man die Subtraktion von lokalen tektonischen Effekten vom regionalen Trend berücksichtigt.

Die neuen Ergebnisse bestätigen die Hypothese einer gleichförmigen Rotation im Uhrzeigersinn, welche nach Osten hin zunimmt, nicht. Aus den paläomagnetischen Daten wird vielmehr klar, dass die Entwicklung durch eine langwellige Faltung, Aufdomungen und deren assoziierten Störungssysteme kontrolliert ist.

Zusammenfassend kann festgestellt werden, dass Paläomagnetismus eine potentiell geeignete Methode zur Separation von lokalen, mittel- oder großskaligen Deformationsprozessen ist. Diverse gesteinsmagnetische Messungen und Experimente, die im Rahmen dieser Arbeit durchgeführt wurden, erlauben neue semiquantitative und qualitative Einblicke in die Magnetomineralogie von niedrig- und hochgradig metamorphen Gesteinen.

### Acknowledgments

*This dissertation was completed at the Institute for Geosciences, Eberhard Karls University of Tübingen.*

*Prof. Dr. Erwin Appel supervised this thesis, and accompanied this research study during several multi-disciplinary field expeditions to southern-Tibet (China) and the Higher Himalaya (eastern Nepal)*

*Prof. Bauchun Huang organized our first fieldwork in southern Tibet in 2005. Prof. Zonghai Zhuang and Dr. Pan Zhongxi kindly provided the sampling.*

*Dr. Khum Paudyal, Otto Dinkelacker and Stephanie Baule supported my first fieldwork in the Everest region, Higher Himalaya, in 2005.*

*Prof. Ding Lin organized the second fieldwork in southern Tibet in 2006. Further contributions and discussions come from Dr. István Dunkl, Dr. Chiara Montomoli, Prof. Rodolfo Carosi and Bastian Wauschkuhn.*

*Prof. Dr. Lothar Ratschbacher and Prof. Dr. Richard Gloaguen granted the use of the remote sensing laboratory during my stay at the University of Freiberg.*

*Xu Qiang and Borja Antolin helped with sampling during my third fieldwork in southern Tibet in 2007.*

*Dr. Lalu Paudel accompanied our second fieldwork in the Everest region in 2007. This work profited from his contributions and discussions during his stay at the University of Tübingen. Oliver Baron and Toya Ghimire supported the fieldwork. Oliver baron and Ursina Liebcke contributed, additionally, with laboratory measurements and some data processing.*

*Dr. Udo Neumann and Dr. Victor Hoffmann and constructively supported my reflected light microscopy scheme. Per Jeisecke and Indra Gill-kopp prepared thin sections and polished samples.*

*Prof. Dr. Stewart Gilder and the laboratory technician Manuella Weiß provided granting and permission of the use of the instrumentation at the palaeomagnetic laboratory in München.*

*Dr. Thomas Frederichs guided me in the MPMS measurements at the University of Bremen.*

*Vamshi Krishna, Nathalie Peres, Khaver Said, Irfan Gani, Birendra Sapkota, Jens Rössiger, Jozseph Hecht, Chisenga Mulenga and Ye Zhao contributed with sample preparations, laboratory measurements and data entries.*

*The fieldwork would not have been possible without the help of our Nepalese porters and guides and the cooperative attitude of our Tibetan drivers.*

*Prof. Dr. Eva Schill was the second reviewer of this thesis.*

*This study was financed by the German Research Foundation (DFG).*

Thank you

# 1. Introduction

## 1.1. Overview

How continental crust responds to collision is a major tackled problem in geodynamics. A spectacular example –in this relationship- is the Himalayan-Tibet late orogen system. This research study focuses on the Himalayan-Tibet orogen system and investigates the link between frontal collision by the Indian indenter and the extrusion of the Tibetan Plateau.

Within the last two decades palaeomagnetism has been proved to be an important tool for the study of rotational and translational motions during the convergence of the Indian subcontinent with Eurasia prior to and after collision. Its potential is yet not fully tapped. Palaeomagnetic investigations in the Tethyan Himalayan Series in southern Tibet and the Higher Himalayan Crystalline, eastern Nepal are thought to contribute to a better understanding of geodynamical processes subsequent to India-Eurasia collision and extrusion of the Tibetan plateau.

The India-Asia collision and continuing convergence of both continents is controlled by a strong northward drift of the Indian plate and by anti-clockwise rotation of India pinned in the western syntaxis. The collision resulted in an intensively deformed continental margin of India, building up the Himalayan orogen with its present day characteristic arc shape between the western and eastern syntaxes and leading to eastward extrusion of the Tibetan Plateau (Tapponnier et al., 1982, 1986).

Secondary pyrrhotite remanences from the Tethyan Himalaya acquired during Eocene (western Himalaya) and Oligocene to early Miocene (central and eastern Himalaya) were evaluated for block rotations. Oroclinal bending (Klootwijk et al., 1985, 1986, 1991) is well reflected by palaeomagnetic data in the western part of the Himalaya also showing a uniform counterclockwise rotation of India versus the Tethyan Himalaya (Schill et al. 2001, 2002, 2004). In contrast, data from the central part and preliminary results from the eastern part (Bhutan) indicate an abrupt change to unexpected clockwise rotations versus India where an oroclinal bending model would predict no rotation or slight counterclockwise rotations (Schill et al. 2004). Our hypothesis is that these clockwise rotations are a result of a large scale dextral shear zone related to lateral extrusion of the Tibetan Plateau, with an onset in central Nepal. The existing gap in suitable data from the eastern part of the Himalaya hinders, till to date, a closer evaluation of this question. In addition to rotations about vertical axes, long-wavelength folding/tilting was frequently observed from inclinations and attributed to ramping along the Main Central Thrust (Appel et al. 1991, Rochette et al. 1994), antiforms and duplex structures (Schill et al. 2003).

Padding the gap in data in the eastern Himalaya and recognizing the rotation pattern perpendicular to the strike of the main tectonic units (i.e., on south-north profiles), the new palaeomagnetic findings will serve to verify the hypothesis proposed above and to discuss different aspects of significant tilting ascertained in the study area.

The study focuses on the low-grade metamorphic sediments of the Tethyan Himalaya because their suitability for palaeomagnetic investigations has been proven in previous studies. Due to the fact that suitable series from the Tethyan Himalaya are only abundant across a west-east striking zone of limited N-S extent, and in order to obtain a section perpendicular to the strike of the main tectonic units, the high-grade metamorphic central crystalline was also sampled.

The proposed sampling areas are located between ca. 86-89°E (Fig. 2), mainly in the Tethyan Himalaya of southern Tibet and eastern Nepal. A further area is the High Himalayan Crystalline in the Solu Khumbu region of eastern Nepal. The locations have been selected according to the following criteria:

- Suitability of Tethyan Himalaya series for palaeomagnetic investigations (stable secondary remanences).
- Possibility for identification of local-, meso- and large-scale variations (combining tectonic and palaeomagnetic information).
- Connecting the high metamorphic gneiss from the Higher Himalaya to the Tethyan zone in the north to obtain a longer south-north section (in the area of expected clockwise rotations).

## 1. 2. Tectonic Background

How continental crust responds to collision is a major problem tackled in geodynamics. A spectacular example –in this relationship- is the Himalayan-Tibet late orogen system.

Within the last two decades several tectonic models have been discussed with regard to the process of the India-Eurasia collision zone and the mechanical evolution of the Tibetan Plateau. The latter can be summarized into two alternative end member models, first the “edge-driven block ” model (e.g., Tapponnier et al., 1982; Peltzer & Tapponnier, 1988; Avouac & Tapponnier, 1993; Replumaz & Tapponnier, 2003), and second the “thin viscous sheet” model (e.g., England & M<sup>c</sup>Kenzie, 1982, England & Molnar, 1997, Flesh et al., 2001). The first one demonstrates the role of the horizontal extrusion of a limited number of rigid/slowly deforming rocks through large strike-slip faults in the accommodation of major India-Asia convergence. In the second model the lithosphere is considered as a thin viscous sheet, its deformation and eastward extrusion are dominated by broadly distributed shortening and crustal thickening. Whether horizontal block extrusion or crustal thickening has been more significant in accommodating the India-Eurasia collision is an open issue. For instance, geodetic data, i.e., global positioning system (GPS) measurements show broadly distributed contraction across the plateau, oriented ~ N30°E, as well as orthogonal extension (Wang et al., 2001), and reveal a complex deformation process coupled to the eastward extrusion of the Tibetan Plateau. Chen et al. (2004) presented a model for these results that demonstrate that strain between the major strike –slip faults is as significant as slip on the faults, and suggested that a large component of the rapid eastward extrusion of Tibet is caused by distributed deformation within the plateau, not only slip on the major faults.

With regard to the significant internal deformation of the plateau the “block – motion” model rather than the “continuum model” is preferred by some authors to describe the kinematics and dynamics of continental deformation. For example, Thatcher (2007) approaches the present day deformation of the Tibetan Plateau by the relative motion of 11 quasi-rigid blocks and fault slip across block boundaries. His model, in contrast to the classic “block motion” model, which emphasizes the roles played by a limited number of large rigid blocks bounded by major strike-slip faults, supports the role of a series of medium sized blocks delimited by all kinds of active faults, to explain the first-order features of the Tibetan Plateau deformation. Alternatively, Shen et al. (2001) compared topography and surface motion of Roydens model (1996) to observations of the Tibetan Plateau and thus proposed a 3-D Newtonian viscous crust model, where a fixed lower horizontal-velocity boundary and a stress-free upper boundary –both deformable- are used to modify the classic “thin viscous sheet” model. The viscosity of the modeled layered lithosphere varied gradually during the growth of the Tibetan plateau to allow at a later stage the development of a viscous channel flow in the lower crust according to the “channel flow model” (Beaumont et al., 2001; Grujic et al., 2004). Magnetotelluric data (Nelson et al., 1996; Unsworth et al., 2005), collected in southern Tibet, reflect a lower resistivity middle crust. The low resistivity combined with heat flow reported by Francheteau et al. (1984) was interpreted as a partially molten layer, present along at least up to 1000 km from the southern margin of the Tibetan Plateau. The deduced low viscosity of this layer is in agreement with the development of climatically (precipitation, and rapid denudation) forced crustal flow in southern Tibet and the Himalaya.

Tapponnier et al. (2001) and Replumaz & Tapponnier (2003) suggest that the Plateau formed by the initial uplift and thickening of southern Tibet, followed by the multiphase tectonic history, i.e., oblique stepwise rise and eastward extrusion. Considering the model proposed by Shen et al. (2001) the Tibetan Plateau underwent –time independent- at least a two stage evolution including, (1) the crustal thickening leading to the present-day elevation of Tibet, and (2) the growth of the plateau to the north-east and east. Thus the east-west stretching and eastward plateau growth dominate the present tectonics of the Tibetan Plateau.

Even based on different assumptions, the model proposed by Tapponnier et al. (2001) as well as by Shen et al. (2001) reveal similarities: The admittance of the two stage evolution history of the Tibetan Plateau would imply that the discussed models above, i.e., “block motion” model, “thin viscous sheet” mode, and “channel flow” model, respectively could explain the collision process and the subsequent mechanical evolution of the plateau. The “block motion model” may be attributed to the early stage of the India-Eurasia collision process. At a later stage the lithosphere had reached the appropriate thickening leading to the development of the viscous channel flow in its lower part. Lateral extrusion probably played a greater role in accommodating India’s indentation into the Asia continent. With regard to the later stage, i.e., “channel flow”, it can be considered that the viscous flow in the lower crust of Tibet might have left his fingerprint manifesting in crustal deformation of the region. Thus domes and antiforms observed in southern Tibet, reflecting its morphology, as well as subsequent extensional structures (e.g., low/high angle normal faulting) might be interpreted as a response to the “channel flow”.

Palaeomagnetic results obtained during this study –including earlier existing data (s. Fig. 1)– contribute to a better understanding of the evolution history of the Tibetan Plateau, and hence are tackled with regard to the tectonic models discussed above.

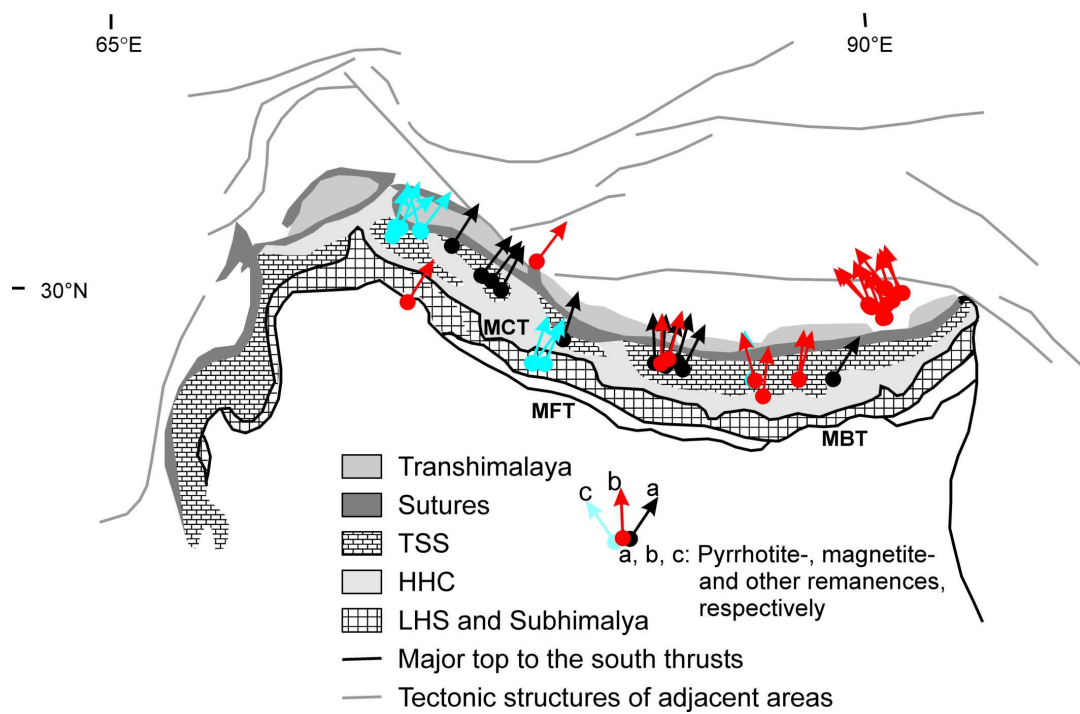


**Fig. 1:** Magnitude and sense of rotation of block segments versus Indian shield along the Himalayan arc, and in southern Tibet (data from Appel et al. (1991, 1995), Besse et al. (1984), Chen et al. (1993), Klootwijk et al. (1985, 1986, 1991), Lin & Watts (1984), Patzelt et al. (1996), Schill et al. (2004))

### 1. 3. Main tectonic units and age constraints

The Himalaya –Tibet orogen system consists of several main tectonic units (Fig. 2): The Indus-Yarlung suture zone (IYSZ) separates rocks of Eurasian and Indian origin. The early collision between India and Eurasia took place along the IYSZ, and the suture formed at the Early Eocene as a consequence of the closure of the Neo-Tethys (e.g., Molnar and Tapponnier, 1975, Gansser, 1980; Burg and Chen, 1984). The IYSZ demarcates the Tethyan Himalaya in the north, comprising the Tibetan Sedimentary Series (TSS), stretching along the Himalayan arc and representing the strongly deformed remnant of the passive northern edge of the Indian subcontinent (e.g. Garzanti, 1999; Hodges, 2000). The nearly east-west striking normal fault system known as the South Tibetan Detachment System (STDS) separates the TSS in the north from the Higher Himalayan Crystalline in the south. The STDS has been interpreted as a result of gravitational collapse (e.g. Burchfield et al., 1992; Hodges et al., 1996), wedge extrusion of the HHC (e.g., Grujic et al., 1996, Chemenda et al., 2000), channel flow in the Tibetan lithosphere (Nelson et al., 1996; Beaumont et al., 2001, 2004; Grujic et al., 2002) or extension caused by increased basal shear of the underthrusting India continent (Liu & Yang, 2003). Recently it was considered as a roof fault of the Greater Himalayan duplex (Yin, 2006). While the HHC is to the north bounded by the STDS, the Main Central Thrust (MCT) is the northernmost of a series of southward propagating thrusts. The Main Boundary thrust (MBT) and the Main Himalayan Thrust (MHT) constitute the southernmost boundary, delimitating the Lesser Himalaya and the Siwalik foreland.

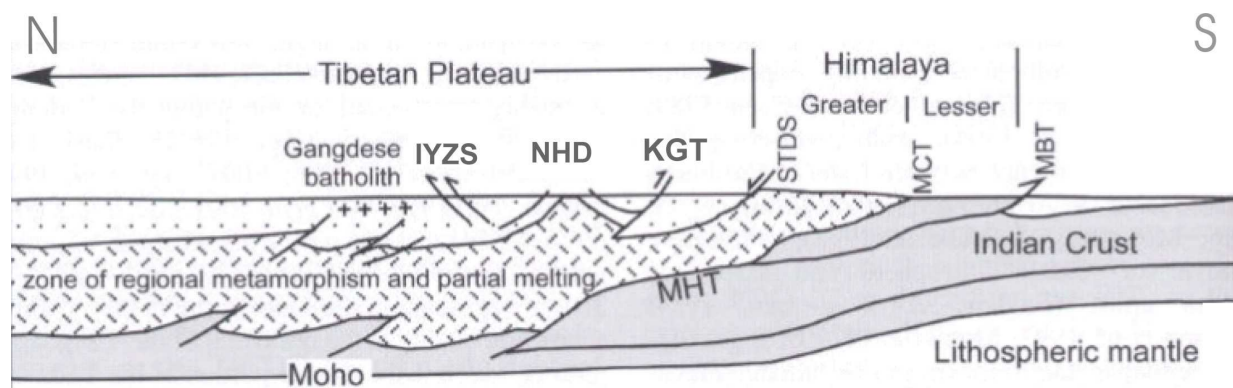


**Fig. 2:** Example of an interpretative north-south cross section, displaying the main tectonic units of the Himalayan Tibet orogen system (modified after Harrison, 2006).

The study area covers two main units, the TSS in southern Tibet and the HHC in eastern Nepal (Solu Khumbu area). In southern Tibet fieldwork has been carried out on an east-west traverse between 86° and 89°E (Fig. 3), encompassing the Nyalam section, the Kharta valley, the Dinggye extensional zone and the Yadong/Pari area. Low grade Ordovician to Mid-Triassic meta-carbonates and slates were sampled. The south Tibetan series are bounded to the south by the STDS and to the north by the IYSZ. The Gyirong-Kangmar thrust system (KGT) related North Himalayan domes (NHD) cored by leucogranites are abundant within this area; they form an anticline structure, which can be followed (Ding et al., 2005) east and west of the study area and is extending approximately east-west. Furthermore, the study areas lay within an extensional – and orthogonal contractional zone (Wang et al, 2001). The west-east extent is cross-cutting a series of north-south striking normal fault zones: the Nyalam fault zone, the Dinggye-Xianza fault system and the Yadong-Gulu rift, all characterized by a left lateral slip component (Gan et al., 2007). In contrast, Zhang et al. (2006) have postulated a right lateral slip component for the north-south striking Dinggye-Xianza rift.

The south-north transect at ca. 87°E is ranging from few km south of Lukla (Solu Khumbu, HHC) to Lhatse close to the IYSZ. Sampling included the high-grade metamorphic gneisses from the HHC, the Tethyan sedimentary series (Ordovician to Carboniferous) and the upper Triassic flysch between Tingri and Lhatse.

With regard to late orogenic processes pyrrhotite has been often demonstrated as a main recorder of palaeomagnetic signals in very low- to low-grade metamorphic rocks as limestone and slates (e.g. Rochette, 1987, Appel et al., 1991; Ménard and Rochette, 1992, Schill et al., 1998, Crouzet et al., 1999). Therefore, secondary pyrrhotite as the characteristic magnetic remanence carrier is of major focus in all sampling areas. It is generally accepted that pyrrhotite in such rocks is formed by the breakdown of diagenetic pyrite and/or magnetite under low oxygen fugacity conditions. An increase in sulfur fugacity may also favor the formation of pyrrhotite by reduction of magnetite.

The mechanism of secondary remanence acquisition in low-grade metamorphic rocks of the Tethyan Himalaya has been extensively discussed (e.g., Crouzet et al., 2001): Pyrrhotite is formed during pro-grade or peak metamorphism. A thermoremanence is blocked during last cooling event if the peak metamorphic temperature ( $T_m$ ) has attained the Curie temperature ( $T_c$ ) of pyrrhotite (~320 °C). If  $T_m$  was lower than  $T_c$  a thermo-chemical mechanism is likely and the time of remanence acquisition might predate the cooling age. For this reason illite crystallinity and K/Ar dating were applied to determine peak metamorphic temperatures and ages of metamorphic cooling: Epi-anchizonal conditions are found to be characteristic for the study area. Therefore, a thermo- as well as a thermo chemical remanence is expected, depending on the influence of the intrusive leucogranites. In the high-grade gneisses of the HHC pyrrhotite is believed to form during the transition from ductile to brittle deformation (i.e., retrograde stage). A thermoremanence is likely acquired and its age will approximately correspond to the age of the last metamorphic cooling event. However, it should also be mentioned that pyrrhotite is capable to grow during pro-grade metamorphism (primary pyrrhotite) and to become re-equilibrated at a later cooling stage (retrograde metamorphose). This mechanism will be extensively discussed in chap. 5.2.

The TSS in the study area comprises Ordovician to Upper-Triassic sediments with very low- to low-grade metamorphism (epi-anchizonal conditions). Due to its low grade the age constraints lack often in the Tethyan Himalaya. For instance, information on the tectono-metamorphic history of the Himalayan-Tibetan orogen system can be derived from the tectono-metamorphic evolution of the HHC: Two main peak metamorphic phases (M1 and M2, respectively) have manifested in the HHC: The early M1 (32-30 Ma) kyanite ± silimanite metamorphism (650-680°C, 7-8 kbar) is linked to crustal thickening and regional Barrovian Metamorphism. The M2 (23-17 Ma) silimanite ± cordierite metamorphism (650-680°C, 4-5 kbar) is attributed to increased heat input and subsequent partial melting in the crust. It is suggested by many authors that crustal melting triggered channel flow and ductile extrusion of the HHC. The timing of motion along the MCT and the STDS zone at the base and the top of the channel respectively has been extensively discussed (e.g., Hodges et al., 1992, Hodges, 2000, Searle and Godin 2003, Godin et al., 2006a). Both ductile shear zones were active during the early Miocene (23-15 Ma). A consistent age older than 16-14 Ma year obtained for hornblende and mica indicates a minimum time constraint on the exhumation history of both shear zones at the ductile/brittle regime transition.  $^{40}\text{K}/^{39}\text{Ar}$  dating on mica and apatite fission track ages (Wang et al. 2001) implies that the Nyalam detachment and its footwall share a rapid cooling history during the interval of ca. 16-12 Ma. New isotopic ages from the Mabja Dome reveal a late Oligocene to early Miocene history of ductile vertical thinning and horizontal stretching, peak metamorphism, migmatization and emplacement of a leucocratic dyke swarm (Lee et al., 2006). Doming is thought to have occurred between 13.0 and 12.5 Ma at temperatures between 370 and 200°C. First thermometric results, mainly based on illite-crystallinity, from measurements running within this study in Goettingen (Dunkl), indicate epi-anchizonal conditions in the study area between 86°E and 89°E.  $^{40}\text{K}/^{39}\text{Ar}$  dating on illite indicates mixed ages, which vary from Early Cretaceous to Late Miocene. “Reliable” ages were obtained at two localities, in the

Permian limestone S of the Kangmar dome (34 Ma) and in the Upper Triassic flysch close to the IYSZ (24-27 Ma).  $^{40}\text{K}/^{39}\text{Ar}$ -dating on illite and zircon fission track dating in adjacent areas in western Nepal give ages of 30-25 Ma documenting the Eo-Himalayan thermal event (Crouzet et al., 2002).

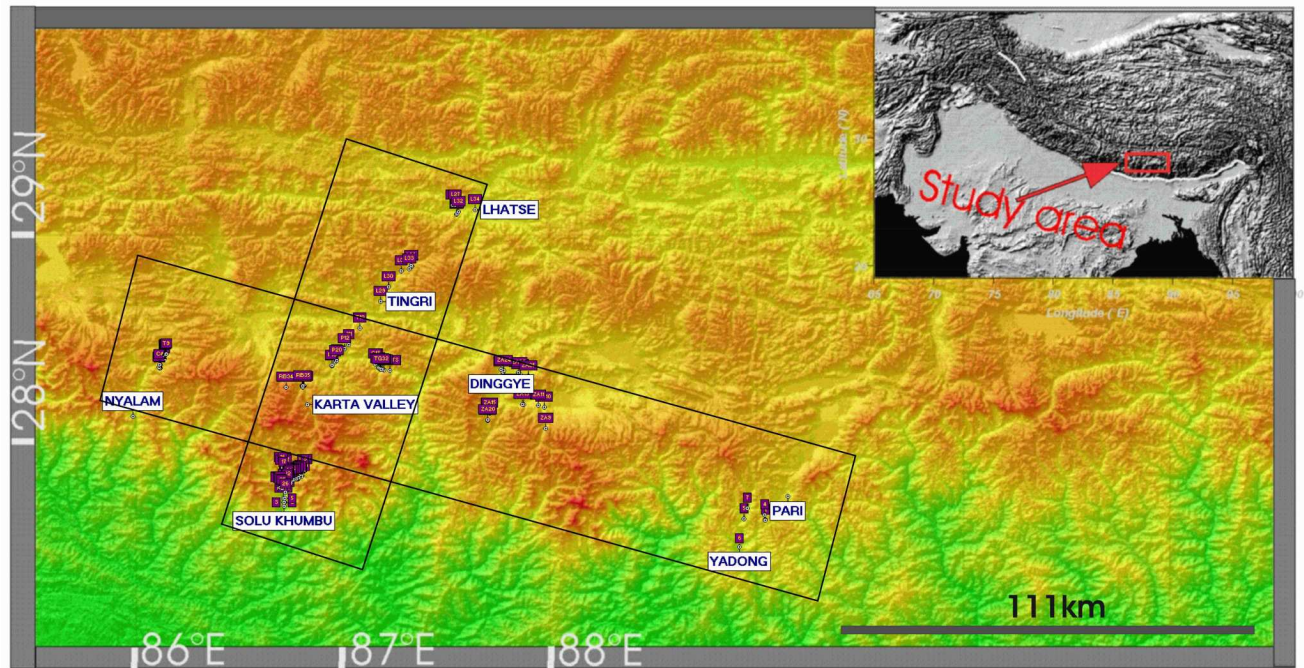


**Fig. 3:** Digital elevation model (shaded relief) from the study area, indicating the sampled areas (with sites localities) on the west-east traverse and the south-north transect (boxes).

## 2. Analytical Methods

### 2.1. Palaeomagnetism and magneto-mineralogy

Core samples (2.5 cm in diameter) oriented with a magnetic compass were cut into standard specimens of 2.2-2.3 cm length. To test the suitability of the samples for palaeomagnetic investigations detailed stepwise thermal (5-10°C, within critical temperature intervals) and alternating field (AF) cleaning were performed for one pilot sample (mostly twin specimens) from each site. For thermal demagnetization (ThD) and subsequent measurements an ASC furnace and a SQUID-magnetometer 2G760 (noise level <math>2.10^{-2}</math> mA.m<sup>-1</sup> for 10 cm<sup>3</sup> samples) were used. A 2G600 automatic degaussing -system attached to the SQUID Magnetometer served for AF demagnetization (AFD). In order to detect possible mineral alteration during heating the bulk susceptibility was measured with a KLY-2 kappabridge (Agico) after each step of heating. Using a pulse magnetometer (Magnetic Measurements MMPM9) the previously AF demagnetized specimens were subjected to isothermal remanent magnetization (IRM) in a direct current (DC) field up to a maximum of 2.8 T, with subsequent stepwise thermal demagnetization of the saturation IRM (SIRM<sup>T</sup>). Depending on the results of pilot studies, and based on the interpretation of IRM acquisition curves and SIRM<sup>T</sup> curves, the specimens of each site were thermally demagnetized, subjected to AF-cleaning, or treated combining both methods.

Thermo magnetic and hysteresis measurements were performed on selected samples (fragments and coarse to fine grained samples) with a Quantum Design XL7 Magnetic Property Measurements System (MPMS; noise level  $\sim 10^{-11}$  Am<sup>2</sup>) at Bremen University: The room temperature (RT) saturation isothermal remanence magnetization (SIRM<sup>RT</sup>) runs were achieved on selected samples using a DC field –applied at RT- with a magnitude of 5 T; cycling from 300 to 5 K (field cooling) and back to room temperature (field warming) in zero-field was monitored in 2.5 K increments. High field hysteresis measurements were done with a focus on the ferri(o)magnetic phase pyrrhotite, in order to verify whether a relationship between selected low-temperatures and measured fields can be established. Reflected light microscopy and Bitter technique were applied to selected polished samples. Transmitted light microscopy (thin section analysis) was applied for petrography analysis of the high-grade metamorphic rocks from the HHC.

Expecting probable differences in behavior and recovery, remagnetization tests were, for the first time, systematically accomplished on selected low- and high-grade metamorphic samples, which are assumed to have acquired either a thermo- or a thermo-chemical remanence (TRM and TCRM, respectively). The selected samples (metacarbonates, pelites and gneisses) were demonstrated to bear pyrrhotite as a dominant magnetic phase while treatment by ThD until 350°C (unblocking temperature interval for pyrrhotite). The application of IRM acquisition and subsequent SIRM<sup>T</sup> applied on these previously treated samples was twofold: (1) confirmation of the presence of pyrrhotite through its re-identification (recovery), and (2) possible characterization of TRM and TCRM acquired in these samples via correlation (linear regression analysis) of their ThD- and SIRM<sup>T</sup> (after remagnetization) results. The data are added to the appendix.

### 2.2. Thermometry and thermochronology

For illite crystallinity, <2micron fractions were produced from every metapelitic sample and analyzed (air-dried and glycolized). Decarbonation of samples, if necessary, precede the preparation of the mounts.

Illite crystallinity is defined through the Kübler Index (KI), where KI is the full width at half-maximum of the first, 10 Å basal reflection of illite-white K-mica (Kübler, 1967; Jaboyedoff, 2000). KI indicates the degree of ordering of illite lattice and thus the metamorphic grade (while KI

decreases, the degree of "crystallinity" increases). The details of the analytical technique can be found in e.g. Crouzet et al. (2006).

For dating illite fractions K/Ar method is used. The selection of samples is made according to the mineral assemblages (whole rock X-ray diffractometry). Separation of different fractions (<0.2, 0.2-0.6, and 0.6-2 microns) enables an estimation of the age of latest re-crystallization. Details of the technique are presented in Árkai et al. (1995) and Frey (1987).

The peak paleotemperature of the black slates is also estimated from the vitrinite reflectance (VR) values. Maximum and minimum VR ( $\% R_{\max}$  and  $\%R_{\min}$  respectively), measured as reflectance of fine dispersed organic matter, is usually obtained in monochromatic (546 nm) polarized light. Here the measurements are performed on a Leica MPV SP microscope.

### **2. 3. Tectonics**

Complementary field surveys (field mapping, structural measurements), analytical work (thin sections, micro-structures) and analysis of landsat images from the area between 86- and 89°E (Yadong/Pari, and Solu Khumbu excluded) is involved as well as investigation on digital elevation models (DEM) and derivation of secondary products of DEM like lineaments extraction, slope, aspect, shaded relief and drainage system from this area.

### 3. Magneto-mineralogy and palaeomagnetic results

#### 3.1. Tethyan Himalaya -southern Tibet

In the study area the South Tibetan Sedimentary series lay within an extensional zone. They are bounded to the south by the STDS and to the north by the IYSZ, and there is a widespread occurrence of North Himalayan gneiss domes bounded to the south by the Gyirong-Kangmar thrust (KGT) fault system (s. Fig. 4). Both structures the STDS as well as the IYSZ and its associated thrusts are striking east-west. In west-east extent there is a cross-cutting series of north-south striking normal fault zones, the Nyalam fault zone, the Dinggye-Xianza fault system and Yadong-Gulu rift.

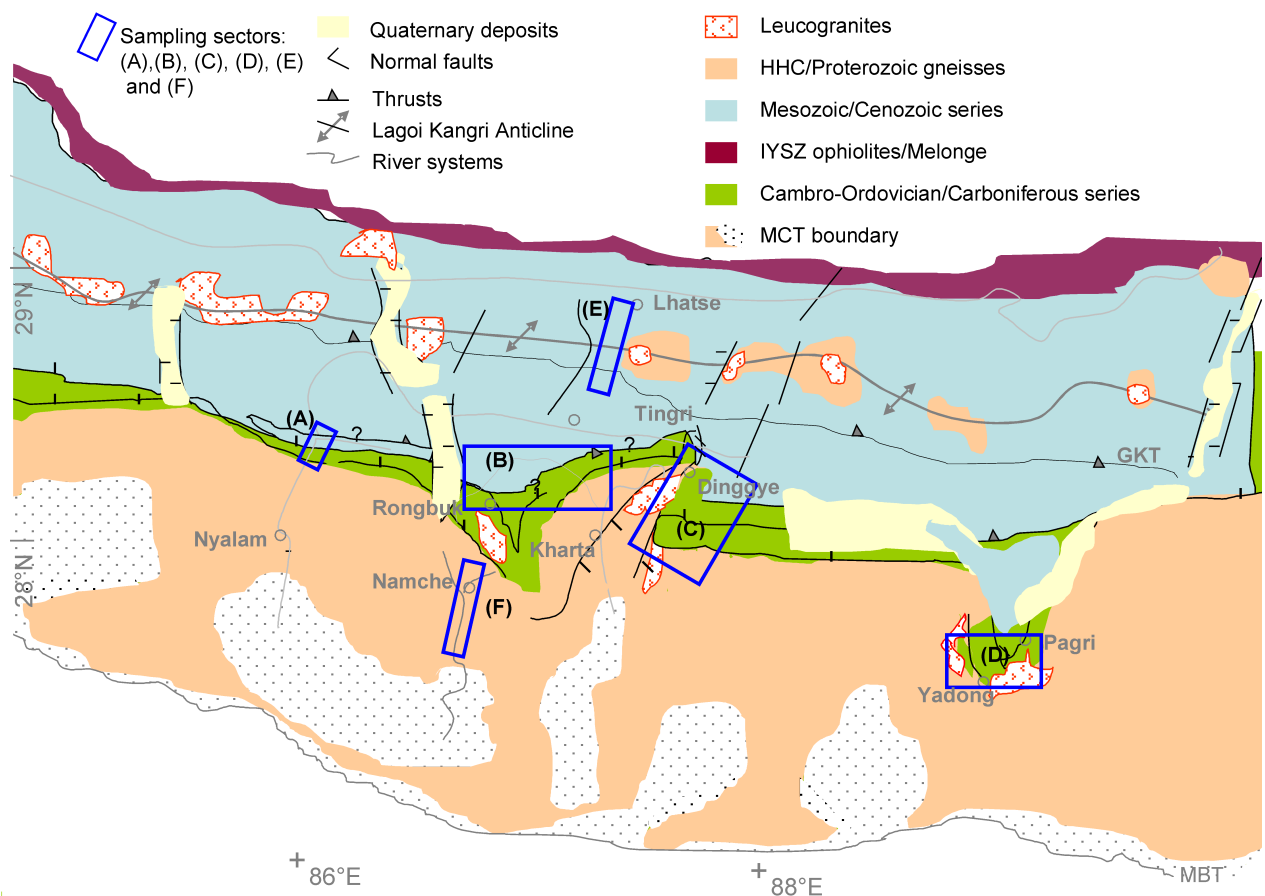


**Fig. 4:** Simplified geological map from the study area -with main relevant tectonic features- showing the sampled sectors along a west-east traverse and south-north transect. Data base for this map have been taken from various sources (Geological map of the Qinghai-Xizang (Tibet) and adjacent areas, Chengdu; Ratschbacher et al., 1994; Ding et al., 2005).

The 67 sampling sites (s. appendix) drilled in the Tethyan Himalaya of southern Tibet cover a west-east extent from 86-89°E (Fig. 3, 4). These samples were taken from six stratigraphic units (Ordovician, Devonian, Carboniferous, Permian and Triassic). For interpretation, the studied area between 86-89°E is divided into 5 main sectors, i.e., (A) Nyalam section (Ordovician to Triassic meta-limestone, and Carboniferous slates), (B) Kharta Valley (Ordovician to Permian meta-

limestone and Devonian slates), (C) Dinggye sector (Ordovician to Permian meta-limestone and siltstone) (D) Yadong/Pari location (Ordovician meta-limestone), and (E) area between Tingri and Lhatse (upper Triassic flysch).

### 3. 1. 1. Nyalam section

Sampling sites for palaeomagnetic investigations at Nyalam section within sector (A) (Fig. 4) consist mainly of Ordovician meta-carbonates and Carboniferous/Devonian slates at the base of the STDS, overlaid laterally by thrusting from the Upper-Permian to Triassic meta-sedimentary series.

#### 3. 1. 1. 1. Results

Regardless a recent remanence carried by goethite and/or low coercivity magnetite, two dominant characteristic remanence components (*ChRM*) were isolated, on the basis of their unblocking temperature intervals and coercivity. Major unblocking between 250-320°C and 370-520°C are attributed to pyrrhotite (*ChRM<sup>pyr</sup>*) and (titano-?) magnetite (*ChRM<sup>mag</sup>*), respectively. *ChRM<sup>mag</sup>* is restricted to the Permian to Mid-Triassic series. Occasionally, a 3<sup>rd</sup> component, identified as hematite, is also observed, but its contribution can be neglected. Isothermal remanence acquisition (IRM) and subsequent thermal demagnetization of saturation magnetization (*SIRM<sup>T</sup>*) support the presence of pyrrhotite, magnetite and hematite. Transition at ~34 K and Morin transition (indicative for stoichiometric hematite) was observed during low temperature thermomagnetic runs (s. the example in Fig. 10b). Further details and additional measurements techniques are discussed below as well as in following chapters. Findings are discussed with regard to the low temperature component (*ChRM<sup>pyr</sup>*). Results of the high temperature component (*ChRM<sup>mag</sup>*) at Nyalam section are connected to those obtained in Kharta valley, and thus tackled in chap. 5.1. 2.

#### *Low temperature component (ChRM<sup>pyr</sup>)*

A *ChRM<sup>pyr</sup>* could be isolated from 5 out of 11 sites at Nyalam section, i.e., Ordovician meta-limestone and Carboniferous slates. The Zijdeveld diagrams (Fig. 5) show a stable component with a consistent south-east direction. IRM acquisition curves and thermal demagnetization (ThD) of NRM and *SIRM* reveals pyrrhotite as the dominant ferro(i)magnetic mineral and carrier of the *ChRM*. Residuals observed in ThD curves (Fig. 5) correspond mainly to trace contribution of hematite as evidenced by *SIRM<sup>T</sup>* (Fig. 6a). Pyrrhotite in the Ordovician limestone is characterized by its high coercivity as it is shown in Fig. 6b. The apparent noisy character of the curves is due to the presence of trace amounts of hematite. The Carboniferous slates reveal a lower coercivity than the Ordovician limestone. A negligible contribution of a low to medium coercivity magnetite is also evident in the Alternating field demagnetization (AFD) of the Carboniferous slates.

Principal component analysis (PCA) (Kirschvink, 1980) and Fisherian vector statistics (Fisher, 1953) show systematically grouped directions (Fig. 7). Statistical data for individual sites is listed in Tab. 1. The overall in situ mean direction is  $D= 167.0^\circ/I=18.5^\circ$  ( $\alpha_{95}=12.0^\circ$ ,  $k=42$ ) ( $D$ ,  $I$ ,  $\alpha_{95}$  and  $k$ , are declination, inclination, confidence angle and dispersion parameter, respectively) for the Nyalam section. Bedding corrected data  $D= 167.2^\circ/I= 40^\circ$  ( $\alpha_{95}=10.2^\circ$ ,  $k=57$ ) show a better grouping. Partial un-tilting is optimum at 66.2% (s. diagram in Fig. 7e). The performed Direction-Correction (DC) tilt test for all sites -with optimum untilting at  $52.4\pm 31.3\%$ - is indeterminate. Depending on sites combinations positive as well as negative DC tilt tests are obtained, augmenting the probability of the occurrence of a syntectonic remagnetization.

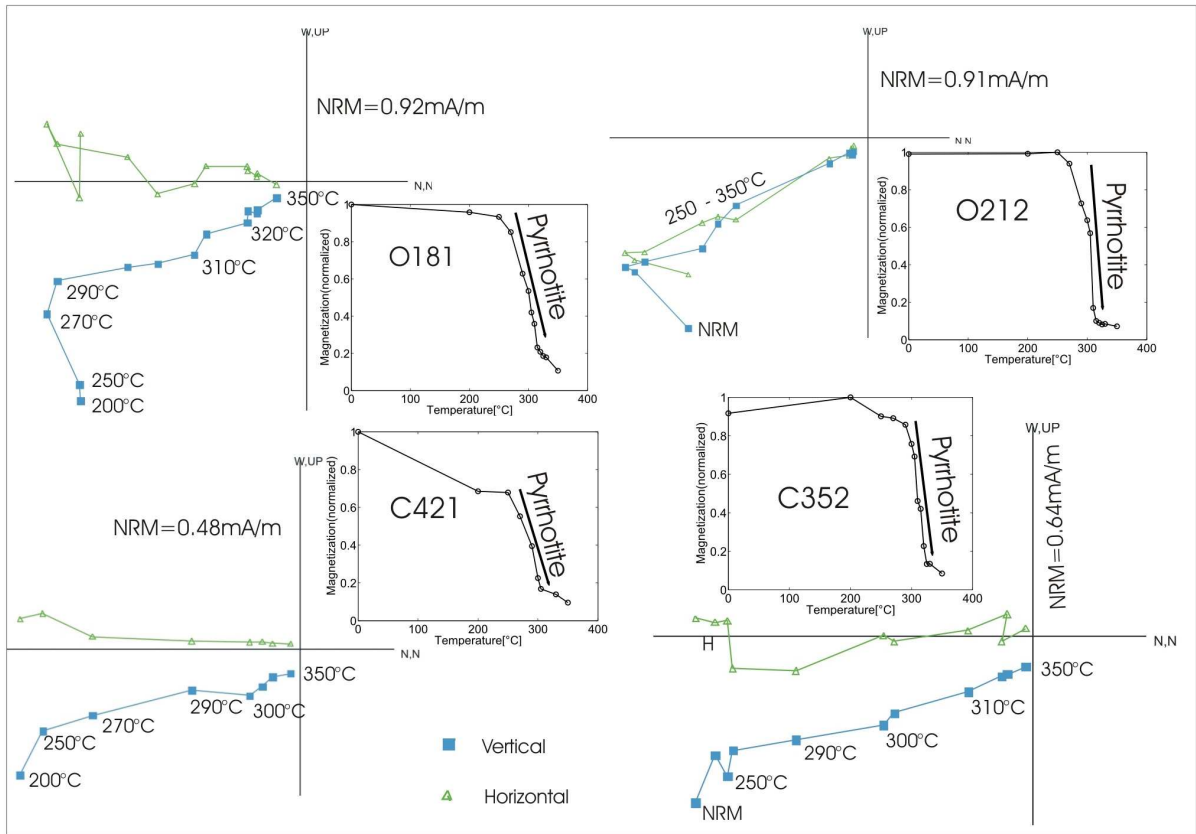


**Fig. 5:** Examples of Zijderveld diagrams and temperature-intensity curves obtained for Ordovician and Carboniferous specimens from the Nyalam section.

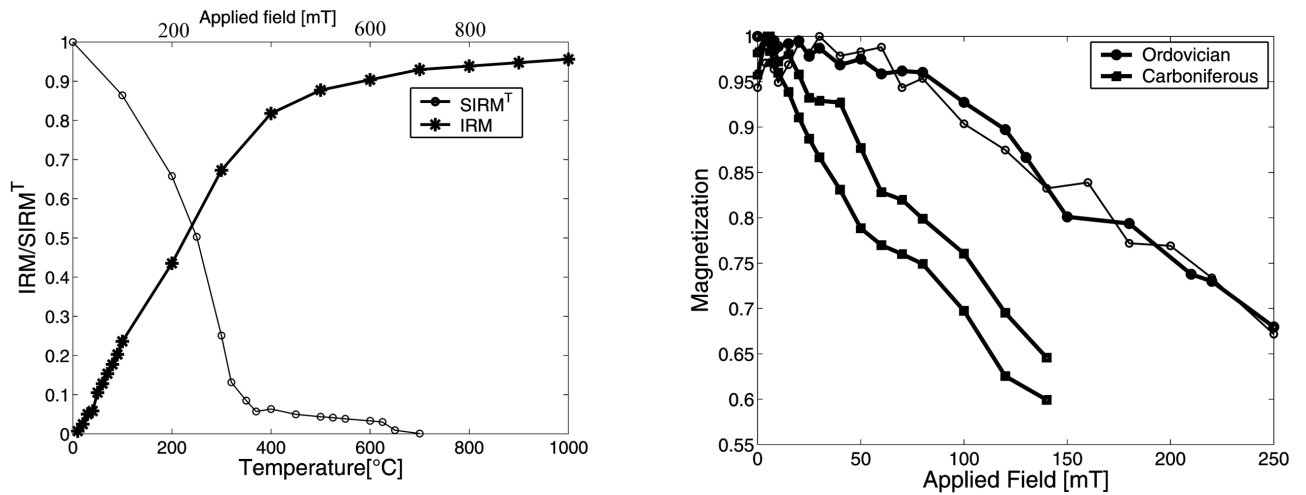


**Fig. 6:** High coercivity – especially in the Ordovician meta-limestone - is reflected by IRM acquisition curves and corresponding thermal demagnetization SIRM ( $SIRM^T$ ), as well as by AF cleaning. The convex character of the AFD is interpreted to be indicative for the presence of fine grained pyrrhotite within the single domain range (SD).

**Tab. 1:**  $ChRM^{DVR}$  directions mean of individual Sites, and overall mean direction (average) of all sites at Nyalam section (g and s indicate geographic and stratigraphic coordinates; N is the number of specimens/sites included in the statistics)

Site	N	Dg (°)	Ig (°)	kg	$\alpha_{95g}$ (°)	Ds (°)	Is (°)	Ks	$\alpha_{95s}$ (°)
ny41	6	169.4	2.5	19.7	15.5	175.5	32.3	19.7	15.5
o1	10	166.3	29.2	71.3	5.8	169.7	49.8	71.2	5.8
o2	8	153.3	24.2	227.9	3.7	169.9	44.9	200.1	3.9
c3	10	171.8	17.9	98.2	4.9	155.7	28.6	97.5	4.9
c4	8	173.5	18.1	27.1	10.8	166.3	43.4	27	10.8
<b>Average</b>	<b>5</b>	<b>167</b>	<b>18.5</b>	<b>41.8</b>	<b>12</b>	<b>167.2</b>	<b>40</b>	<b>57</b>	<b>10.2</b>

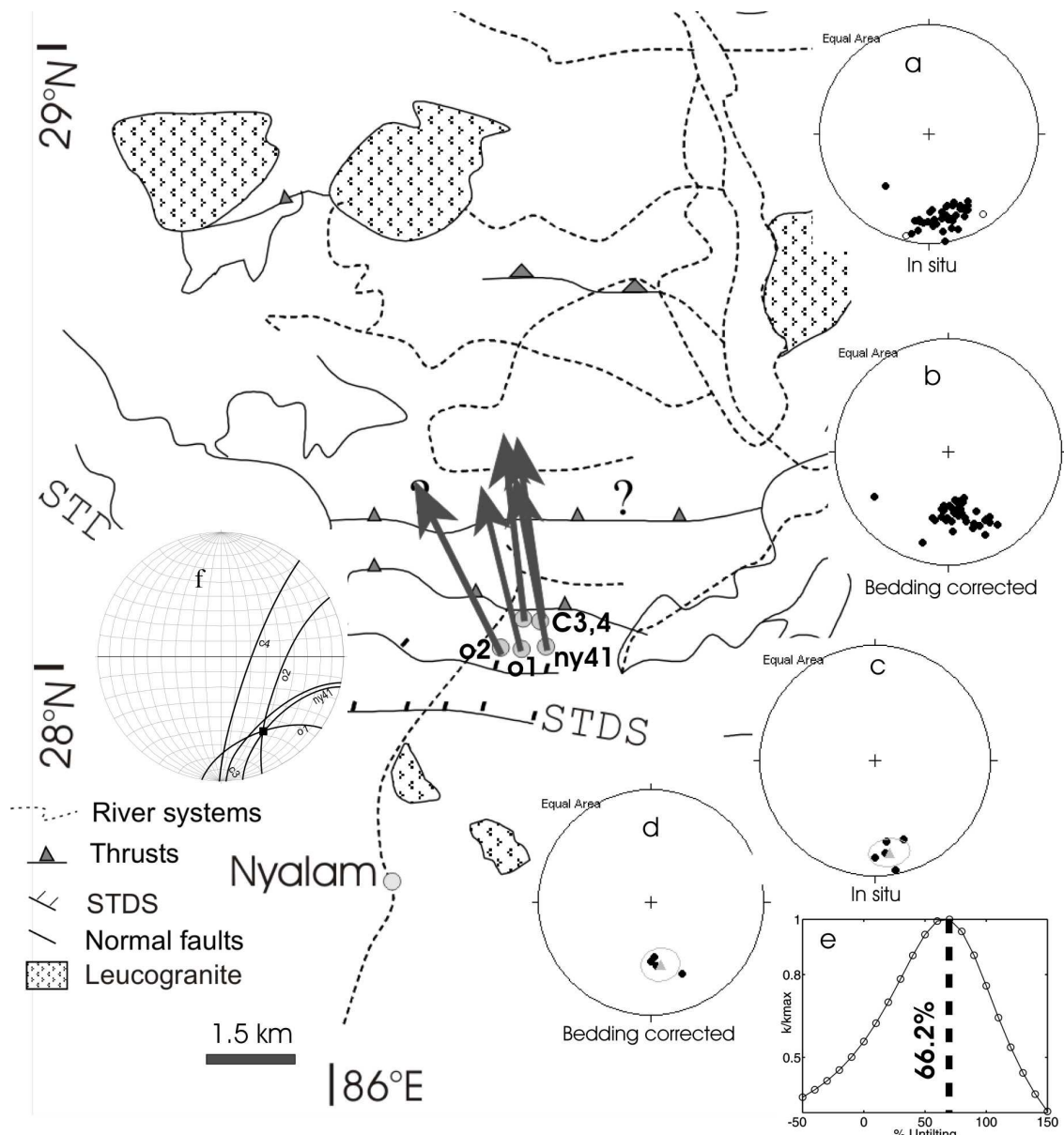


**Fig. 7:**  $ChRM^{DVR}$  directions of individual specimens (a, b), and site mean directions/overall mean direction (circles and triangles, respectively) (c, d) with  $\alpha_{95}$  confidence circle of Ordovician and Carboniferous meta-sediments at Nyalam section. Dots and open circles represent lower- and upper hemi-sphere projections, respectively. Arrows at sampling sites (filled grey circles) indicate observed declinations versus north (all in situ). (e) Partial untilting diagram for Nyalam sites with optimum at 66.2% untilting. (f) Common remanence intersection obtained for three sites.

### 3. 1. 1. 2. Discussion

Following the structures and constrained cooling ages discussed in Chapter 3 an Oligocene - Miocene age of remanence acquisition can be suggested. However, the measured “anomalous” inclinations (s. Tab. 1 and Fig. 7) give rise to several questions, and possible explanations:

- 1) A basically simplest model to explain the “anomalous” inclinations is a large-scale sub-horizontal folding after remanence acquisition (s. Fig. 8A). This model would explain the regional occurrence of these inclinations. For instance, this assumption remains questionable, since, it has been often demonstrated in the Tethyan Himalaya that the remanence acquired in pyrrhotite has a post folding character. In contrast, the proposed model emphasizes a probable primary remanence acquisition in pyrrhotite.
- 2) Assuming that no tilting has taken place a Paleocene/Eocene age of remanence acquisition in this area at southern latitudes deduced from the APWP, after Acton (1999), can also be considered.
- 3) The polarity in Nyalam is rather reverse, and an Oligocene –Miocene age can be expected. In this case a strong tilting after remanence acquisition resulting in “anomalous” inclinations is rather obvious.

In this case, remagnetization might have had manifested at the end, or after the first order folding (main Himalayan folding), and before the commencement of the second order tilting, probably, related to the development of extensional tectonic structures the STDS and the antiforms/synforms. Taking into account the discussed considerations, the first model might not be completely excluded. The second assumption would imply that pyrrhotite has recorded the progressive suturing until Early Eocene in Eastern Himalaya (southern Tibet). This stresses the discussion - as by the first assumption - about the nature of the remanence acquired in pyrrhotite and its age: a burial related process for the formation and magnetization of pyrrhotite is not improbable.

The Ordovician limestone at Nyalam indicates very low-grade conditions of metamorphism (anchizone); microscopic observations imply simple shear. Deformed large crystals of detrital white mica, calcite twin laminae and early stage of graphite crystallization are indicative for deformation and temperatures not exceeding 300°C. Therefore, a thermo-chemical origin can be proposed for this remanence. Despite pyrite observed on polished thin sections by reflected light microscopy, the very fine grained iron sulfides (<5µm) dissimilated in the matrix, identified as pyrrhotite, as well as the very high coercivity observed during alternating field demagnetization, support the thermo-chemical nature of the remanence (TCRM). The high coercivity of the pyrrhotite is probably a result of existing exsolved pyrrhotite structures: assemblages of single domain (SD) grains and probably additional magnetostatic interaction between the latter.

The TCRM can, under circumstances, be related to a peak-temperature event (Barrovian?). In any case it can be suggested that the cause (metamorphism) is regional since it affects already two different stratigraphic units showing similar magnetic behavior (Ordovician limestone and Carboniferous slates). The known metamorphism (M1) in the Tethyan Himalaya is derived from the tectono-metamorphic evolution of the HHC, and is considered to have occurred at ~ 32Ma. This assumption and the fact that pyrrhotite is regarded to acquire a secondary remanence emphasize the 3<sup>rd</sup> assumption indicating that polarity in Nyalam is rather reverse and strong tilting might be related to the proximity of the sites locations to the STDS. In this case a “folded” or curved STDS (variation in dipping directions and angles) can be proposed (s. Fig. 8B). It should be mentioned that such tilting can also be caused by minor curved normal faults within the sequence. The “folding” of the STDS itself, superimposed to its “primary” undulation, parallel to the extension direction (long wave length folding) might be related to a late or coeval event considered as a consequence of the deformation caused by the channel flow: similar to salt diapirism phenomenon and associated dissolution, partial melting and viscous flow in the lower crust might have caused doming in the crust, accentuated by isostatical uplift as a response to pronounced

denudation. Buckling and basal shearing might also have contributed to deformation. If we consider the M1 and associated main D1 deformation (Eo-Himalayan deformation) discussed above than a maximum age for the remanence-acquisition can be defined (Oligocene); on the other hand the remanence acquisition could predate or be coeval with STDS (Nyalam detachment) and leucogranites exhumation and cooling and thus be a recorder of their associated deformation during the Miocene.

#### *Rotation and tilting:*

Even though a slight apparent counter-clockwise rotation is obtained for the Nyalam area (Tab. 1), which would be in agreement with the oroclinal bending proposed by Kloodwijk et al. (1985, 1986, 1991), a systematic and progressive decrease in this anti-clockwise rotation toward east and north is observable by the calculated in situ remanence directions (s. also Tab. 1 and Fig. 7). However, it should be mentioned that this assumption is rather tentative, due to the small number of the sampling sites (5 sites) in the Nyalam area.

Remarkable at Nyalam as well as in the adjacent sectors of the study area, is the distribution of the remanence directions on small circles. This phenomenon has been observed in the western Alps and discussed by Ménard (1988) and Crouzet (1996). In the India-Asia collision zone it was the first time discussed by Waldhör et al. (1999, 2001) (Pamir range), and further detected in the Tethyan Himalaya by Schill et al. (2003). Besse et al. (1984) remarked that their palaeomagnetic results in the Tingri area (southern Tibet) are not Gaussian distributed, but did not recognize that their calculated remanence directions are reflecting a small circle dispersion, identified by a reconsideration of their data within this study. In the Higher Himalayan Crystalline the small circle distribution is recognized the first time along the studied south-north transect in Solu Khumbu.

From data observations it can be assumed that dispersion of remanences has developed by syntectonic remanence acquisition throughout a certain period in which tilting around a nearly north-south axis have had occur followed by a second tilting around an axis approximately parallel to the main strike (east-west tilting, long wavelength folding. Additionally, a small vertical axis rotation might have had happened. The occurrence of minor normal faults within the sequence parallel to the STDS would support a detachment related anti-clockwise rotation. The en echelon normal faults would trigger a domino effect. The deduced anti-clockwise rotation would in turn imply that the concerned segment was previously clockwise rotated (adjustment effect).

In summary: (1) The 1<sup>st</sup> and 2<sup>nd</sup> assumption are not improbable; (2) The bedding corrected inclinations favor younger ages of remanence acquisition, for this reason an Oligocene-Miocene age of remanence is proposed which may approximately satisfy the considerations discussed above. However mixed ages cannot be excluded. Dispersion of remanence directions on small circles, similarity - in situ and tilt corrected- in calculated overall mean remanence directions, and the variance in performed fold tests (positive, negative, and indeterminate, depending on combined sites), all emphasize a synfolding remanence acquisition (Shipunov, 1997; Enkin, 2003) at Nyalam section. Common small circles remanence intersection value for Ordovician sites at Nyalam coinciding with results from the Dinggye and Yadong area, give evidence for a regional trend along the strike of the study area (west-east transect). More details are discussed in following chapters, and summarized in chap. 5. 1. 6.

From the magnetic point of view, the observed “anomalous” inclinations can be explained by auto-inversion or partial oxidation of pyrrhotite in the presence of magnetite and/or hematite. Due to the fact that the anomalous inclinations show a regional trend (two different stratigraphic units, Ordovician and Carboniferous) –they are not restricted to a small number of samples or sites- such a process seems to be rather improbable.

For the systematic and progressive change in remanence directions arrangement from north-west at Nyalam section to north-east in the adjacent area of Kharta-valley south, as it is discussed below, an alternative model expressed as a large lateral ramp-flat-ramp (s. Fig. 8C) can be proposed. Note that antiforms (domes) and synforms (basins) with their major and minor axes parallel and perpendicular to the extension direction might have the same effect. The circular distribution of remanence directions support a major effect attributed to the latter. A combination and interaction of all these contractional extensional structures as summarized in Fig. 8 is not excluded.

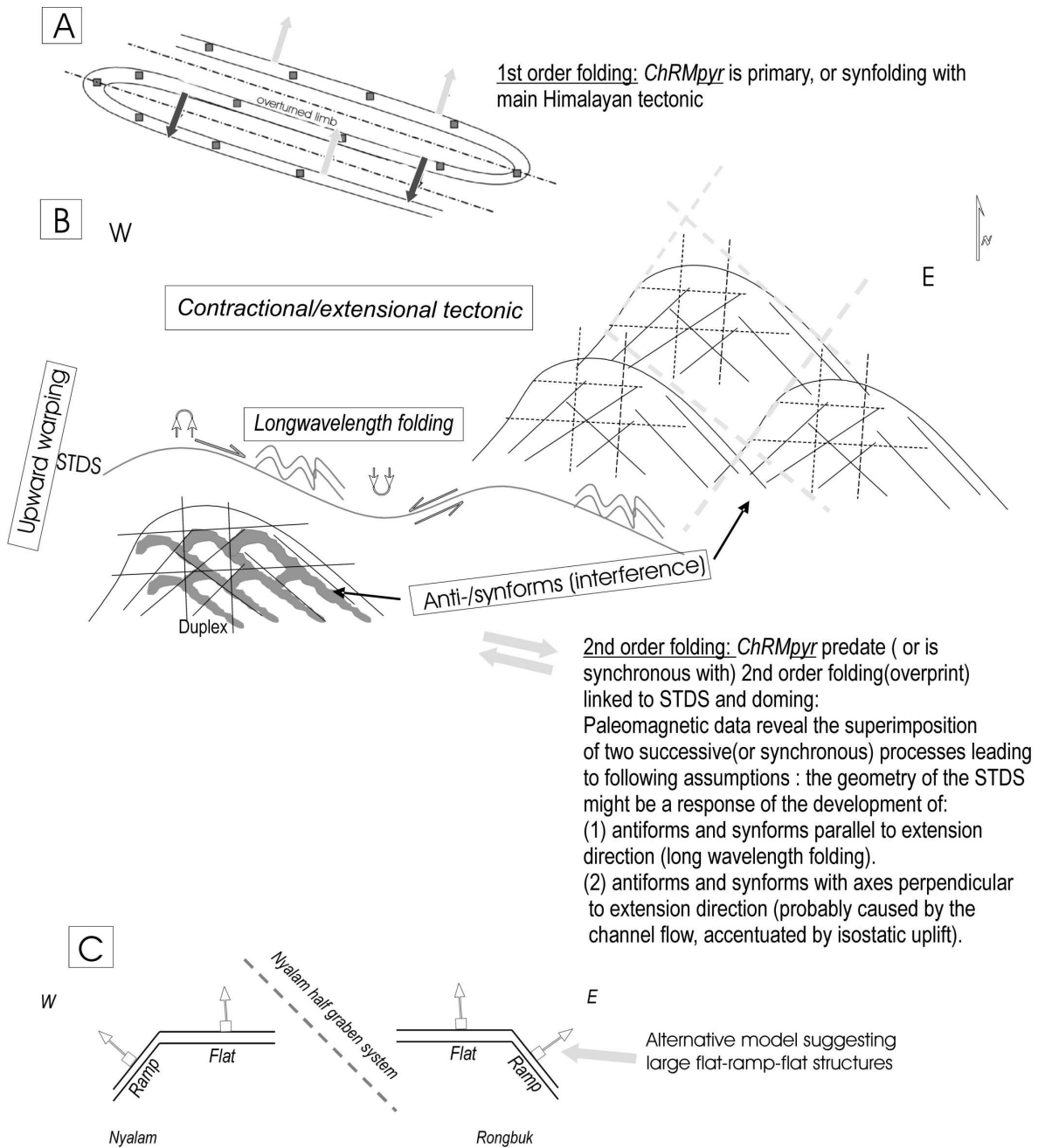


**Fig. 8:** simplified sketches visualizing models and assumptions discussed in chap. 5. 1. 1. 2.

### 3.1.2. Kharta Valley

Sampling in sector (B) was carried out close to Rongbuk and its north-west surroundings (Fig. 4). The sampling areas are termed Kharta valley south (KVS) and south (KVN), respectively. In KVS 5 sites were taken from the Ordovician meta-limestone, close to the STDS. Further 12 sites were drilled in KVN in Ordovician to Permo-Triassic TSS.

#### 3.1.2.1. Results

Sampling sites with significant results for the low temperature component pyrrhotite were taken from the Ordovician limestone in KVS (5 sites), and the Ordovician to Devonian limestone and slates in KVN (7 sites). Finding of the high temperature component magnetite are restricted to the Upper-Permian to Lower-Triassic series.

Low temperature component ( $ChRM^{pyr}$ )

The sampled sites lay within a normal fault (STDS)/thrust system dipping to the north.

$ChRM^{pyr}$  is dominant in the sampling sites mentioned above. Examples of ThD curves and Zijderveld diagrams are represented in Fig. 9a, revealing properties similarity to the  $ChRM^{pyr}$  component obtained at Nyalam section. However, the sites tightened to the STDS have, partly, lower coercivity (Fig. 9b), due probably to a larger grain size and/or the presence of a composite pyrrhotite. The large decay in remanence (pyrrhotite transition at  $\sim 36$  K), during  $SIRM^T$  field cooling might be an indication for such a relatively soft magnetic character (Fig. 10a).

Similar to Nyalam, unexpected inclinations are also partly observed in KVS. Normal and reverse polarity occur, as well as, occasionally, antipodes within a specimen. Reverse polarity is observed in two sites (one with very shallow negative inclination, and one with steep negative inclination). It should however be mentioned that remanence might change the hemisphere through tilting. Bedding corrected and in situ remanences are similar. Normal (in 3 sites) and reverse polarity (in 4 sites) is also present at KVN. A trend of increasing slight clockwise rotation is toward the ductile shear zone. Statistical data for both areas is summarized below in Tab. 2 and visualized in Fig. 12.

Data at KVN failed the Enkin (2003) fold test at 95% confidence level (optimal untilting is  $24.4 \pm 73.1\%$ ); partial untilting is maximum at  $29.8\%$  ( $D/I=20.53^\circ/32.9^\circ$ ,  $k=7.5$ ,  $\alpha_{95}=12.1$ ).

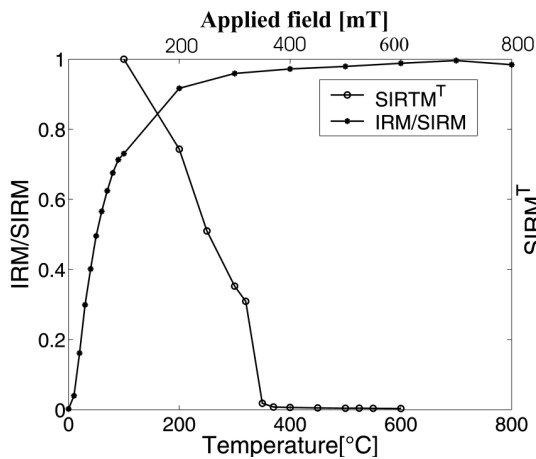
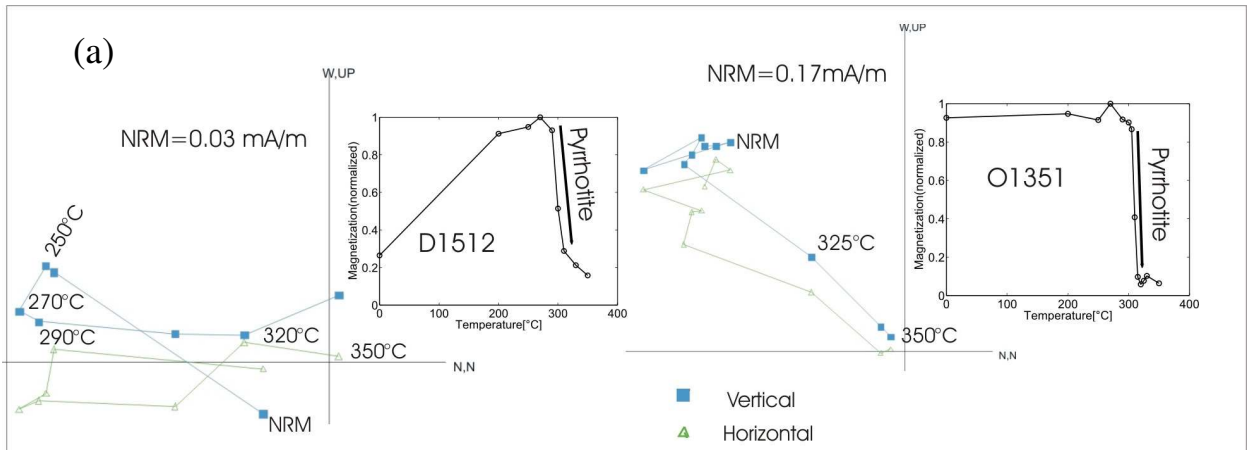


**Fig. 9:** (a) Examples of Zijderveld diagrams and temperature-intensity curves obtained for Ordovician and Devonian specimens from Kharta valley; residuals in ThD curves are due to the small contribution of hematite and magnetite. (b) Example of IRM and SIRM curve of Ordovician sample, revealing the dominance of pyrrhotite (with relatively lower coercivity). The sample is supposed to have acquired a thermoremanence through shear heating, and overprint, while the exhumation of the STDS. A gradual increase in temperature is observed in other samples (not shown), documented by an increase in the contribution of hematite and low coercivity magnetite. In this case, pyrrhotite might be regarded as the represent of the “350°C” -STDS related-isotherm.

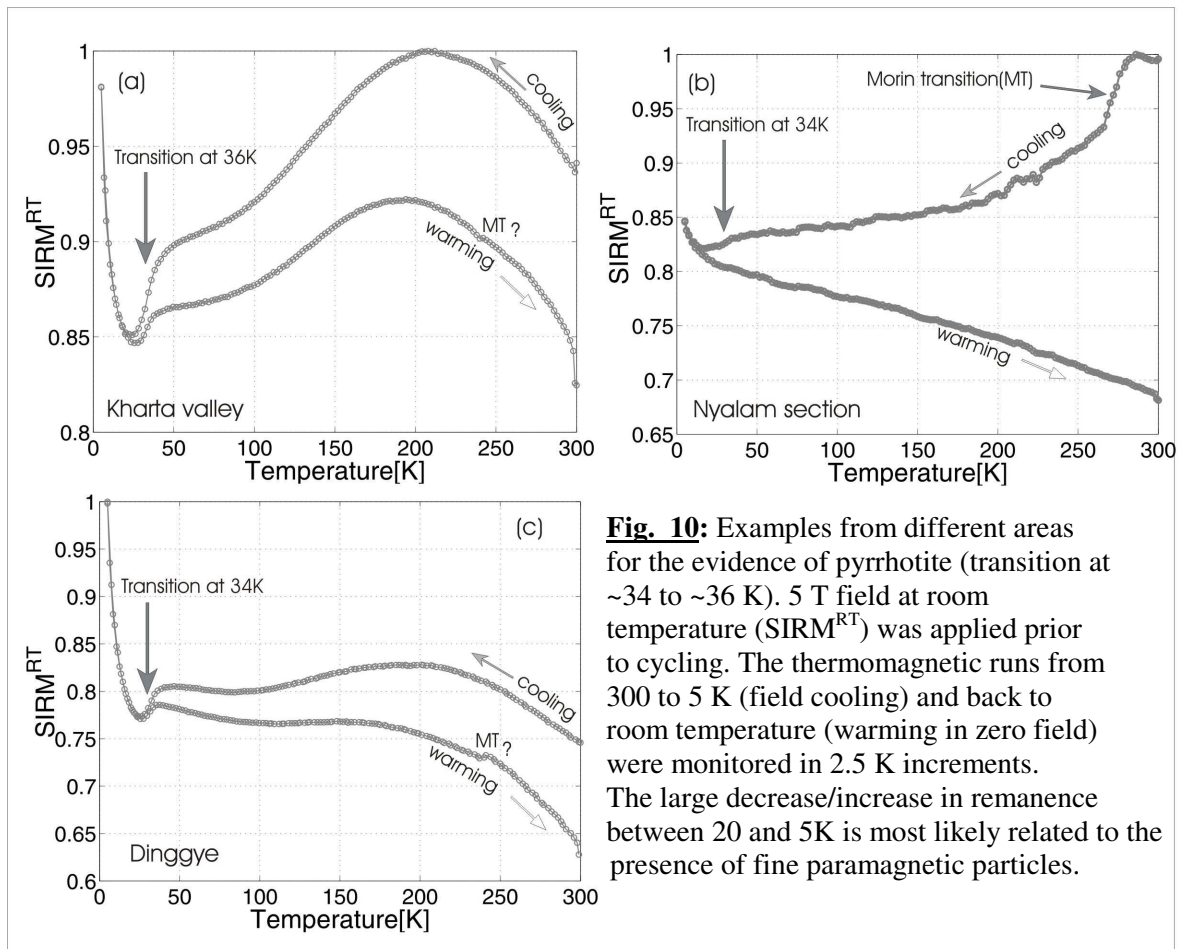


**Fig. 10:** Examples from different areas for the evidence of pyrrhotite (transition at ~34 to ~36 K). 5 T field at room temperature ( $SIRM^{RT}$ ) was applied prior to cycling. The thermomagnetic runs from 300 to 5 K (field cooling) and back to room temperature (warming in zero field) were monitored in 2.5 K increments. The large decrease/increase in remanence between 20 and 5K is most likely related to the presence of fine paramagnetic particles.

**Tab. 2:**  $ChRM^{DVR}$  directions mean of individual Sites, and overall mean direction of all sites at Kharta valley. Site rb37 is excluded in average1.

Site	N	Dg (°)	Ig (°)	kg	$\alpha_{95g}$ (°)	Ds (°)	Is (°)	ks	$\alpha_{95s}$ (°)
<b>Kharta valley south</b>									
rb33	6	205.7	32.4	9.7	25.1	206.3	10.7	8.7	26.6
rb34	5	208.7	-5.3	41.4	13.5	207.4	-22.1	28.3	16.4
rb35	7	202.2	18.3	17.9	15.9	200.1	-1.7	18.1	15.9
rb36	9	195.1	6.1	45.6	8.2	191.2	-2.9	45.2	8.2
rb37	6	199.7	-61.1	23.7	15.4	non	non	non	non
<b>Average1</b>	<b>4</b>	<b>202.8</b>	<b>12.9</b>	<b>29.8</b>	<b>19.9</b>	<b>201.1</b>	<b>-4</b>	<b>37.3</b>	<b>17.7</b>
Average2	5	202.5	-0.2	6.7	36.5				
<b>Kharta valley north</b>									
d15	10	180.5	-40.1	24.3	10.1	143.4	-59.9	24.8	9.9
o13	8	215.9	-31.7	110.2	5.3	203.3	-16.6	110.2	5.3
o14	4	166.3	-22.2	55.9	12.4	166.1	27.7	56.8	12.3
tg30	4	44.1	44.5	10.8	29.3	32	10.6	10.7	29.4
tg32	6	202.6	-29.3	11.5	20.6	194.6	2.6	11.5	20.6
tg29	6	348.1	50.9	10.8	21.3	11.1	40.2	10.8	21.4
tg31	6	35.2	34.7	6.6	28.3	25.6	0.1	6.5	28.4
<b>Average</b>	<b>7</b>	<b>196.4</b>	<b>-38.3</b>	<b>14.5</b>	<b>16.4</b>	<b>192.4</b>	<b>-14.4</b>	<b>5.5</b>	<b>28.3</b>

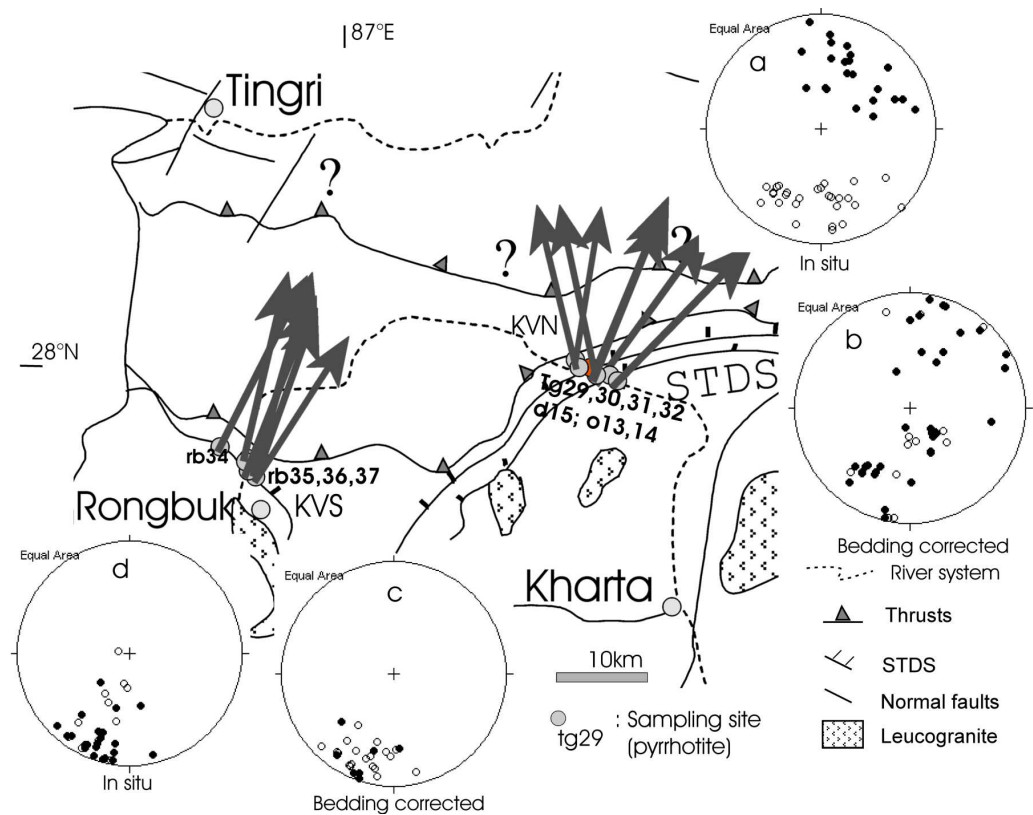


**Fig. 11:** Relevant structures from the sector (B), and  $ChRM^{DVR}$  directions of individual specimens (a, b, c and d) from Ordovician and Carboniferous meta-sediments at Kharta valley. Full and open circles indicate lower- and upper-hemisphere projections, respectively. Arrows indicate observed declinations versus north (all in situ).

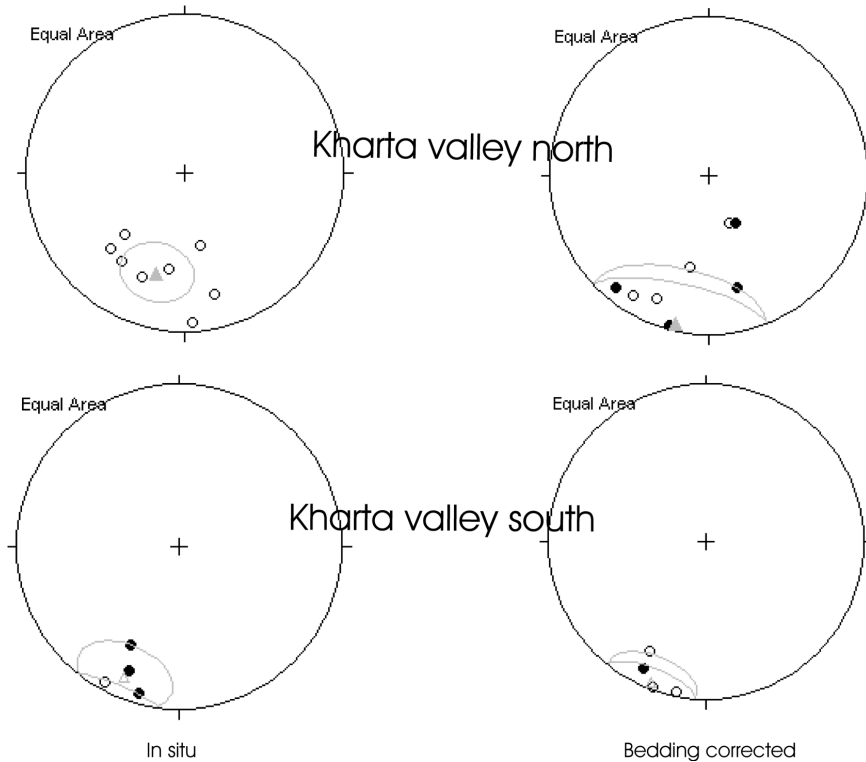


**Fig. 12:**  $ChRM^{DVF}$  overall mean direction (triangle) with  $\alpha_{95}$  confidence circle for Ordovician and Carboniferous meta-sediments at Kharta valley. Dots/triangles and open-circles/triangles indicate lower- and upper hemi-sphere projections, respectively. From data evaluation (s. also Tab. 2) syntectonic remanence is most probable at KVS, whereas, a composite of syn- and postfolding remanence can be proposed for KVN.

#### High temperature component magnetite ( $ChRM^{mag}$ )

In contrast to Ordovician limestone and Devonian/Carboniferous slates Triassic meta-carbonates and slates characterized by a very low grade of metamorphism show a dominant component with low to medium coercivity and unblocking temperatures at 370-520°C which is likely corresponding to magnetite ( $ChRM^{mag}$ ). Occasionally, a 2<sup>nd</sup> and 3<sup>rd</sup> component is also observed residing in low coercive magnetite, pyrrhotite and hematite. The coexistence of these minerals is characterized by partial overlapping during demagnetization for both thermal and AF treatment (Fig. 13). VRM is carried by goethite and low coercivity magnetite.

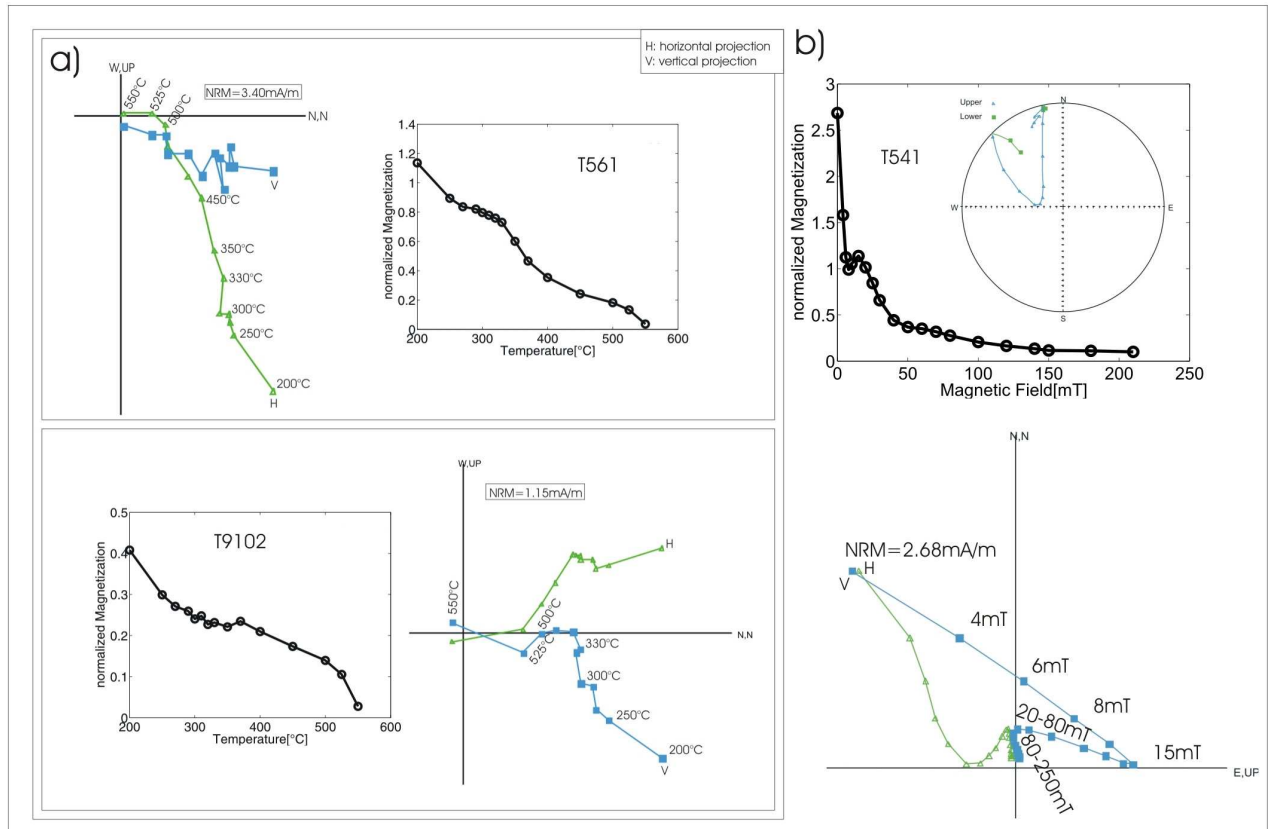


**Fig. 13:** Examples of Zijderveld diagrams and intensity-temperature/applied field curves showing ChRM components behavior during thermal (a) and AF demagnetization (b).

As mentioned above and in contrast to Ordovician meta-carbonates at Nyalam section Triassic series are characterized by a dominant low to medium coercivity component in IRM acquisition curves (Fig.14). Demagnetization is mostly reached at 80mT. Residuals (plateau) reside in hematite (clear indication in  $SIRM^T$  curves) and possibly pyrrhotite -additionally occurring-. Continuation with ThD treatment after AF cleaning confirmed in rare cases the presence of pyrrhotite. In major cases, the residuals are a hint for the presence of hematite -partly in trace amount- as it is clearly evidenced through the application of  $SIRM^T$ . Often, during ThD treatment, the onset of a VRM at higher temperature steps hinders the identification of this component.

Results of data evaluation (PCA and vector statistics) for 4 sites yielding significant findings with regard to  $ChRM^{mag}$  are listed below (Tab. 3).

An overall mean direction (site t5 excluded) of  $D=332.6^\circ/I=-12.2^\circ$  ( $\alpha_{95}=11.8^\circ$ ,  $k=165.7$ ) is obtained for in situ, and  $D=315.5^\circ/I=-53.7^\circ$  ( $\alpha_{95}=16.2^\circ$ ,  $k=88.5$ ) for bedding corrected. Normal polarity is dominant.

The sampled Triassic series correspond to the Mukut Formation in the western and central Himalaya. The geological age of this formation is about 250-220 Ma (Crouzet et al. 2003). The bedding corrected overall mean direction from Nyalam is close to the expected direction for a primary direction ( $D\sim 305^\circ/I\sim -55-60^\circ$ ) calculated from the APWP of India (Crouzet et al. 2003). These results are similar to those ones obtained from adjacent area in the Tethyan Himalaya (Thakkhola:  $D=323^\circ$  to  $329^\circ/I=-43^\circ$  to  $-48^\circ$ , Klootwijk and Bingham 1980; Manang:  $D=334^\circ/I=-54^\circ$ , Appel et al. 1991). They would point to a clockwise rotation versus India of  $\sim 25-30^\circ$ . However, data show a better grouping in situ ( $k_g \cong 2 \cdot k_s$ ) which is in contradiction with a primary origin, even indeterminate partial untilting and DC fold test does not support a primary origin of  $ChRM^{mag}$ .

Generally, Upper-Permian to Triassic meta-series in Kharta valley shows a demagnetization behavior similar to that observed by the Triassic samples discussed above. Magnetic mineralogy is also similar with a, partly, strong contribution of magnetite, also some pyrrhotite and hematite (Fig.15). This could be attributed to a uniform degree of metamorphism. Thermo-magnetic runs ( $SIRM^{RT}$ ) as it is indicated in the example of Fig. 15d reflect the complexity (partial overlapping of multi-components) of the magneto-mineralogy as described above for the Triassic meta-series. Furthermore, the detection of various Fe-Ti phases would imply the presence of titanomagnetite and hematite as carriers of remanence.

Normal polarity is dominant for all acquired  $ChRM^{mag}$  directions. An overall bedding corrected mean direction (site rb38 excluded, s. Tab. 3) of  $D=340.4^\circ/I^\circ=-55.3^\circ$  ( $\alpha_{95}=13.7^\circ$ ,  $k=32.2$ ) is obtained for 5 sites. A positive fold test (data pass the fold test after Enkin (2003) at 95% confidence level) supports a pre-folding age of remanence acquisition. The acquired overall mean directions, after bedding correction, is similar to that obtained for the Triassic sites from the Nyalam section. An apparent clockwise rotation ( $\sim 35^\circ$ ) versus India is indicated.

**Tab. 3:**  $ChRM^{mag}$  directions mean of individual Sites, and overall mean direction of all sites at Nyalam section and Kharta valley

Site	N	Dg (°)	Ig (°)	kg	$\alpha_{95g}$ (°)	Ds (°)	Is (°)	ks	$\alpha_{95g}$ (°)
<b>Nyalam section</b>									
t5	4	353.1	64.1	20.1	21.1	2.1	-19.8	20.1	21.1
t6	4	341.6	-11.7	53.3	12.7	329.5	-53.5	53.3	12.7
t7	5	327.4	-13.3	127.5	6.8	300.4	-59.5	127.5	6.8
t9	5	328.8	-11.5	48.5	11.1	314.6	-46.5	49.3	11.1
<b>Average1</b>	<b>4</b>	<b>335.2</b>	<b>4.6</b>	<b>4.5</b>	<b>48.7</b>	<b>331.5</b>	<b>-47.6</b>	<b>10</b>	<b>30.6</b>
<b>Average2</b>	<b>3</b>	<b>332.6</b>	<b>-12.2</b>	<b>110.5</b>	<b>11.8</b>	<b>315.5</b>	<b>-53.7</b>	<b>59</b>	<b>16.2</b>
<b>Kharta valley</b>									
rb38	3	336.1	47.8	29.3	23.2	272.1	56.8	30.3	22.8
rb39	4	330.6	-27.6	47.3	13.5	310.8	-60.9	47.3	13.5
rb40	8	285.1	-61.7	47.7	8.1	330.9	-52.5	28.3	10.6
p18	4	4.2	-4.4	49.4	13.2	355.5	-42.2	53.3	12.7
p19	9	0.4	-24.6	18.2	12.4	332.1	-54.7	18.2	12.4
p20	6	305.4	-75.5	92.5	7.1	7.2	-58.8	95.2	6.9
<b>Average1</b>	<b>6</b>	<b>340.1</b>	<b>-28.6</b>	<b>3</b>	<b>47.3</b>	<b>330.7</b>	<b>-46.4</b>	<b>3.1</b>	<b>45.8</b>
<b>Average2</b>	<b>5</b>	<b>340.9</b>	<b>-42.1</b>	<b>4.9</b>	<b>38.3</b>	<b>340.4</b>	<b>-55.3</b>	<b>32.1</b>	<b>13.7</b>

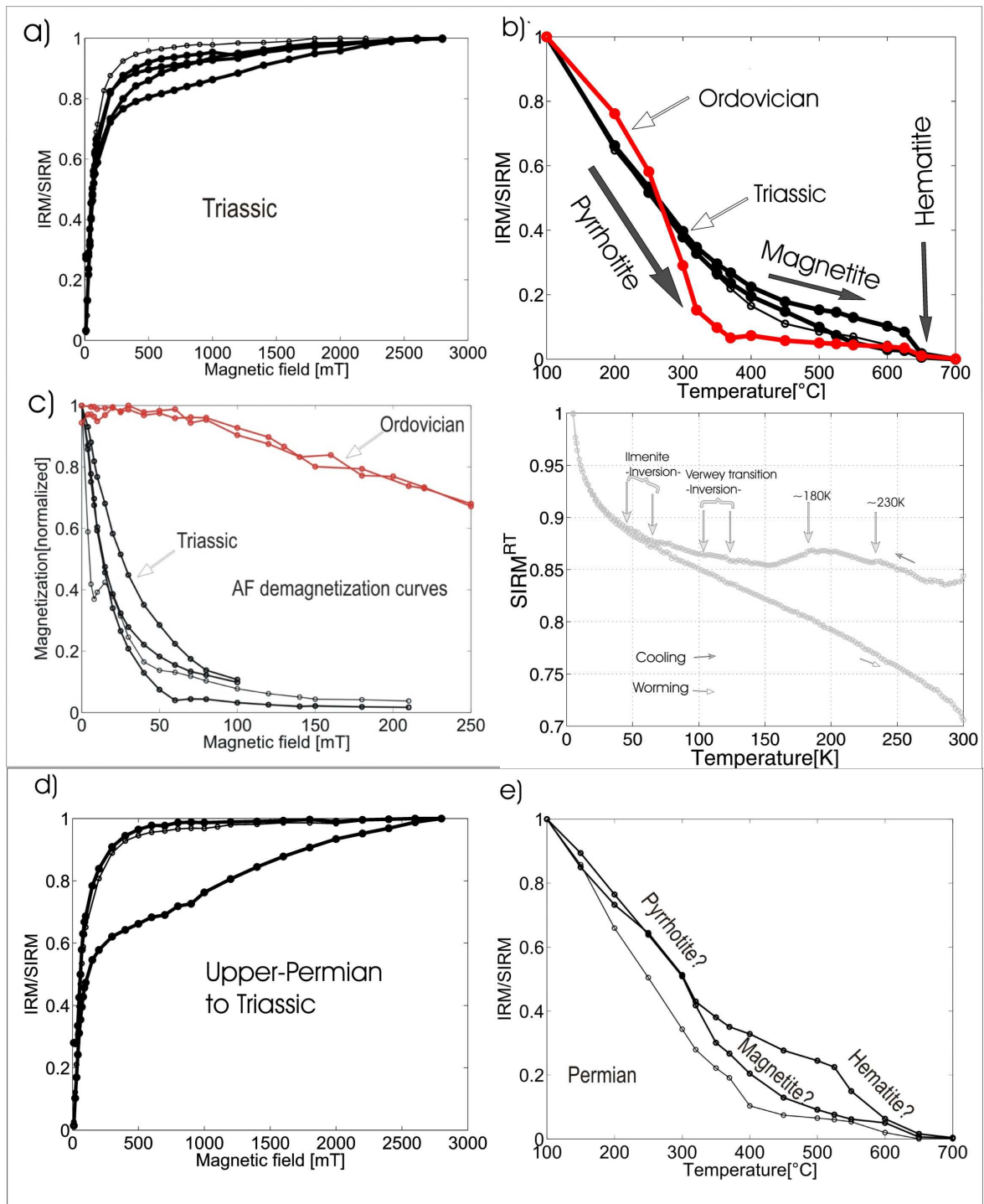


**Fig. 15:** curves of IRM acquisition (a, e) and  $SIRM^T$  (b, f) for Triassic and Upper-Permian to Triassic specimens, respectively. Variation in saturation fields (e) indicates the presence of a low to medium component (magnetite) associated with higher coercive pyrrhotite and hematite components (f). (c) Coercivity of Triassic specimens compared to Ordovician samples. (e) Field cooling (300 to 5 K) and warming (5 to 300 K) of a normalized 5 T room temperature SIRM ( $SIRM^{RT}$ ). The transitions between 250 and 180 K are interpreted to be corresponding to existing various Fe-Ti phases. The example show a characteristic curve for Ti-rich oxide phases, revealing a reversal behavior in cooling and warming between 110 K and 5 K. Undulations in the cooling curves, detected on cooling above 210 K might indicate the presence of titano-hematite phases

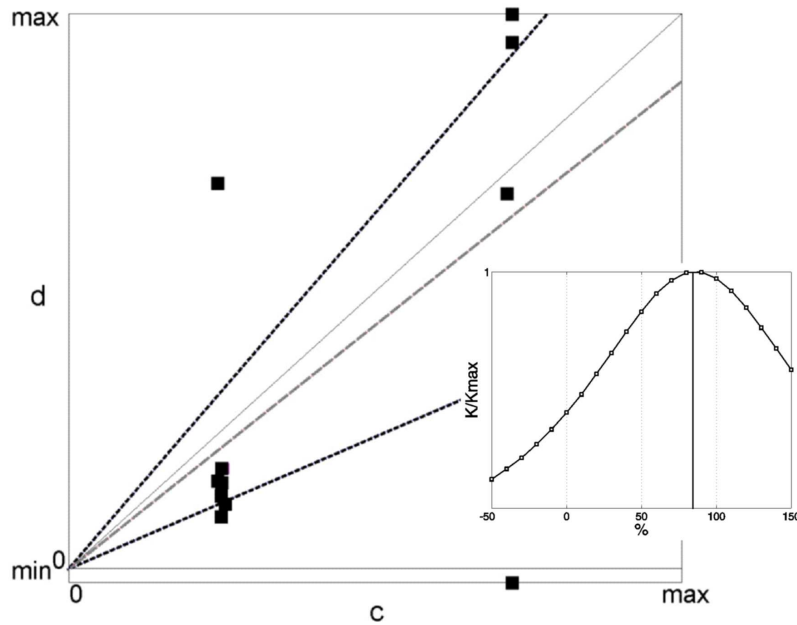


**Fig. 16:** Positive Direction-Correction (DC) test (after Enkin, 2003) performed for Upper-Permian to Triassic sampling sites in Kharta valley, and partial untilting (~86%) support a primary origin of  $ChRM^{mag}$

From one further positive fold test obtained for the  $ChRM^{mag}$  directions in 2 sites sampled from both limbs of a “late” fold (second order folding) in Kharta valley it can be concluded that the  $ChRM^{mag}$  is at least predating the  $ChRM^{DVF}$ .

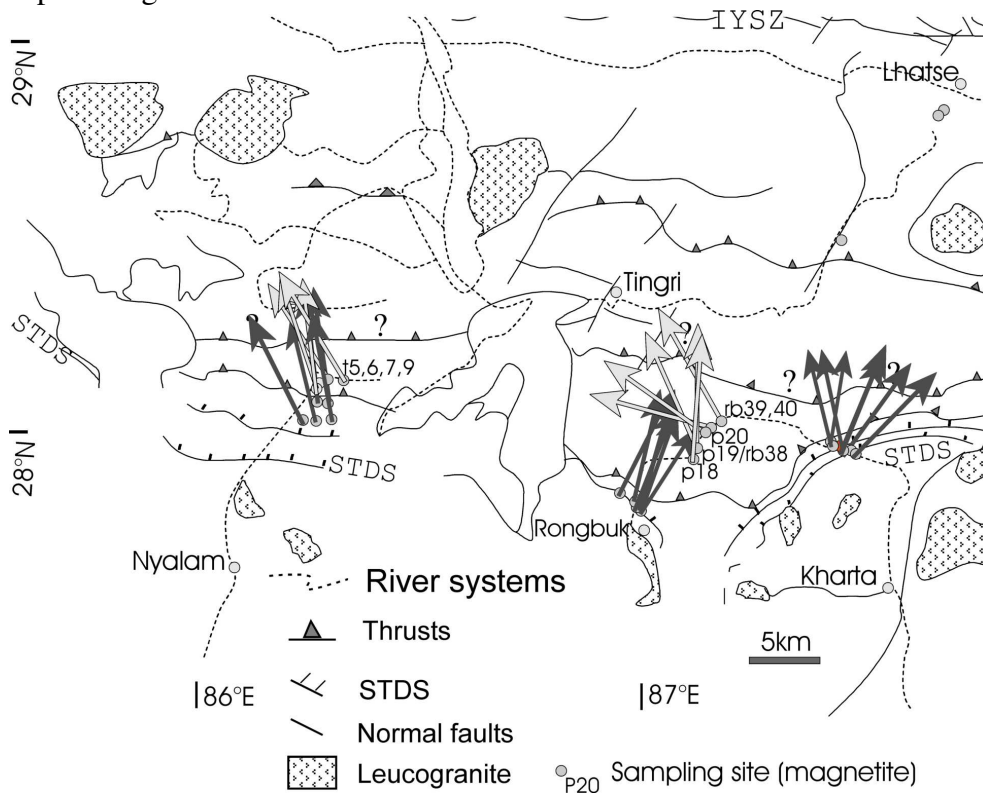


**Fig. 17:** Sense and magnitude of displacement –in situ– of  $ChRM^{mag}$  directions determined for Nyalam section and Kharta valley (light grey arrows). For comparison  $ChRM^{DVF}$  directions are indicated by dark arrows (all in situ).

### 3. 2. 2. Discussion

Does palaeomagnetic data record the exhumation history of the STDS?

Similar to Nyalam, unexpected inclinations are also partly observed in Kharta valley south (s. Tab. 2). Normal and reverse polarities occur, as well as occasionally antipodes within a sample. Reverse polarity observed in two sites (one with very shallow negative inclination, and one with steep negative inclination) favor the third assumption discussed for the Nyalam section. It should however be mentioned that remanence might change the hemisphere through tilting. This fact should not be ignored in the course of extensional faulting, and associated thrusting by folding and ramping.

The proximity of the sampling sites to the STDS should be mentioned. The latter lay within a normal fault (STDS)/thrust system dipping to the north. Keeping in mind that shallow as well as steep inclinations occur, a flat-ramp structure (extensional structure) can be proposed.

Similar to KVS, the sampled sites at KVN are situated within a condensed high strain zone. Laterally, a thrust to the top and a ductile shear zone (STDS) to the bottom delimitate the sites.

Normal (in 3 sites) and reverse polarity (in 4 sites) is present. The closest sites to the shear zone show normal polarity (probably documenting the last cooling event); the distal ones have a reverse polarity. A trend of increasing slight clockwise rotation is observed toward the shear zone.

It can be assumed that a thermo-remanence was acquired which is related to shearing and exhumation of the STDS (heating through shear, in situ melting and overprint). The record of normal and reverse polarity might document a longer protracted cooling history of the STDS covering at least one reversal of the earth magnetic field.

The measured inclinations in KVN (s. Tab. 2) match with the expected one for the area during Miocene (~24 Ma), deduced from the APWP (Acton, 1999). Remanence directions grouping better in situ as well as a negative DC fold test obtained for the area support its secondary character, postdating the Eo-Himalayan main folding.

The origin and nature of  $ChRM^{mag}$  obtained from the Triassic Mukut formation at Nyalam remain disputable. Measured bedding corrected directions are similar to those observed in the adjacent areas, and ascribed to a primary remanence; however, neither the performed partial untilting (absence of a maximum between 0 and 150% untilting), nor the indeterminate DC fold test would support its primary origin. Partial imprint is therefore not improbable. The positive DC tilt test and the 86% optimum partial-untitling obtained for Kharta valley would support a primary origin of  $ChRM^{mag}$ . However, a composite of a syntectonic and primary remanence is not excluded. Therefore, the suitability of the data for paleo-latitude calculations remains questionable.

#### Rotation and tilting

The directional arrangement of the remanences in KVS is consistently north-east as it is shown in Fig. 13. Following the oroclinal bending model no rotation to a slight counter-clockwise rotation would be expected for this area. Therefore, an apparent slight clockwise rotation might have had happened. In KVN a north-west arrangement occur, as well, toward the north dipping thrust, but the north-east direction is dominant, and an increase in the apparent clockwise rotation is evident toward the ductile shear zone. Whether a right lateral shear has occurred is not completely clear, due to the small number of sites. In satellite images from this area (s. appendix), this zone (ductile STDS) is demarcated by a sharp wedge. Further branches striking parallel to the wedge were also detected by DEM analysis. Right lateral shear within the vicinity of this zone of high strain might therefore not completely be excluded. More conspicuous is the circular distribution of the

remanence directions in a systematic mode similar to that evidenced at the Nyalam section. In this case a similar scenario as at Nyalam can be proposed for Kharta valley, but this time with an apparent slight clockwise rotation. Alternatively, the progressive change in the remanence arrangement from north-west in Nyalam to north-east at Kharta valley might be considered as a consequence of tilting adjustment effect due to a existing large lateral ramp, or duplex structures and antiforms. Probable would also be a vertical axis rotation coeval with tilting or postdating it.

### 3. 1. 3. Dinggye extensional zone

The surveyed area lays within the Xainza-Dinggye rift. This north-south trending structure extends from the central Qiangtang block in the north into the HHC in the south across the Lhasa block, the Yarlung Zangbo suture, the Tethyan Himalaya, and the STDS (Zhang and Ding, 2003). The rift is a brittle fault system defined by narrow half graben with main faults on their western boundaries; dominating normal faults are dipping to north-west in the Tethyan Himalaya, and south-east in the HHC. This effect is interpreted within this study as a response to doming in the crust.

The sampling area covers the southern Xainza-Dinggye rift in the Tethyan Himalaya of southern Tibet. It consists of a sequence of Paleozoic-Cenozoic limestone, mudstone and sandstone; the latter underwent low-grade metamorphism to build slate and phyllites. The High Himalaya is separated from the Tethyan Himalaya by the STDS. The half graben system cuts off the High- and Tethyan Himalaya and the STDS. It is characterized by a normal fault and a dome cored by leucogranites in the Tethyan Himalaya (Mabja dome). In the HHC it is represented by a north-south striking quasi- detachment fault with a right lateral slip component (Zhang, 2006).

#### 3. 1. 3. 1. Results

Regarding the unexpected inclinations first observations reveal similarities in palaeomagnetic results as in Nyalam and Kharta valley south. It should however be mentioned that the scatter in declinations and inclinations is much more significant in the Dinggye area, and a systematic dispersion on a small circle is absent.

ThD, as it is shown in Fig. 18b, demonstrate the dominance of a low temperature component, again identified as the ferro(i)magnetic phase pyrrhotite. Thermomagnetic measurements ( $SIRM^{RT}$ ) (s. Fig. 11b) also identify pyrrhotite, characterized by a clear transition at ~34 K.

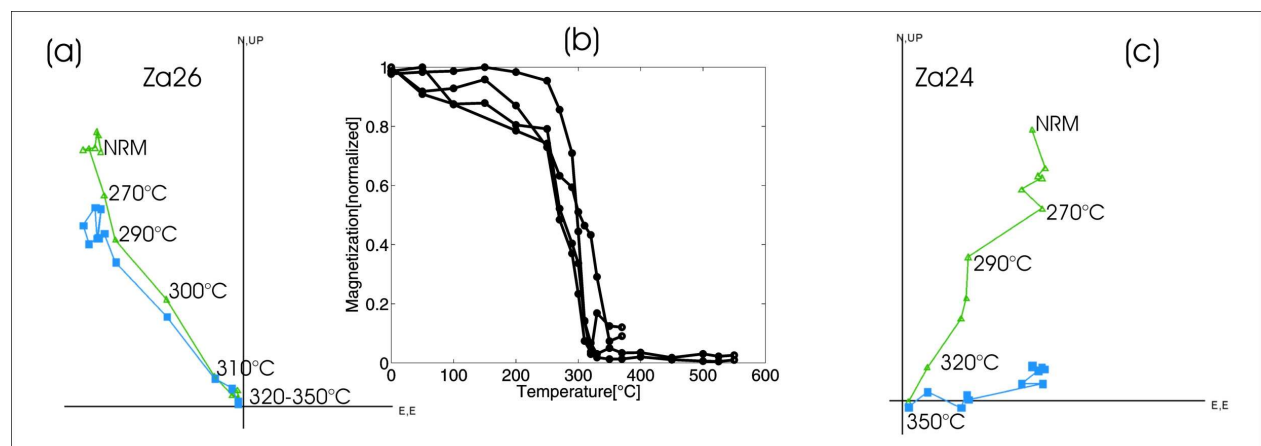


**Fig. 18:** (a) and (c) are examples of in situ observed north-west (dominant) and north-east (less dominant) arrangement of the  $ChRM^{pyr}$  directions in the Dinggye area. (b), clearly demonstrate the dominance of the ferro(i)magnetic phase pyrrhotite, which is thought to have mainly acquired a TRM.

Data evaluation (PCA analysis and Fisher statistics) of representative sites reveal stable, and partly well grouping  $ChRM^{pyr}$  component directions. With the exception of one site (Za8) showing normal polarity, and one site (Za13) indicating reverse polarity, the majority of the sites reveal unexpected inclinations like in Nyalam and Kharta valley south. Zijderveld diagrams in Fig. 18(a) and (c) show examples of the sense of measured remanence directions. A predominating north-west arrangement occurs, but a north-east trend is also observed, occasionally within a site. For final evaluation, data of sites with a non Gaussian distribution ( $k < 10$ ) are excluded from the statistics listed below:

**Tab. 4:**  $ChRM^{pyr}$  directions mean of individual Sites, and overall mean direction (average) of all significant sites in the Dinggye area with a consistent, but “unexpected” ( site za8 and za13 excluded) inclination.

Site	N	Dg (°)	Ig (°)	kg	$\alpha_{95g}$ (°)	Ds (°)	Is (°)	ks	$\alpha_{95s}$ (°)
za10	6	151.4	30	29.5	13.8	non	non	non	non
za11	6	344.3	-8.4	39.7	11.8	non	non	non	non
za18	5	335.7	-19.9	15.1	23.1	335.1	-28.8	23.4	12.5
za26	8	352.7	-18.8	23.3	12.6	342.8	-32.5	15.1	23.1
za27	7	353.1	-32.4	164	5.1	328.5	-44.2	165	5.1
<b>Average</b>	<b>5</b>	<b>343.4</b>	<b>-22.1</b>	<b>48</b>	<b>12.5</b>	<b>335.8</b>	<b>-35.3</b>	<b>101.3</b>	<b>15.1</b>
za13	5	178.2	-48.1	57.3	11.4	186.5	-14.4	57.1	11.4
za8	6	16.6	17.2	24.5	11.2	19.4	6.7	25.1	11.1

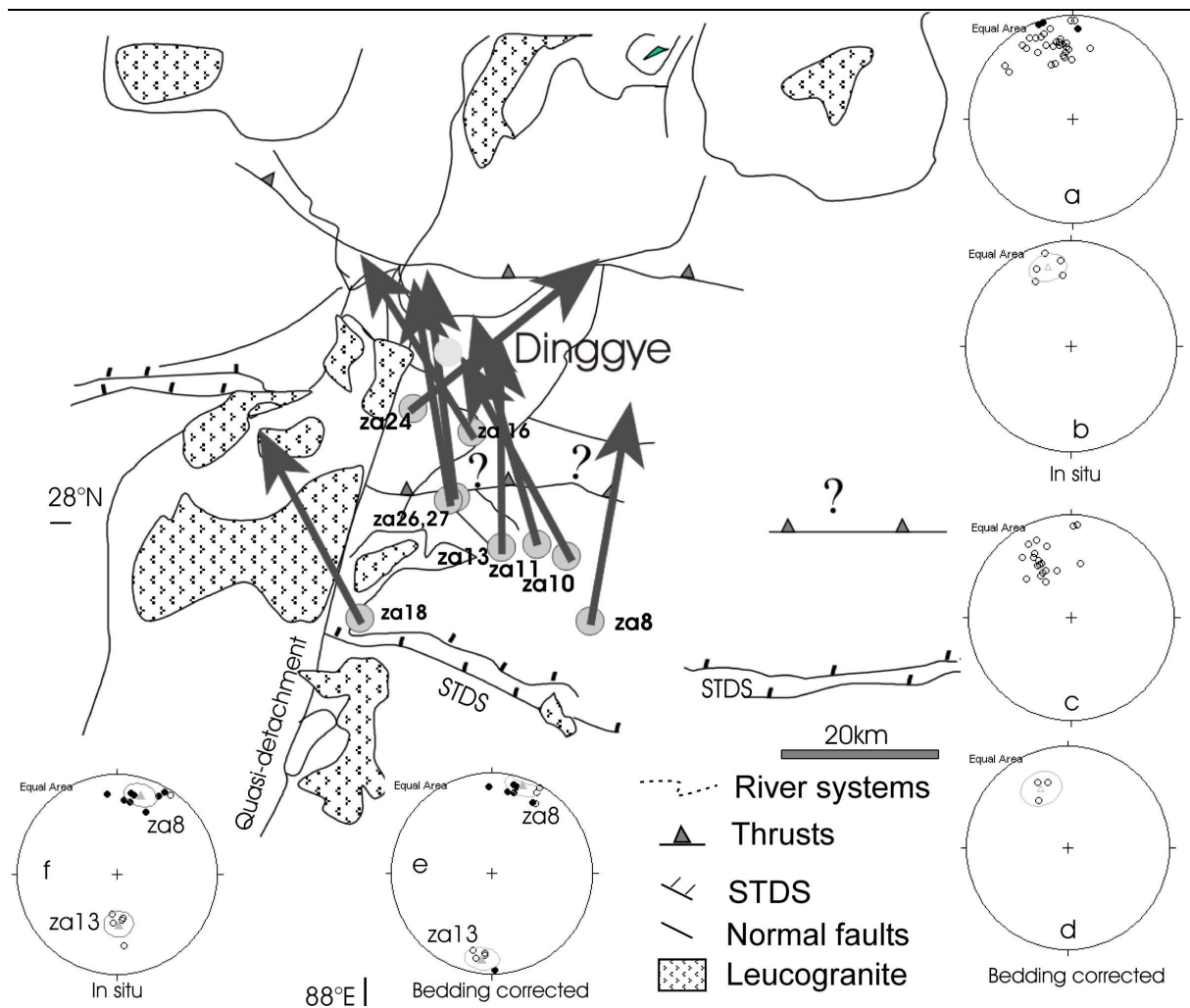


**Fig. 19:**  $ChRM^{pyr}$  directions of individual specimens (a, c) in the Dinggye area (s. sector (C) in Fig.4), and overall mean direction (triangle) (b, d) with  $\alpha_{95}$  confidence circle of Ordovician and Carboniferous/Devonian meta-sediments at Kharta valley. Full and open circles indicate lower- and upper hemisphere projections, respectively. (e) and (f) represent the individual sites za8 (with normal polarity) and za13 (with reverse polarity), respectively. Arrows indicate magnitude and sense of displacement since remanence acquisition in pyrrhotite.

### **3. 1. 3. 2. Discussion**

Regardless the absence of a systematic distribution of measured remanence directions on a small circle, unexpected inclinations and overall mean directions calculated for sampling sites in the Dinggye area reveal similarities to those obtained for the Nyalam area, and therefore, give arise to the different cases, and the proposed explanations discussed for Nyalam section.

### 3. 1. 4. Yadong/Pari area

The Yadong-Gulu Graben system trend approximately N30°E and cross cut from south to north the HHC, the IYSZ, the Lhasa block, and the Nyainqantanglha range (Armijo et al., 1986).

The 7 sampled sites taken in this area are from the south extremity of the rift. Ratschbacher et al. (1994) report sinistral strike-slip within this domain, and propose an extension-fracture model for the formation of the right stepping en-echelon normal faults of the Yadong-Gulu rift indicating sinistral strike slip in addition to rift extension.

Ductile high strain shear zones have been identified in southern and northern Yadong-Gulu rift (Burchfield et al., 1991; Harrison et al., 1995). Zoning and shear sense of these high strain zones might be linked to extension and thus opening of the rift. Cogan et al. (1998) suggest that the opening of the rift is being accommodated at depth by flow in the middle crust, perhaps a consequence of the middle crust being partially molten as suggested by INDEPTH data (Nelson et al., 1996).

#### 3. 1. 4. 1. Results

Pyrrhotite with variable contribution has been found in all sampled 7 sites. However stable  $ChRM^{pyr}$  could be isolated only in 3 sites (Yd2, Yd3 and Yd6); the remaining sites (Yd1, Yd4, Yd5 and Yd7) show a large scatter in remanence directions increasing toward the STDS, regarded in this area as a ductile shear zone. IRM and  $SIRM^T$  (Fig. 19b) reveal the dominance of the low temperature component pyrrhotite, and occasionally, the existence of trace amounts of magnetite and hematite. Antipodes, together with single components, are ascertained by ThD as it is shown in Fig. 19a.

Reflected light microscopy investigations imply different degrees of metamorphism, and therefore different mechanisms on the formation of pyrrhotite, and on the subsequent remanence acquisition in the latter. Further details are elucidated in Fig. 21.

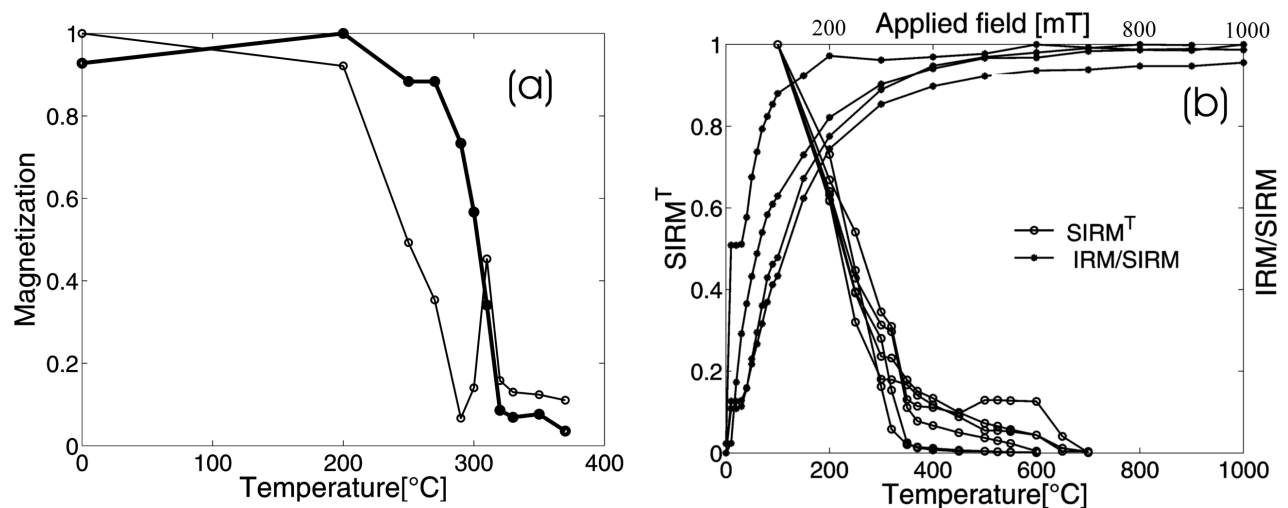


**Fig. 20:** Examples of single and antipodal pyrrhotite remanence components demonstrated by ThD (a), and confirmation of the dominance of pyrrhotite, accompanied by trace amounts of magnetite and hematite, evidenced through application of IRM/SIRM and subsequent  $SIRM^T$ .

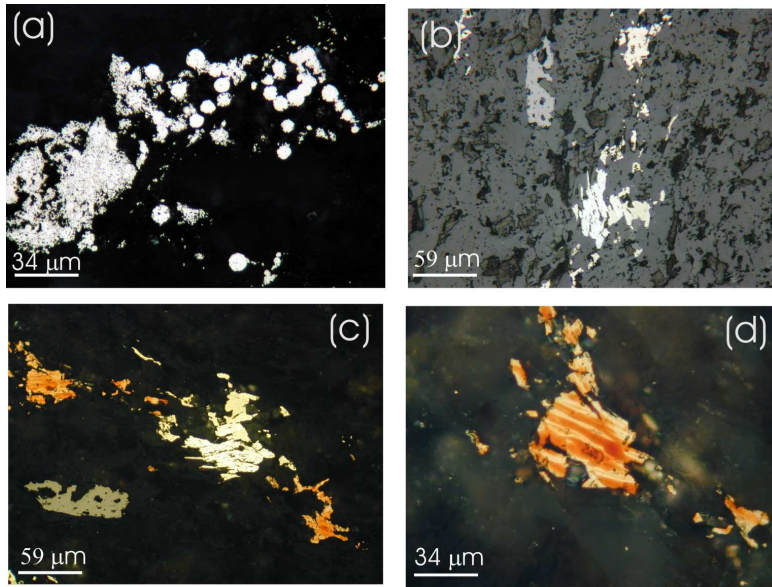


**Fig. 21:** Reflected light microscopy on polished sections from selected samples bearing pyrrhotite: degraded pyrite showing triple junctions, and pyrite fromboids in one metacarbonate (a) indicates retrograde condition, and a probable formation of pyrrhotite while the break-down of pyrite. (b) Intergrowth of monoclinic and hexagonal pyrrhotite in a biotite-schist evidenced by the application of the Bitter-technique (c). (d) Bitter pattern indicate branching; the “180°- case” is characteristic for monoclinic pyrrhotite (enlarged (c)). The grain size is very variable ranging from SD/PSD (dissimilated in the matrix) to MD.

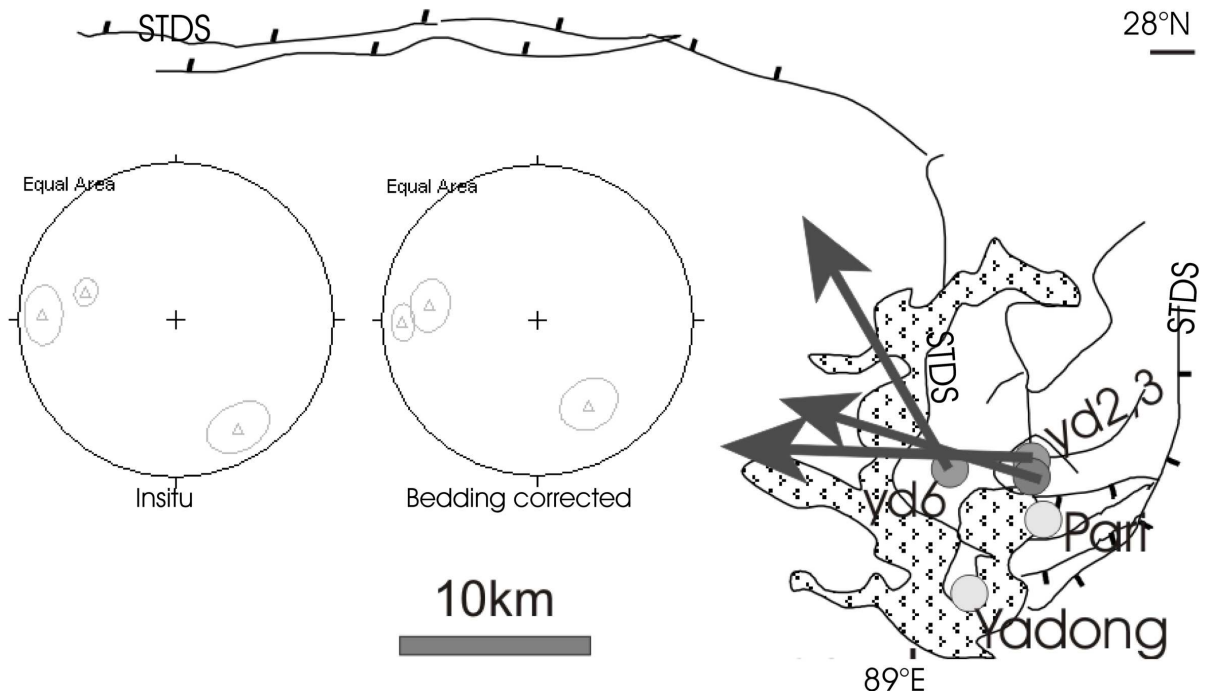


**Fig. 22:** Simplified structure of the sampling sector (D) in the Yadong/Pari area. The Arrows indicate sense and magnitude of displacement of measured  $ChRM^{DVI}$  directions. Stereo plots show the calculated site means (open triangle, upper hemisphere).

**Tab. 5:**  $ChRM^{DVI}$  directions mean of individual Sites in the Yadong/Pagri area. Normal polarity is proposed to have acquired in yd2 and yd3 while a reverse polarity has been recorded by yd6.

Site	N	Dg (°)	Ig (°)	kg	$\alpha_{95g}$ (°)	Ds (°)	Is (°)	ks	$\alpha_{95s}$ (°)
yd2	18	287.1	-39.5	29.3	6.5	271.6	-10.2	28.9	6.5
yd3	4	271.9	-15.6	55.3	12.5	277.8	-29.1	58.7	12.1
yd6	5	149.8	-25.6	38.3	12.5	148.2	-40.1	30.2	14.1

### 3. 1. 4. 2. Discussion

From field and microscopic observations it can be concluded that Yd2, Yd3 and Yd6 have suffered low-grade metamorphism conditions, probably sub-green- to green schist facies. Degraded Pyrite fromboids in Yd6 (Fig. 21a) identified through reflected light microscopy would support the formation of pyrrhotite while break down of pyrite. In contrast, the coexistence and intergrowth of monocline and hexagonal pyrrhotite identified by Bitter technique is already an indicator for higher temperature ranges (epizone). Hexagonal pyrrhotite is usually expected by higher degree of metamorphism. Nearly symmetric antipodal components dominate in Yd2 and Yd3, the directional arrangement of the components is east-west, and is thus nearly parallel to the main strike. For instance, it can be assumed that a tilting around an east-west trending fold axis has occur, probably accompanied with a slight clockwise rotation. The observed slight anti-clockwise rotation in yd6 would neither be in disagreement with the oroclinal bending model (Klootwijk, 1986), nor with the strike-slip related extension predicted by Ratschbacher et al. (1994).

#### Tilting and rotation

In analogy to Nyalam section- and Kharta valley results, the obvious distribution of remanence direction on small circles in the Yadong/Pari district, and the encountered anti-clockwise vertical axis rotation emphasize a systematic regional trend over the whole length of the examined east-west traverse, between 86- and 89°E. Further aspects are discussed in chapter 5. 1. 6.

### 3. 1. 5. Area between Tingri and Lhatse

The sampling sites in sector (E), indicated in Fig. 4, were taken in the vicinity of the Lagoi Kangri dome delimited to the south by the Gyrong Kangmar Thrust (GKT) and to the north by the IYSZ. With the exception of one meta-carbonate site the remaining 4 sites are exclusively slates from the widespread Upper Triassic flysch in this area. This formation is supposed to be similar to the Lamayuru unit in Zaskar.

#### 3. 1. 5. 1. Results

AF cleaning reveals a noisy character, and a better demagnetization behavior was observed during thermal treatment. The noisy character is probably a response to the presence of various Fe-Ti oxide phases, mainly hematite characterized by its Morin transition, but also some magnetite, observed during thermomagnetic runs ( $SIRM^{RT}$ ). A clear transition at ~30 to ~34 K is not observed in this example; nevertheless, the overlap of the cooling and warming curves around 30 K is interpreted to be indicative for the presence of pyrrhotite.

In 4 sites a dominant  $ChRM^{pyr}$  component could be separated (Fig. 26), partly showing antiparallel directions within the same specimen (Fig. 23b). The presence of pyrrhotite as a carrier of the characteristic magnetic remanence is additionally demonstrated by  $SIRM^T$  (Fig. 24b) with a relatively low coercivity (Fig. 24a). Pyrrhotite has been additionally identified through reflected light microscopy by its high degree of anisotropy, distinguishing it from the pyrite coexisting with it. Goethite is usually surrounding MD pyrrhotite. Graphite is observed in the meta-carbonate sample. An intergrowth of hexagonal and monocline pyrrhotite is ascertained through Bitter-technique. A two-phase branching is visible through the applied ferrofluid. Two phase, or an echelon-branching usually occurs in large crystals with strongly miss-oriented surfaces.

On the basis of PCA, well-grouping specimen directions are obtained for 3 sites with predominantly reverse polarity (Fig. 8). One site with normal polarity shows rather a much more scatter in the remanence directions, but still within the range ( $k = 11.8$ ), and was therefore included in the Fisherian vector statistics. The overall mean  $ChRM^{pyr}$  direction for these 4 sites is  $D=204.5^\circ/I=-41.3^\circ$  ( $\alpha_{95}=25.7^\circ$ ,  $k=18.3$ ). Statistical data for individual sites is listed in Tab. 6.

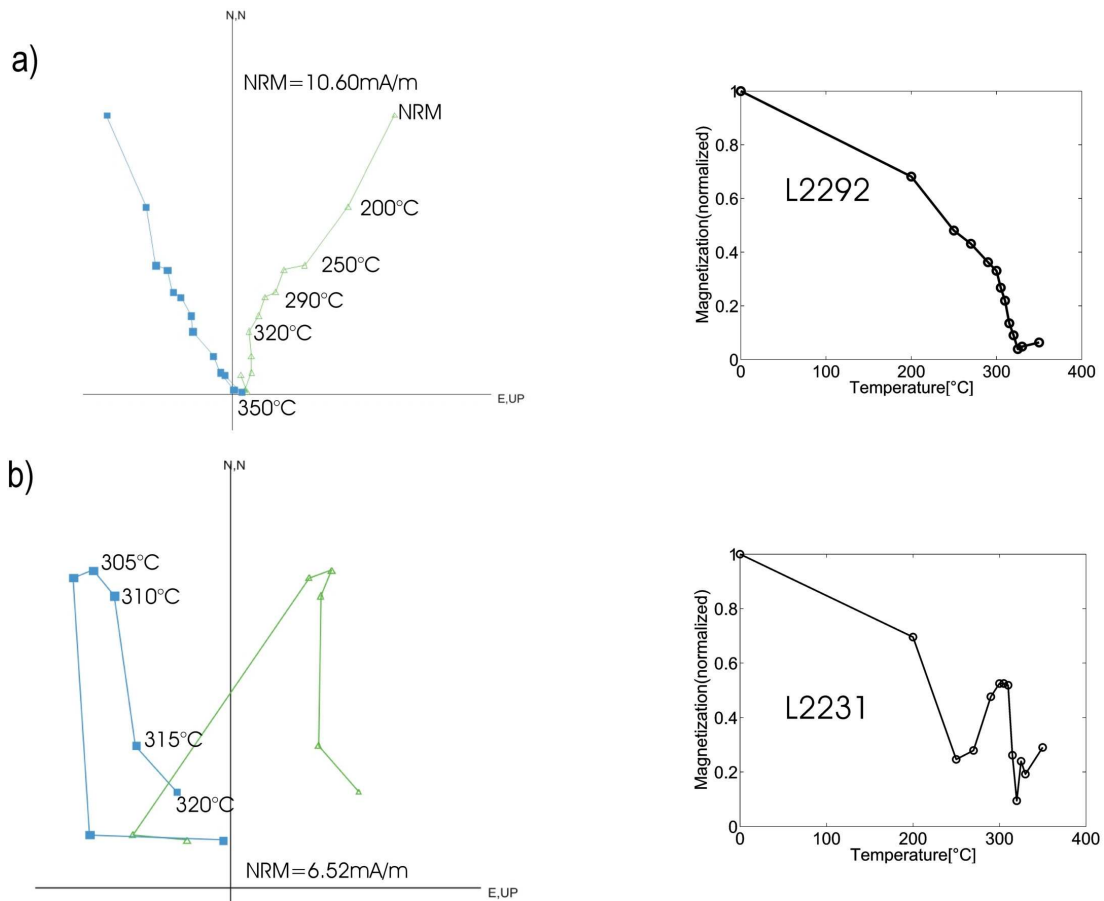


**Fig. 23:** Examples of Zijderveld diagrams and temperature-intensity curves for the Upper Triassic flysch between Tingri and Lhatse indicating single (a) and antiparallel (b) components.

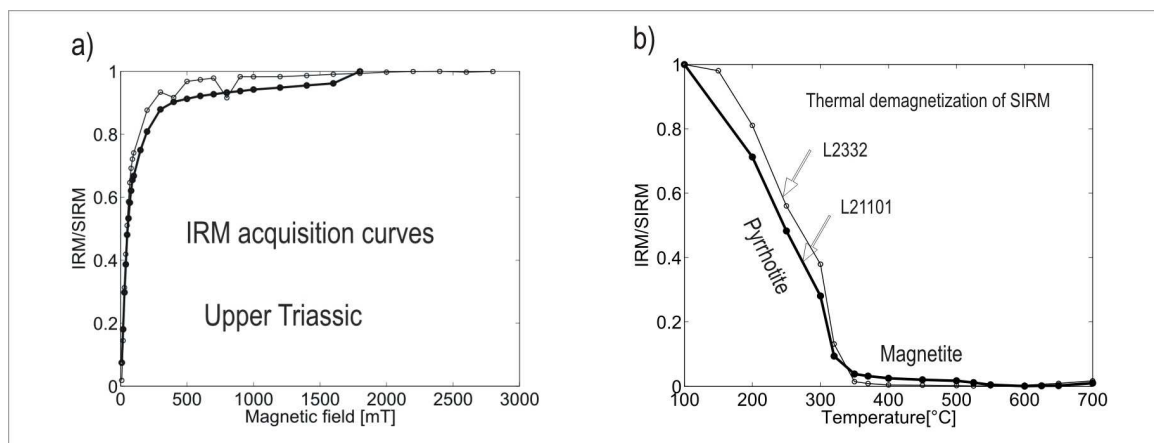


**Fig. 24:** IRM acquisition curves for specimens of the Upper Triassic flysch (a) and corresponding thermal demagnetization diagrams of SIRM (b)

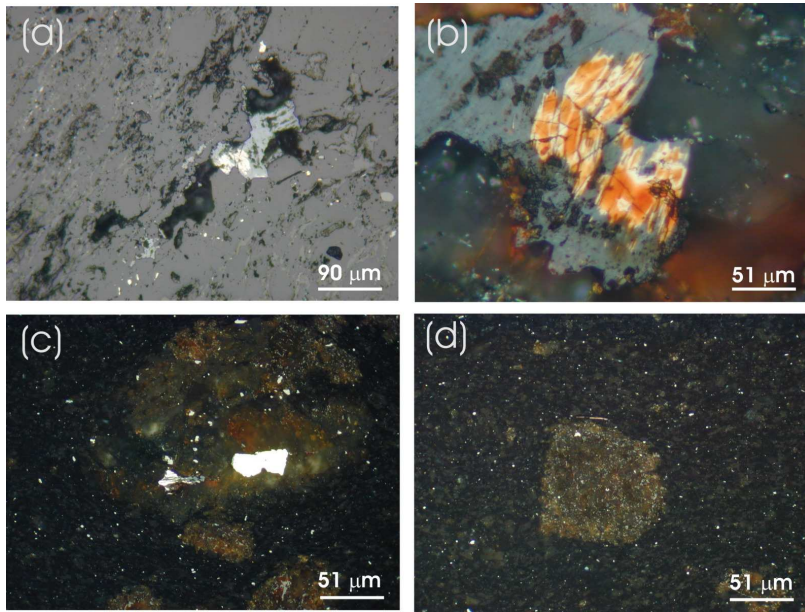


**Fig. 25:** Reflected light microscopy on selected polished sections reflecting the progressive increase of the degree of metamorphism in (E): (a): Pyrrhotite, identified by its high anisotropy, in a biotite rich slate (epizone). Goethite surrounding pyrrhotite, indicate oxidation at a later stage. (b): Bitter-pattern in enlarged (a), after the application of a ferro-colloid, and partly intergrowth of hexagonal and monoclinic pyrrhotite. En echelon pattern reveal a strongly miss-oriented surface of

pyrrhotite. (c): Coexistence of pyrite and pyrrhotite in an organic rich metacarbonate (sub-green schist). In the same section (d) shows the growth of graphite crystals in the vicinity of romboidric patches.

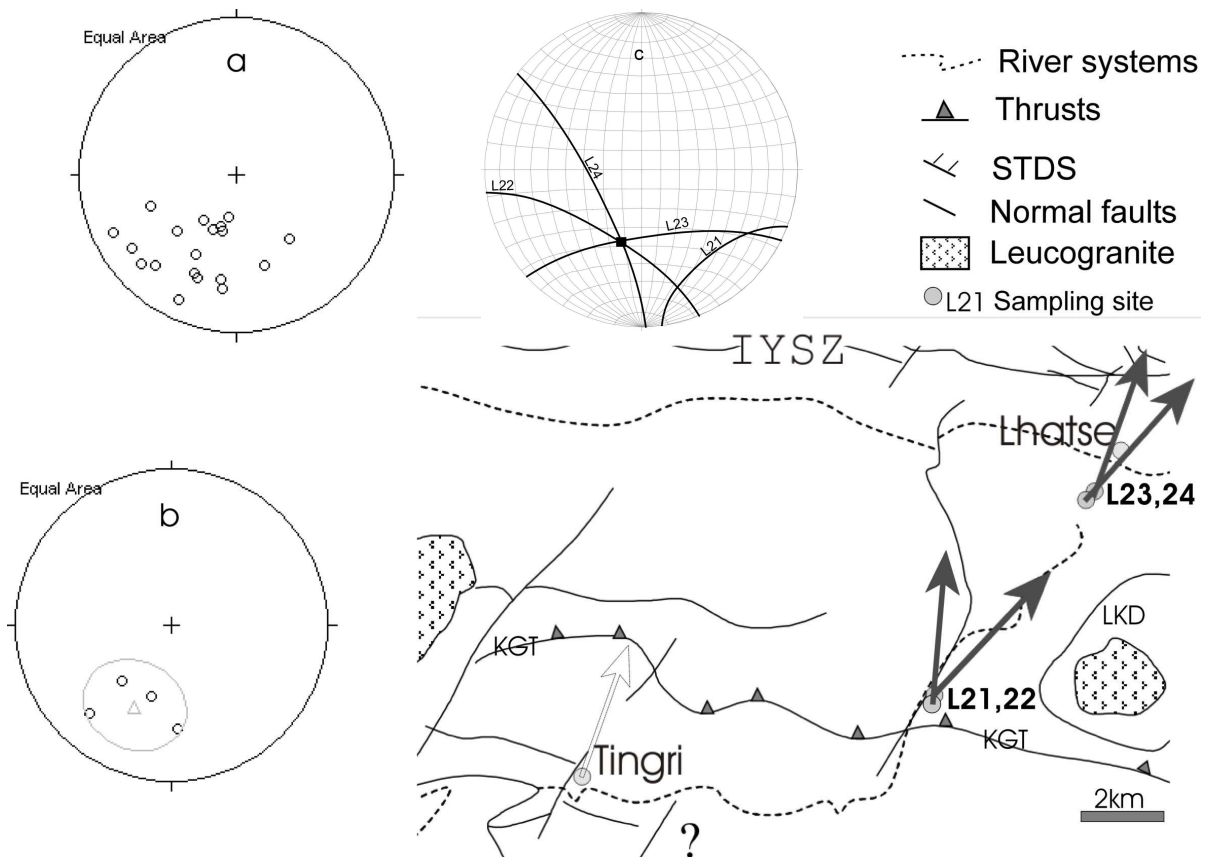


**Fig. 26:**  $ChRM^{DVR}$  directions (dark arrows) –in situ– of individual specimens (a) in sector (E) (Fig. 4), and overall mean direction (triangle) (b) with  $\alpha_{95}$  confidence circle. Full and open circles/triangles indicate lower- and upper hemisphere projections, respectively. (c) Common small circle intersection obvious for three sites. White arrow represents a secondary remanence direction –in situ– of Besse et al. (1985), obtained from 3 limestone sites.

**Tab. 6:**  $ChRM^{DVT}$  directions mean of individual Sites of sector (E) in the area between Tingri and Lhatse.

Site	N	Dg (°)	Ig (°)	kg	$\alpha_{95g}$ (°)	Ds (°)	Is (°)	ks	$\alpha_{95s}$ (°)
L21	4	357.2	33.6	11.8	32.7				
L22	5	223.2	-23.5	22.1	18.8				
L23	4	195.4	-50.8	30.6	19.6				
L24	6	221.9	-50.1	21.6	16.3				
<b>Average</b>	<b>4</b>	<b>204.5</b>	<b>-41.3</b>	<b>18.3</b>	<b>25.7</b>				

### 3. 1. 5. 2. Discussion

The presence of coarse grain-sized pyrrhotite ranging from PSD (disseminated in the matrix) to MD state support the relatively low coercivity observed during SIRM<sup>T</sup>. The observed low coercivity during IRM acquisition is also a hint for the existence of a composite pyrrhotite: An intergrowth of hexagonal and monocline pyrrhotite is ascertained through Bitter-technique. Domain wall motion, as well as multi-phase branching is visible after the application of a magnetite based nano-particles ferro-fluid on the polished surface of the sample section. Two phase, or an echelon- branching usually occurs in large crystals with strongly miss-oriented surfaces. This might indicate in the case of the analyzed sample that a second strong deformation phase, after the formation of pyrrhotite and the acquisition of its remanence has had happened which has deformed the pyrrhotite, and probably partly overprinted its first remanence (2<sup>nd</sup> partial re-magnetization). This would explain the large scatter in  $ChRM^{DVT}$  component in other sites, from this area, here, excluded from the statistics, and therefore not further discussed.

The presence of hexagonal pyrrhotite phase is indicative for a higher degree of metamorphism. Abundance of large pyrite crystals and MD pyrrhotite in the slates could be indicative for a formation mechanism of pyrrhotite within the vicinity of a sulfur fluid rich milieu (high sulfur fugacity) during the retrograde phase. Following the observations through reflected light microscopy, an increase in the degree of metamorphism is observed toward the suture: while the selected sample from site L21 rather shows sub-green schist conditions, the sample from site L23 indicates already epizone conditions. On the basis of the observations discussed above and the presence of anti-parallel components it can be assumed that pyrrhotite has acquired a thermoremanence. It is possible that the second deformation did not affect strongly the L21 site, and that  $ChRM^{DVT}$  in L23 (sample from sites close the IYSZ) has recorded it. The calculated inclination –in average- is similar to that expected for the area during the Miocene, and its age can be approximately compared to that of the last cooling event, which has been yet found within this study to be late Oligocene to Miocene (24-27 Ma), applying K/Ar dating on illites from samples L23, 24, 25. Not ignored should be the trend of increasing steepening of inclinations toward the IYSZ, probably caused by a north ward tilting. The characteristic “double-peak” observed in the illite thermometry curves for these sites, and the calculated mixed age (24-27 Ma), would support the observations discussed above, giving rise to the assumption of a superimposition of two events, in this case, the Barrovian M1 metamorphism (Oligocene), followed by a partial overprint (M2?) in the vicinity of the dome while exhumation and cooling during the Miocene time.

#### Rotation and tilting

Calculated declinations for these four sites between Tingri and Lhatse point to a slight clockwise rotation of a magnitude of ~10-20° versus India/Asia. Due to tilting shallow as well as steep inclinations occur, and a systematic scattering in remanence directions is evident; The small

number of the sites leads in its average to higher confidence errors, and thus to a broad estimation of the possible vertical rotation ( $\sim 10\text{-}20^\circ$ ) which might have happened.

Tilting occurring after remanence acquisition in pyrrhotite for each individual site will displace the latter away from its “primary” position following a small circle. Defining a small circle for each site, the resulting common intersection point (remanence), if existing, will define the initial remanence, before tilting, and thus the net magnitude of vertical axis rotation since remanence acquisition. The application of this principal to the above discussed sites clearly indicate the existence of an intersection remanence for 3 sites with a predominating reverse polarity and systematically well grouping remanence directions. The 4<sup>th</sup> site (L21), already characterized by its normal polarity and less well grouping remanence directions seems to have been tilted relative to the previous sites. It is probable that the first 3 sites represent a common mod of rotation and/or tilting, while L21 underwent different ones.

In any case, the calculated common remanence  $D=196.5^\circ/I=-51^\circ$  ( $\bar{\alpha}95=\pm 18.2^\circ$ ) for the intersecting small circles of the 3 sites indicate a slight clockwise rotation versus India. Furthermore the steepening in inclinations would imply a northward tilting.

Beside a primary remanence, Besse et al. (1984), have calculated from 3 sites a secondary remanence direction in the Tingri area (represented in Fig. 26 by a white arrow) of  $D=17.2^\circ/I=11.8^\circ$  ( $a95=10.1$ ,  $k=84$ ) in situ, and  $D=20.7^\circ/I=-8.0^\circ$  ( $a95=71$ ,  $k=3$ ) bedding corrected; also pointing to a slight clockwise rotation. They have remarked that their calculated remanences are not following a Gaussian distribution. From a closer reconsideration of this data within this study it can be remarked that their results are reflecting a circular dispersion of the remanence direction around orthogonal tilt axes similar to those obtained for Nyalam and Kharta valley. Their calculated “primary” remanence directions are tilted around a northwest-southeast oriented axis while the secondary ones appear to be dispersed on a small circle with a tilt axis orthogonal to it.

Generally, and due to the limited number of significant sites in view of pyrrhotite, it can be rather tentatively assumed, that a trend of apparently increasing clockwise rotation toward the IYSZ occur.

The data obtained for the sector (E) between Tingri and Lhatse will be connected to the palaeomagnetic results obtained for Kharta valley and the Higher Himalayan crystalline (ChRM overall means, only), and discussed in chapter 5. 1. 7 with regard to a south-north section. Further details from the HHC will follow in chapter 5. 2.

### 3. 1. 6. Discussion with regard to east-west traverse

In southern Tibet along a west-east traverse between 86° and 89°E the sampling area has been subdivided in 4 main sectors (A), (B), (C) and (D) corresponding to the Nyalam section, the Kharta valley (KVN and KVS), the Dinggye extensional zone and the Yadong/Pari area, respectively. In order to separate local and regional tectonic effects manifesting in this region palaeomagnetic results have been analyzed and discussed for each sector in individual chapters, and are combined for discussion within a regional tectonic frame.

Regardless the alternating directional arrangement of the  $ChRM^{DVF}$  being north-west in (A), north-east in (B), again north-west in (C), north-east between (C) and (D), and finally north-west in (D), a remarkable non Gaussian-, but systematic small circle distribution of the  $ChRM^{DVF}$  directions is revealed in nearly all sectors, likely as consequence of tilting and/or vertical axes rotation. Since this behavior it is not restricted to a small number of sites within a sector, it is expected that it reflects a regional trend related to the structures discussed in previous chapters (s. also Fig. 8B).

From a closer data evaluation for all sectors a relationship is established, confirming the regional occurrence of this phenomenon:

#### Data base:

The following palaeomagnetic data (all in situ) along the west-east traverse are considered and visualized in Fig. 27:

#### Nyalam section

- (1) Common intersection remanence calculated for 3 Ordovician sites

#### Kharta valley

- (2) Overall site mean for KVN
- (3) Overall site mean for KVS

#### Dinggye extensional zone

- (4) Site mean for za8 (with predominantly normal polarity)
- (5) Site mean for za13 (with reverse polarity)
- (6) Site mean for za10
- (7) Overall Site mean for za10, 18, 26, 27 (all with unexpected inclinations  $I < 0$ )

#### Yadong/Pari

- (8) Site mean for yd2
- (9) Site mean for yd3
- (10) Site mean for yd6

yd2, 3 reveal nearly symmetric antipodal directions oriented approximately east-west, while yd6 indicate predominantly reverse polarity.

As discussed in previous chapters calculated inclinations for different sectors are partly reflecting expected inclination during the Miocene (~25 Ma) ( $I \sim 40^\circ$ ) and the Oligocene (~32 Ma) ( $I \sim 30^\circ$ ) deduced from the APWP after Acton (1999) for the study area. These data is therefore involved in the concept below for calculations.

### Observations and presupposition:

(1), (6) and (10) are similar.

Apparently declinations of (2), (3), (4), (5), (8) and (9) are demarcating a small circle (SC) while vector directions of (1), (6) and (10) are approximately perpendicular to this SC. This implies that vectors of (1), (6) and (10) are coinciding with the tilt axis corresponding to SC, and a small circle defined for (1) and (10) would in this case be parallel to SC, and coincide with it at a certain critical half apical angle ( $\beta$ ). Note that specimen directions of (1) and (8) reveal a circular distribution.

Small circles with a horizontal axis are determined for (1), (6) and (10) as follows:

Trend of axis =  $D^{\rightarrow}$  of (1), (6) and (10), respectively ( $D^{\rightarrow}$  = vector declination direction).

Plunge of axis = 0 (assuming horizontal tilting)

$\beta = 2 * I$  ( $I$  = inclination of (1), (6) and (10), respectively).

Calculated small circles (Fig. 27 I, II) are termed N, D and Y corresponding to Nyalam, Dinggye and Yadong, respectively.

The non Gaussian dispersed palaeomagnetic data obtained for KVN, KVS, particular sites (za8 and za13) in the Dinggye area as well as yd2 and yd3 in Yadong/Pari is approached by calculated SC N, Y and D.

For errors minimization a common mean SC (A) is additionally calculated for N and Y.

D is defined as the upper limit SC, and thus with maximum  $\beta = 60^\circ$  ( $I = 30^\circ$  is taken as reference value for expected remanence direction during the Oligocene (~32 Ma)).

Generally, the determined small circles will approach the mean SC, which would best fit the data.

The calculated mean SC represented in Fig. 27 by its upper and lower SC confidence indicates that palaeomagnetic data considered above plot within the mean confidence angle interval ( $\alpha_{95} = \pm 11.5^\circ$ ) (defined as mean of all three  $\alpha_{95}$  calculated for (1), (6) and (10)), and thus satisfy the assumption above.

### Quantification and interpretations

The summary of palaeomagnetic results geometrically visualized in Fig. 27, confirm the observations discussed in previous chapters pointing to the occurrence of a consistent systematic regional trend in the area between  $86^\circ$  and  $89^\circ$ . A non stochastic case is therefore valid, and a relationship can be established. The ascertained regional trend is expressed as a dispersion of palaeomagnetic data from different sectors on a common mean small circle, with a tilt axis described above.

Toward separation and quantification of the palaeomagnetic data, a 2-case concept (visualized in Fig. 27) is established, and data is evaluated with regard to vector remanence directions, expected for Oligocene/Miocene time.

As it is indicated in Tab. 7 representative mean amount of rotation for the surveyed west-east traverse have been calculated with regard to Miocene and Oligocene expected directions deduced from the APWP, after Acton (1999). The latter are found to be  $20^\circ$  and  $13^\circ$  for Miocene and Oligocene, respectively. The resultant mean value  $\vartheta = 16.5^\circ$  ( $\pm \alpha_{95} = 11.5^\circ$ ) is regarded as the

characteristic regional value for the whole studied area. The termed difference rotation in Tab. 7 is interpreted as a consequence of rotational under-thrusting and oroclinal bending. Thus the obtained mean difference rotation amount of  $7^\circ$  is accepted within this concept as the amount reflecting rotational under-thrusting; yet not the net amount, since a small effect linked to oroclinal bending manifesting in a slight anti-clockwise rotation in this area might still be needed to be subtracted. For a determined amount of rotational under-thrusting of the Indian plate beneath the Tibetan Plateau  $<5^\circ$  since late Eocene (Acton, 1999), the calculated difference rotation within this study can be regarded as the sum of  $5^\circ$  of rotational under-thrusting and of  $2^\circ$  of oroclinal bending effect averaged for the area between  $86^\circ$  and  $89^\circ\text{E}$ . Despite the deduced values for rotational under-thrusting and oroclinal bending, the inferred mean value ( $\vartheta$ ) of rotation is surprisingly very close to those reported in the adjacent area to the west (s. Tab. 8 for comparison), and therefore support the occurrence of a uniform pattern of rotation on a large regional scale. Furthermore, it can be concluded that no rotation has occurred before Oligocene ( $\sim 32$ ). The mean tilting value ( $\delta$ ) reflect the ascertained east-west tilting in the Yadong area discussed in chapter 5. 1. 4., and best represented by palaeomagnetic results of yd2 (s. also Fig. 27).

The iterative orthogonality of tilt axes (two sense/phase of tilting) on a regional scale inferred from palaeomagnetic data reflects a “periodic” distribution of contractional extensional structures as discussed in previous chapters (s. also Fig. 8B). This pattern deduced from palaeomagnetic data is expected along the Himalayan arc, and is in agreement with geodetic data, i.e., global positioning system (GPS) measurements revealing broadly distributed contraction across the plateau, oriented  $\sim \text{N}30^\circ\text{E}$ , as well as orthogonal extension (Wang et al., 2001).

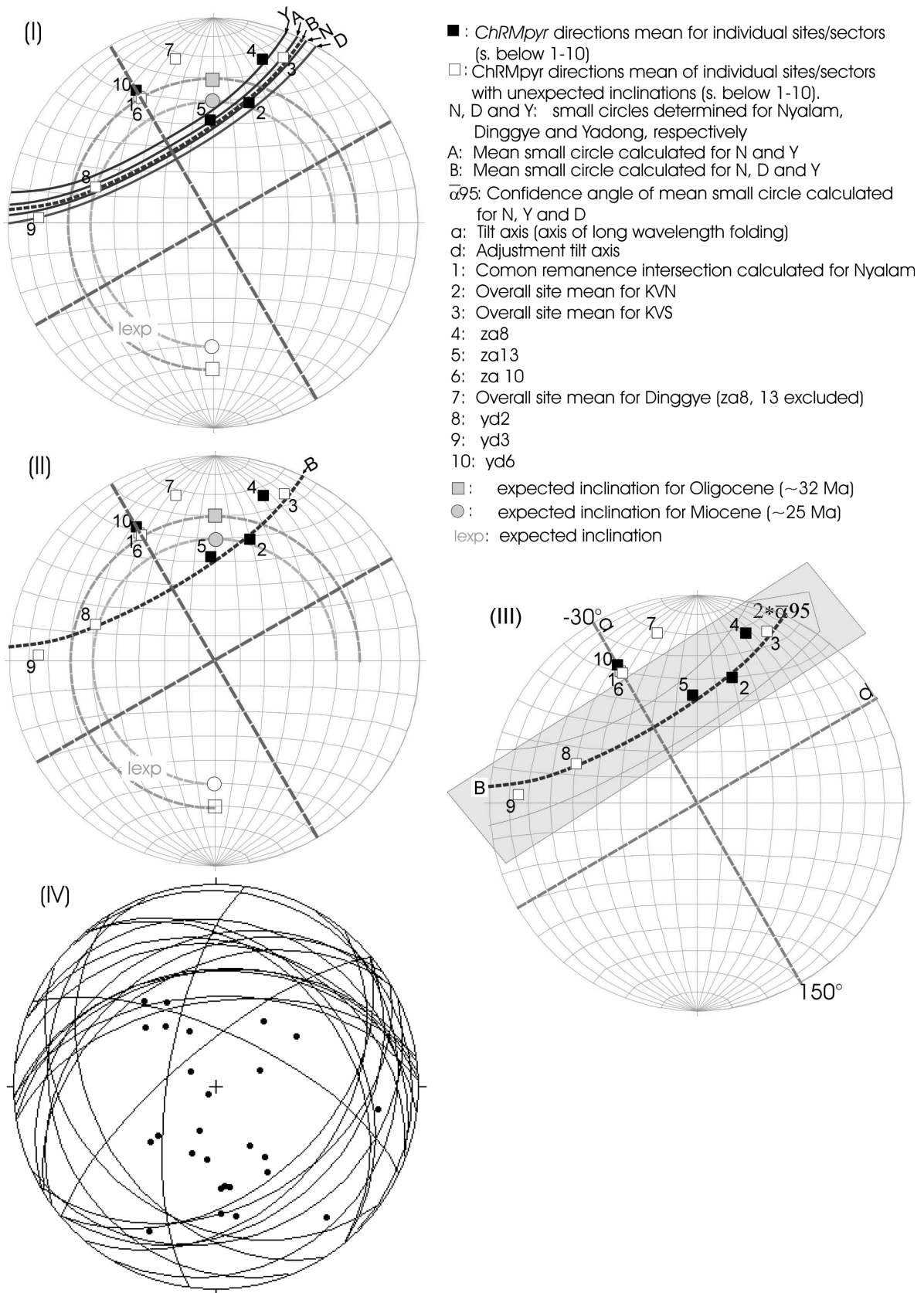


**Fig. 27:** Stereographic projection (equal area) of palaeomagnetic results (in situ) obtained for all 4 sectors along the west-east traverse in southern Tibet between 86° and 89°E ((I), (II), (III)). Generally (assumed) normal polarity directions are shown. The established relationship is demonstrated in (I) and (II), showing a dispersion of remanence directions along a small circle. In (II) and (III) only small circle of N and statistical confidence limits of a mean small circle of N, Y, D are shown. In (IV) Bedding/foliation poles (dots) and planes (circles) for sampling sites are represented (equal area projection).

**Tab. 7:** Summary of palaeomagnetic results (reconstruction and quantification) determined for the west-east traverse between 86° and 89°E in southern Tibet. Numerical results are absolute values. Calculated clockwise rotation and tilting are obtained by back tilting to expected inclination for the area. Note that coincidentally the ~32 Ma- as well as the ~25 Ma ages are considered as upper and lower limits for Eocene and Oligocene geological times.

Nyalam (N) SC	Rotation(°)	Tilting (°)	Difference rotation(°)	Difference tilting(°)
Oligocene(~32 Ma)	21	98.2		
Miocene(~25 Ma)	15	104.4	6	6.2
Dinggye (D) SC				
Oligocene(~32 Ma)	25	95.3		
Miocene(~25 Ma)	19	100.7	6	5.4
Yadong (Y) SC				
Oligocene(~32 Ma)	13	106.0		
Miocene(~25 Ma)	4	115.1	9	8.6
A= mean(N,Y) SC				
Oligocene(~32 Ma)	18	101.7		
Miocene(~25 Ma)	10	108.9	8	7.2
Mean(N, Y, D) SC				
Oligocene(~32 Ma)	20	100.1		
Miocene(~25 Ma)	13	106.8	7	6.7
Mean value	$\vartheta = 16.5^\circ$	$\delta = 103.5^\circ$	□	□
Trend of tilt axis reconstructed from palaeomagnetic data				(°)
Oligocene(~32 Ma)				130/110*
Miocene(~25 Ma)				137/124*
Trend of tilt axis (for comparison with palaeomagnetic data) reconstructed from bedding/foliation data for sampling sites ( $\pi$ -circles)				133
				53

**Tab. 8:** Palaeomagnetic results from adjacent areas to the west (from Schill et al. 2003) compared to data from this study.

	Hidden valley	Thakkhola	Manang	Nar/Phu	Shiar	This work
Latitude	28.8°N	28.7°N	28.7°N	28.8°N	28.6°N	~27.5 ~- 28.5°N
Longitude	83.6°E	83.7°E	84.0°E	84.3°E	85.1°E	86°-89°E
(a)	30 ± 1	?	27.5 ± 2.5	32 - 25	25 - 17	32 -25
(b)	357.2/59.2	184.4/-54	196.4/-65.9	355.5/61.4	206.9/-27.2	small circle distribution
	-3.6	-12.2	-3.2	non	non	
(c)	-2.3°	4.9°	16.6°	Fisherian	Fisherian	
				16.0°	26.5°	16.5°
(a)	Age of remanence acquisition in Ma					
(b)	observed remanence direction					
(c)	calculated mean amount of rotation (clockwise)					

### 3. 1. 7. Discussion with regard to south-north transect

In addition to the examination of a west-east trend in southern Tibet (parallel to the main tectonic unit of the Himalayan arc), a south-north section approximately perpendicular to the main strike of the Himalayan arc is surveyed. The latter comprises from the south to the north, the HHC of Solu Khumbu, the Kharta valley and the area between Tingri and Lhatse, termed sector- (F), (B) and (E), respectively. Palaeomagnetic results for (B) and (E) are presented and extensively discussed in chapter 5. 1. 2 and 5. 1. 5; from (F) the sites overall mean value only is involved here. Further details will follow in chapter 5. 2.

Despite differences on site scale, the overall mean for 12 sites ( $D=355.6^\circ/I=45.7^\circ$ ,  $\alpha_{95}=12.2^\circ$ ,  $k=14.9$ ) suggests that no rotation (or a slight apparent counter-clockwise rotation) has had happened in Solu Khumbu (F). To the north in the Tethyan sedimentary series, sector (B) subdivided in KVS ( $D=202.8^\circ/I=12.9^\circ$ ,  $\alpha_{95}=19.9^\circ$ ,  $k=29.8$ ) and KVN ( $D=196.4^\circ/I=-38.3^\circ$ ,  $\alpha_{95}=16.4^\circ$ ,  $k=14.5$ ) as well as sector E ( $D=204.5^\circ/I=-41.3^\circ$ ,  $\alpha_{95}=25.7^\circ$ ,  $k=18.3$ ) indicate that a clockwise rotation slightly increasing toward the north has occurred on this transect.

#### Pro and con

Indications for possible right lateral shear in KVN along the STDS are mentioned in chapter 5. 1. 2. Along the IYSZ dextral shear might occur, perhaps initiated by an echelon oblique right lateral strike slip (landsat and DEM reveal structures which might support an oblique dextral normal motion). The offset of the main Karakorum Fault zone to the east was debated by some of the authors. The suggestion of its cessation set at ca.  $81^\circ\text{E}$  by Murphy et al. (2000, 2002) was disproved by Lacassin et al. (2004). They propose its continuation to the east as a dextral transpressive structure reactivating the IYSZ. Strike slip in the Rinbug area has been reported by Ratschbacher et al. (1994).

Generally, with regard to results of this study, the top to the north sense of shear of the extensional structures, STDS, KGT system included, and sigmoidal oblique dextral normal shear along the IYSZ would support the development of a clockwise rotation slightly increasing toward the IYSZ. Furthermore, it is not excluded that block rotation is triggered by motion transferred by accumulation and/or accommodation from the STDS in the south to the IYSZ in the north (both considered as interacting 1<sup>st</sup> order faults) via first order thrusts and numerous all kind of small sized 2<sup>nd</sup> order thrusts, oblique and parallel to the main strike normal faults. An interpretative sketch is represented in Figure 28. On the other hand, however, not in contradiction with these assumptions, the calculated common intersecting declination  $D = 16.5 \pm 18.2^\circ$  coincident with the mean value  $\vartheta = 16.5 \pm 11.5^\circ$ , representing the regional trend between  $86^\circ$  and  $89^\circ\text{E}$ , might at first glance invoke a contradiction with the these of an increasing clockwise rotation toward the IYSZ. However, a separation of local effects manifesting as described above, from the regional trend characterized by  $\vartheta$  renders again the assumption plausible.

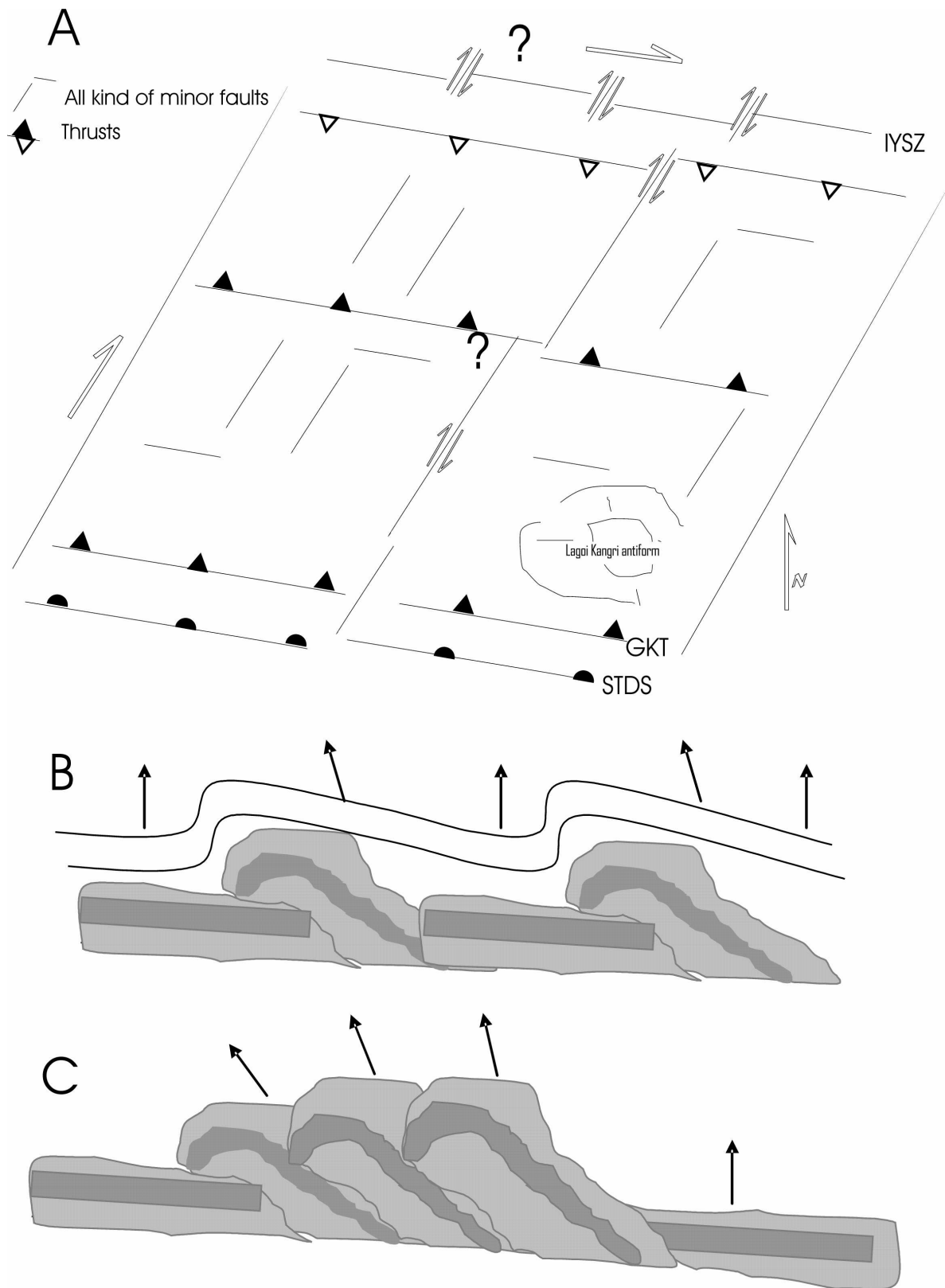


**Fig. 28:** Simplified sketches visualizing the assumptions discussed in chap. 5. 1. 7. A: general working model assuming the interaction of STDS and IYSZ to explain the slight increase of clockwise rotation toward the IYSZ. B and C demonstrate possible role of thrust-ramps/antiforms and duplex structures in the accumulation and/or accommodation of rotation (near field effect). Black arrows indicate remanence vector directions.

## 3. 2. Higher Himalayan Crystalline of Solu Khumbu

### 3. 2. 1. Geological setting and sampling

High-grade metamorphic gneisses (upper amphibolite to granulite facies) of the High Himalayan Crystalline (HHC) have been examined for their suitability for palaeomagnetic investigations: Field work, including sampling and detailed geological mapping, has been conducted in the Solu Khumbu area on a south-north transect at ca. 87°E along the Dudh Kosi from a few km south of Lukla (close to the Main Central Thrust) to Dugla in the North (south of Everest). A total of 47 sites (all indicated in the geological map in Fig. 29) were taken from different formations ranging from amphibolite to granulite facies.

Details on the geology of the sampled transect are presented in the geological map of Fig. 29, accomplished on the basis of compiled field data and petrographic analysis.

Detailed field mapping and thin-section analysis show that the sampled transect underwent at least three metamorphic events (M1, M2 and M3). M1 and M2 represent pro-grade metamorphism (amphibolite to granulite facies, and granulite facies, respectively) overprinted by M3 retrograde metamorphism during exhumation and cooling (green schist facies). Hence, the sampled transect is divided in a (1) south segment which underwent M1 and M3, and a (2) north segment characterized by M1, M2 and M3.

Palaeomagnetic investigations are completed for 20 sites from the south segment. For 27 sites from the north segment the results of a pilot study are presented awaiting the achievement of further measurements.

### 3. 2. 1. Results from magneto-mineralogy

In this region the HHC consists of the Barun gneisses (upper amphibolite to granulite facies) and the Namche migmatite gneiss, a granitic orthogneiss deriving from granites of Early Paleozoic age. A total of 20 sites were collected from this area for palaeomagnetic investigations. ThD and AF cleaning were tested on pilot samples. AF treatment shows a noisy character (Fig.31j). Improvement could be reached by repeated cleaning in AF (at the same steps, respectively) (Fig. 31k). Nevertheless, due to variability in the magnetic behavior, ThD (in steps of 5-10° within critical intervals) turned out to be the more suitable method. Pyrrhotite, with variable contribution, was observed in all sites (Fig.31a-f). Regardless the complexity and variability in the remanence behavior between sampling localities and within specimens, two different characteristic magnetic remanence components were separated, depending on their unblocking temperature spectra. Temperature intervals of unblocking between 200-350°C and 450-600°C are most likely related to pyrrhotite ( $ChRM^{pyr}$ ) and magnetite ( $ChRM^{mag}$ ), respectively. IRM acquisition and  $SIRM^T$  (Fig. 32a-b) support the dominance of pyrrhotite and the presence of magnetite.  $SIRM^{RT}$  reflect the complexity in the magneto-mineralogy observed partly by examined specimens. Hematite could neither be clearly identified during ThD nor while IRM acquisition: onset of a viscous remanence at higher temperature steps often hindered the evaluation of its endpoints. IRM acquisition curves mainly adopt an asymptotical behavior to the horizontal (saturation line) around 500 mT. However,  $SIRM^T$  reveal its presence in trace amounts. Petrographic analyses often show its intergrowth with magnetite. Reflected light microscopy identifies large grain-sized hemo-ilminite. Morin transition in  $SIRM^{RT}$  cycling curves is characterized by a large decrease in remanence, supporting the presence of large grain size stoichiometric hematite. In contrast, the overlap to inversion of the cooling and warming curves at around 34 K in G2 and G3 is interpreted as a response to existing SD/PSD pyrrhotite grains. The transition at ~34 K in G12 is an indication for the presence of larger grains up to 30-40 µm as it is recognized through reflected light microscopy on a polished section (Fig. 35B,a). While G2 and G3 share similarities in their cooling and warming curve, and thus in

their magneto-mineralogy, G12 reveal a different magnetic behavior. This difference can be considered as a qualitative attribute, distinguishing between different gneiss facies. These observations corroborate with the petrographic analysis: G2 and G3 are petrographically identified as migmatitic paragneiss; G12, in contrast, is determined as a migmatitic orthogneiss. Examples for both facies (G3 and G12) as well as for further formations within the study area are presented in Fig. 35A

With a focus on the ferri(o)magnetic phase pyrrhotite, and in order to verify whether a relationship can be established between selected low temperature steps and measured fields, high field hysteresis measurements were run for a 7 T SIRM, at RT, 25-, 32- and 36 K. Results and further details are summarized in Fig. 33d. Whether the identified ferri(o)magnetic phase at the selected low temperature steps (25-, 32- 36 K) can be restricted to pyrrhotite, as assumed, remains questionable, and further measurements are required to elucidate this case.

From the remagnetization experiments (s. chapter 2, methods, for details), a 100% recovery obtained between RT and 350 °C is interpreted as a response to the presence of a ferri(o)magnetic mono-phase –in this case the pyrrhotite. A characteristic correlation coefficient  $r = 1.00$  is calculated for the majority of the examined samples (migmatitic paragneisses). An exception in this relation is found for a migmatitic orthogneiss, where  $r = 0.96$  is calculated. Comparing these results with those of previous measurements (e. g. cycling, s. Fig. 33) the difference in the calculated  $r$  might be ascribed to grain size changes, being within a PSD/SD mono-range in the paragneiss samples, and widely dispersed (PSD/SD-MD) in the migmatitic orthogneiss. Errors in measurements are not excluded.

### 3. 2. 2 Mechanism of remanence acquisition

#### Low temperature component pyrrhotite ( $ChRM^{pyr}$ )

Generally, pyrrhotite can be formed at ~ 200 °C. Within higher temperature conditions its growth and stability is dependent of the sulfur fugacity (at. % S); up to a given 50% S pyrrhotite can exist with other iron phases within a wide temperature range 200-1000°C (Craig et al., 1997).

In the high-grade metamorphic gneisses of the Solu Khumbu area existing pyrrhotite is believed to have formed at the ductile/brittle deformation transition regime, during the retrograde stage M3 (green schist facies) discussed above, and to acquired its remanence shortly thereafter, below its Curie temperature (~325°C). Pyrrhotite is, however, also capable to grow at higher temperature (primary pyrrhotite), as aforementioned, and to became re-equilibrated at a later stage, i.e., retrograde phase. To gain more insights in its magnetization it is necessary to examine given conditions favoring its formation. As discussed in the magneto-mineralogy results two main facies were examined: (1) The Barun gneiss, a paragneiss related to the M1 event and subsequent M3, (2) the Namche migmatite, a migmatitic ortho- and paragneiss linked to the M1, M2 and M3.

Paragneisses usually derive from shales and pelites, while orthogneiss derive from the proterozoic granite. Due to the fact that sulfur is required for the formation of pyrrhotite, the latter will then rather be expected in paragneisses, and supposed to be absent in the orthogneisses. However, pyrrhotite is evidenced also in the latter. By a closer view on the constrained geological map as well as modified sections, it is clear that the migmatitic orthogneisses mainly intercalate migmatitic para- and calcgneisses, supposed to be the natural sulfur fluids donator by infusion/diffusion. Due to the fact that migmatitic orthogneisses (leucosomes), in the majority of cases results from in situ partial melting fluids infusion is expected at the contact to the para- and calcgneisses, and a scenario as discussed above for the formation of pyrrhotite and its magnetization is available. With regard to the conditions discussed above it can be assumed that pyrrhotite has had formed/re-equilibrated and thermo-magnetized at the ductile/brittle transition during the last cooling event.

The occurrence of normal and reverse polarity in some sites, simple- and multi antipodes within specimens (1) support the thermo-magnetic nature of the acquired remanence, and (2) prove that averaging on secular variation has been achieved. It implies a protracted cooling history, covering at least one reversal of the earth magnetic field.

#### High temperature component ( $ChRM^{mag}$ )

Stable and well grouping  $ChRM^{mag}$  directions, matching with those of  $ChRM^{pyr}$ , have been isolated for 3 sites (G3, G13 and G18) in the southern segment. G3 is a migmatitic paragneiss (M1, M2 and M3), and G13 and G18 are Barun gneisses (M1 and M3). A thermoremanence acquisition in magnetite is questionable. Blocking during cooling at elevated temperatures in the ductile range would lead to scattering remanence directions. It is much more plausible to assume a secondary magnetite formed during the M3 stage, which has acquired a thermo-chemical remanence. Magnetization of magnetite might predate that of pyrrhotite, if a longer protracted exhumation and cooling history is assumed. On the other hand, rapid cooling would rather emphasize their contemporaneous magnetization. Nevertheless, the development of a thermoremanence, at earlier stage of M3, and the acquisition of a thermo-chemical remanence at its later stadium are not completely excluded.

As it has been previously mentioned pilot results from the northern part, which underwent M1 overprinted by M2 and M3 reveal an increase of the contribution of magnetite at the expense of pyrrhotite. A north-west arrangement of the remanence directions occurs, however, a consistent north-east sense of directions is dominant. The northern sector, generally, reflects high temperature conditions. It is remarkable that the  $ChRM^{pyr}$  - and  $ChRM^{mag}$  directions are reflecting a traceable continuous cooling path clearly indicating a successive magnetization of magnetite and pyrrhotite, respectively, most likely within the greenschist conditions. For instance, a thermoremanence acquisition in both magnetic minerals magnetite and pyrrhotite is emphasized. Nevertheless, this assumption persists questionable until statistically sufficient new data is involved, and will be tackled on this basis in future work. The adopted north-east arrangement in the remanence directions reflect similarities to those measured in Kharta valley. Randomly dispersed  $ChRM^{hem}$  directions isolated for the high temperature component hematite indicate its instability, and are therefore not considered.

### 3.2.3. Palaeomagnetic results and tectono-metamorphic implication

Does palaeomagnetic data document the cessation of the channel flow?

$ChRM^{pyr}$  directions were derived from PCA and Fisher statistics. Normal and reverse polarity occur partly within a site. Simple and multi-antipodal directions within a specimen are observed as well, indicating that the time cover for the closure temperature of pyrrhotite was long enough to average on the secular variation. Only sites with statistically significant results ( $k \geq 10$ ) are involved in the final consideration. Vector analysis for 9 sites (with  $k \geq 10$ ) yields an in situ overall mean direction (average1 in Tab. 9) of  $D=353.8^\circ/I=45.3^\circ$  ( $\alpha_{95}=14.4^\circ$ ,  $k=15.4$ ) (Fig.17b). Site G5 has been excluded from the statistics as it shows an unexpected positive inclination which might be the result of auto inversion in the presence of magnetite or of strong tilting after remanence acquisition; here it should be mentioned that recumbent collapse folds were frequently observed in the sampling area. Assuming, as discussed above, that the  $ChRM^{mag}$  obtained for 3 sites match those of  $ChRM^{pyr}$  directions, the latter were included in the statistics for data comparison; an in situ overall mean direction (average2 in Tab. 9) of  $D=355.6^\circ/I=45.7^\circ$  ( $\alpha_{95}=14.9^\circ$ ,  $k=12.2$ ) is obtained. From both averaged directions it can be assumed that no significant vertical block rotation versus India has occurred. According to the APWP curve from Acton (1999), the calculated average1 inclinations would correspond to a minimum remanence age of ~11 Ma, whereas average2 inclinations would

imply a minimum age of ~ 7 Ma, both of them not in contradiction with late Miocene cooling ages reported for the area (e.g. Searle et al., 2006) (s. time/temperature diagram in Fig. 37). Furthermore, it can be assumed in this case that the recorded remanence in pyrrhotite will document the last cooling event which might have had happened. In situ melting itself is supposed to be triggered by partial melting in the crust and the “adiabatic” ascent and exhumation of leucogranites. Therefore, if the hypothesis of a southward extruding channel flow is accepted, it can be proposed that by a continuous partial melting feeding beneath southern Tibet, the channel has extruded episodically. Therefore, the determined age for the recorded remanence will correspond to the cessation of the channel flow. A closer consideration of individual site means results indicate differences in calculated inclinations, corresponding to remanence ages ranging from Oligocene to Miocene. Frequently measured steep inclinations are compatible with the inclinations reported by Appel et al. (1991) and Rochette et al. (1994) and attributed to a ramping along the MCT. The effect of ramping along the MCT might not be excluded especially for sampling locations close to the MCT. However, large antiform- and synform structures becoming more frequent toward the north as observed within this study and reported by Carosi et al. (1999) emphasize the effect of doming and thus the development of duplex structures reflecting long wavelength folding.

Generally, beside a retrograde stage (M3) two main peak metamorphic phases (M1 and M2, respectively) have manifested in the HHC: The early M1 (32-30 Ma) kyanite ± silimanite metamorphism (650-680°C, 7-8 kbar) is linked to crustal thickening and regional Barrovian Metamorphism. The M2 (23-17 Ma) silimanite ± cordierite metamorphism (650-680°C, 4-5 kbar) is attributed to increased heat input and subsequent partial melting in the crust. Despite the proposed model of its extrusion as a Coulomb wedge (Royden & Burchfiel 1987, Platt, 1993), it is suggested by many authors that crustal melting triggered channel flow and ductile extrusion of the HHC (Beaumont et al., 2004; Jamieson et al., 2004). The timing of motion along the MCT and the STDS zone at the base and the top of the channel, respectively, has been extensively discussed (e.g., Hodges et al., 1992; Hodges, 2000; Searle and Godin 2003; Godin et al., 2006a). Both ductile shear zones were active during the early Miocene (23-15 Ma). A consistent age older than 16-14 Ma year obtained for hornblende and mica indicates a minimum time constrain on the exhumation history of both shear zones at the ductile/brittle regime transition.  $^{40}\text{K}/^{39}\text{Ar}$  dating on mica and apatite fission track age (Wang et al. 2001) implies that the Nyalam detachment and its footwall share a rapid cooling history during the interval c. 16-12 Ma. New isotopic ages from the Mabja Dome reveal a late Oligocene to early Miocene history of ductile vertical thinning and horizontal stretching, peak metamorphism, migmatization and emplacement of a leucocratic dyke swarm (Lee et al., 2006). Doming itself is thought to have occurred between 13.0 and 12.5 Ma at temperatures between 370 and 200°C. Tacking into account the regional condition parameters, and with regard to the pyrrhotite component, as it would document the ductile/brittle transition regime, from measured remanence directions, and subsequent deduced upper remanence age (~11 Ma) it can be concluded that the Higher Himalayan Crystalline and the North Himalayan domes share similarities in their exhumation cooling histories. Coeval events are therefore not excluded.

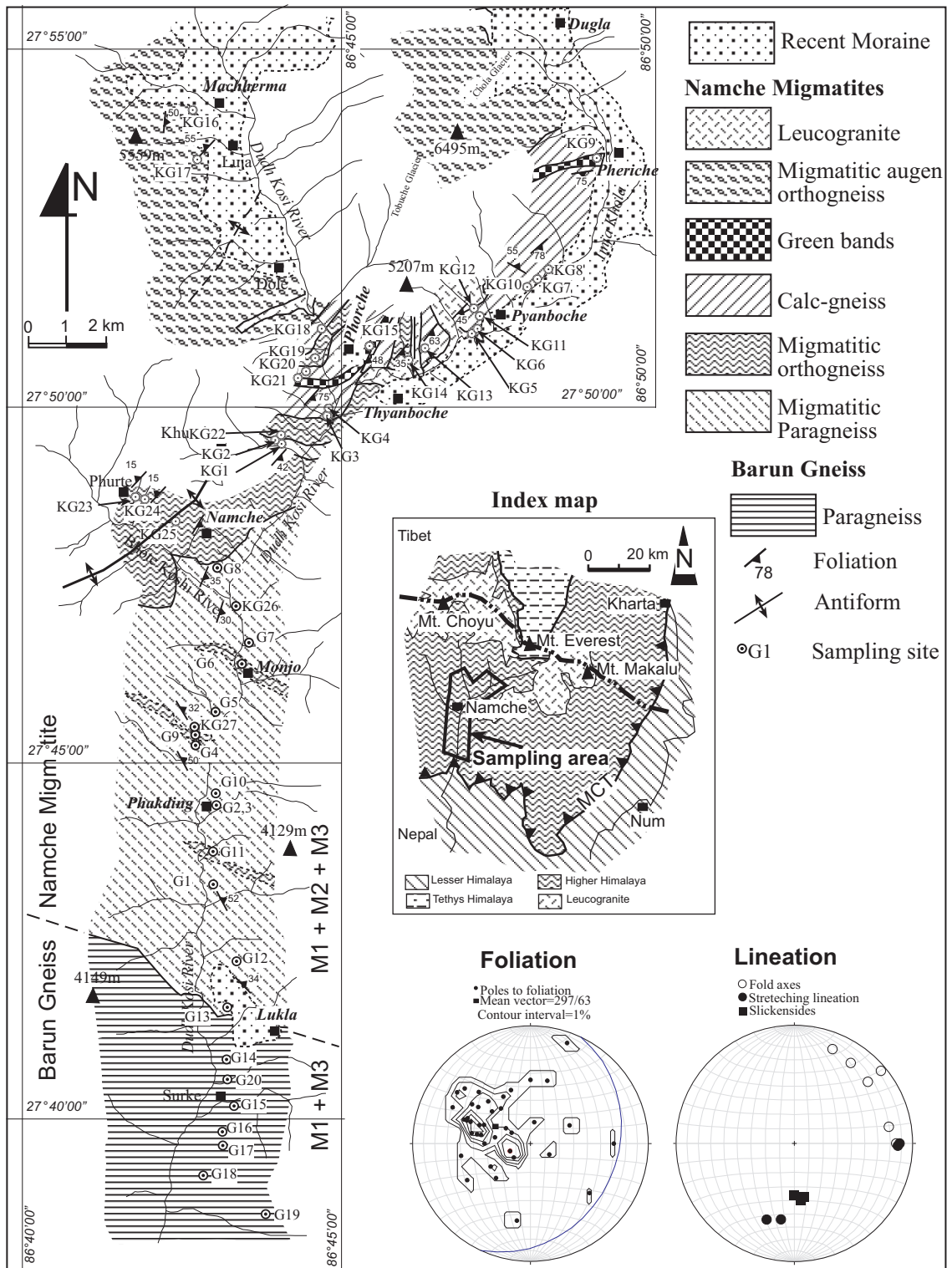


**Fig. 29:** Constrained detailed geological map for the studied south-north transect in the HHC of Solu Khumbu on the basis of field- and petrographic observations. Measured structural data are represented in a stereographic projection (equal area). Slickensides indicate top to the south sense of shear. South-west/north-east as well as east-west oriented stretching lineation is measured, indicating the presence of two components with approximately orthogonal sense of shear (similar observations were reported by Pêcher (1991) and Brun et al. (1985) for the HHC of the Garwhal- and Nyalam-Zahm area, respectively). Measured fold axes give rise to the assumption of a progressive reorientation toward east-west.

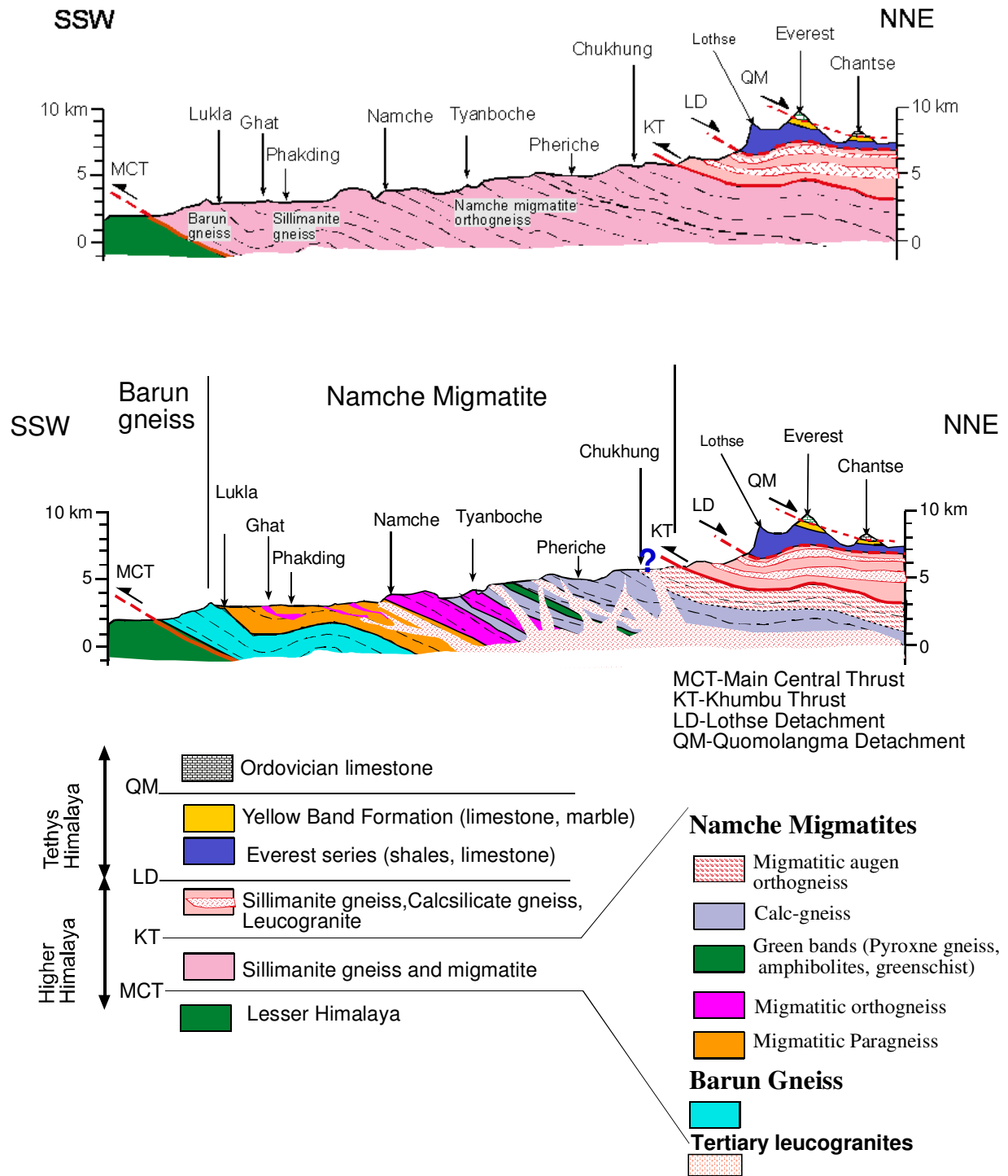


**Fig. 30:** Simplified geological cross section along the Everest, after Gessup et al. (2006) including the sampled south-north transect within this study (Upper profile). The cross section is modified on the basis of our new field surveys and petrographic analysis (Lower profile). Details on sampled facies are visualized in the geological section and termed in the appended legend.

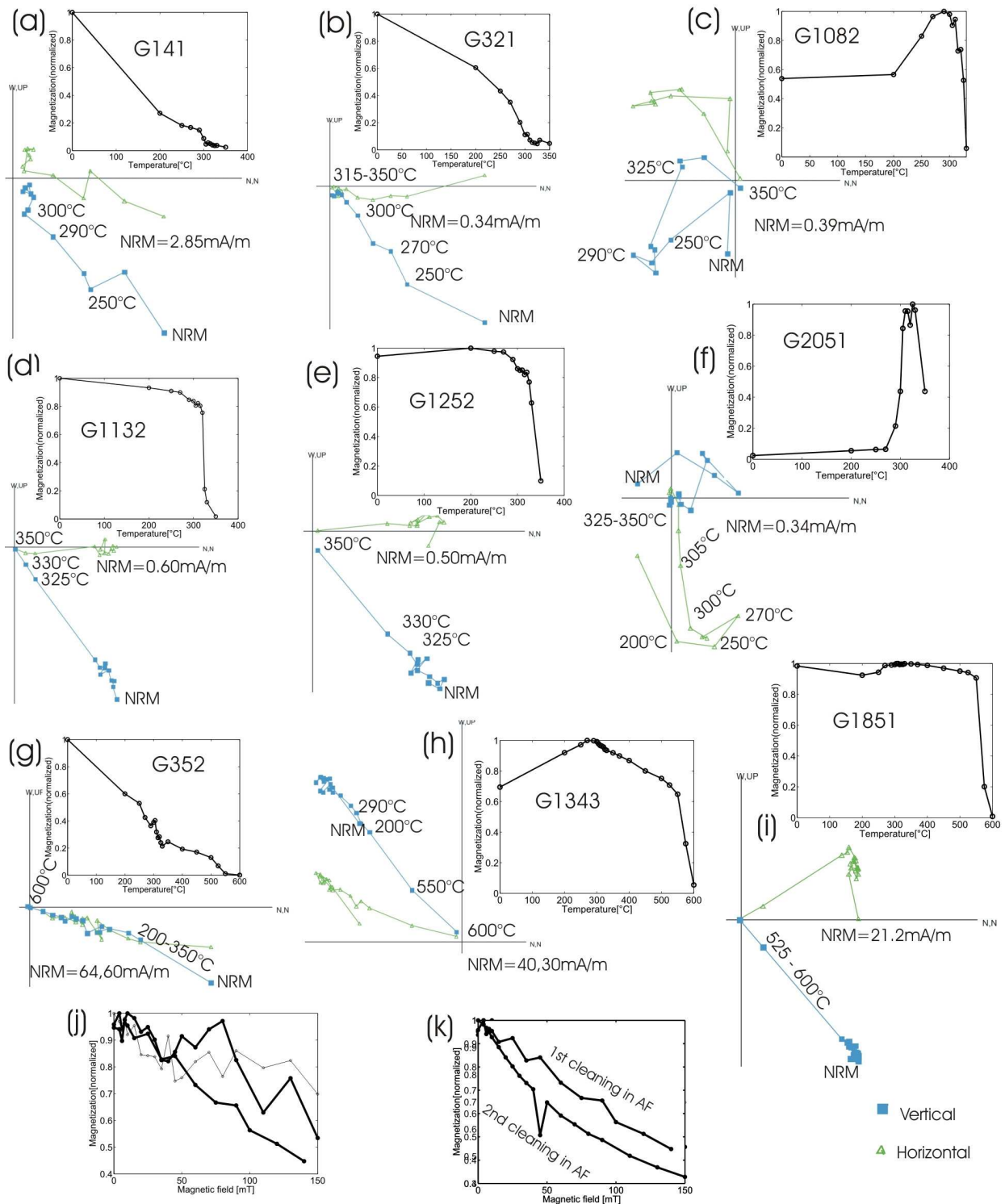


**Fig. 31:** Migmatitic para- and orthogneisses from the southern segment of the studied south-north transect in the Solu Khumbu area - Temperature-intensity curves and Zijderveld diagrams for pyrrhotite (a-f) and magnetite (g-i) bearing specimens during thermal demagnetization; (g) indicates coexistence of pyrrhotite and magnetite in G3. AF demagnetization shows a noisy character (j) which could be smoothed by repeated cleaning at the same steps (k), respectively.

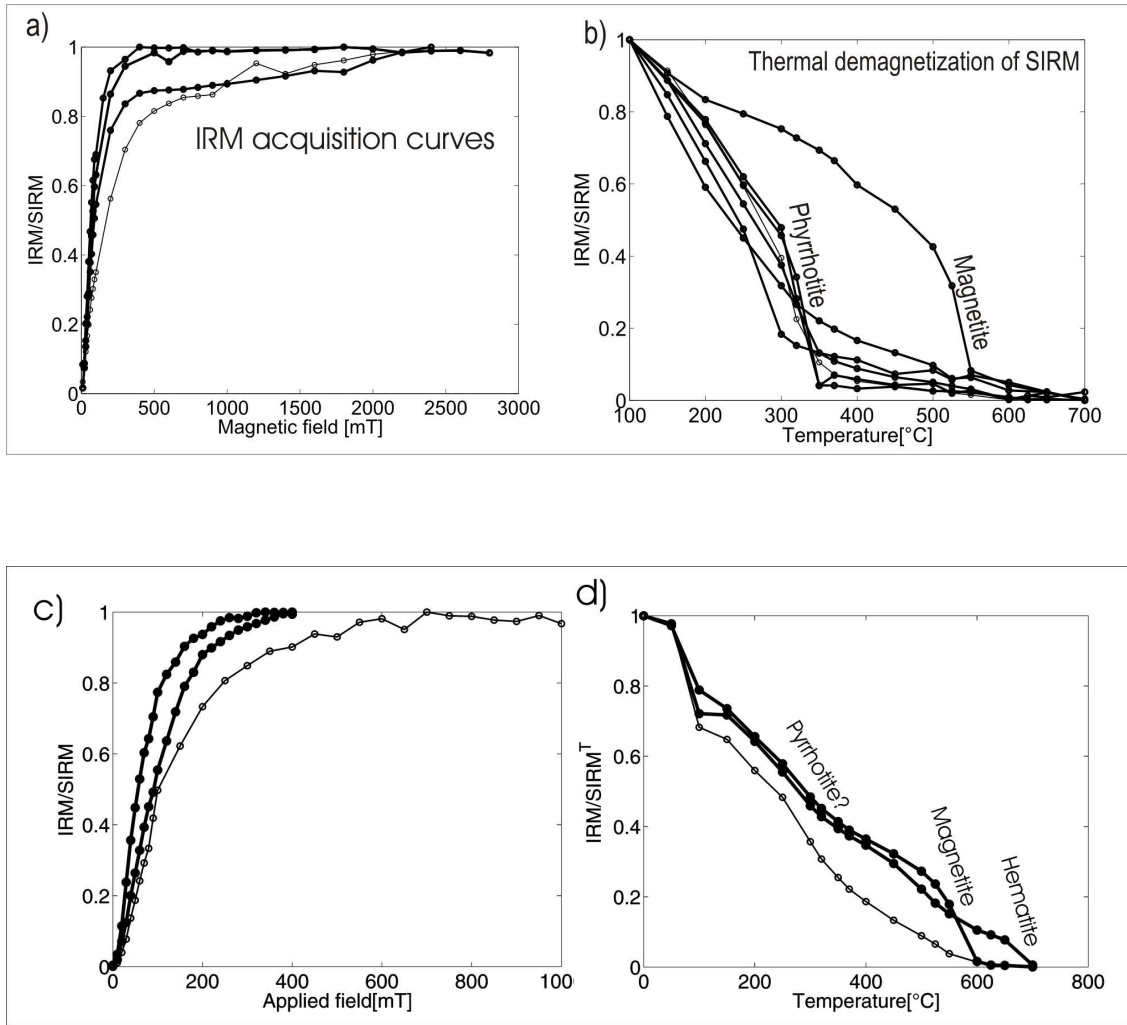


**Fig. 32:** IRM acquisition curves and thermal demagnetization of SIRM for gneisses from the southern (a, b) and northern (c, d) segment containing pyrrhotite and magnetite with low to medium coercivity. The non saturation by fields higher than 1T is rather indicative for the presence of goethite. Trace amounts of hematite are exclusively identified by SIRM<sup>T</sup>. From further measurements it has been observed that in the absence of goethite saturation is mainly asymptotically approached at around 0.5 T during IRM acquisition, signaling the presence of magnetite and pyrrhotite, however subsequent SIRM<sup>T</sup> revealed in the majority of cases also the presence of hematite, even in negligible amounts. Pyrrhotite seems to be dominant (with the exception of 2 magnetite sites) in the southern sector (s. (b)). In contrast, pilot studies from the northern sector reflect the increase in the contribution of magnetite (s. (d)).

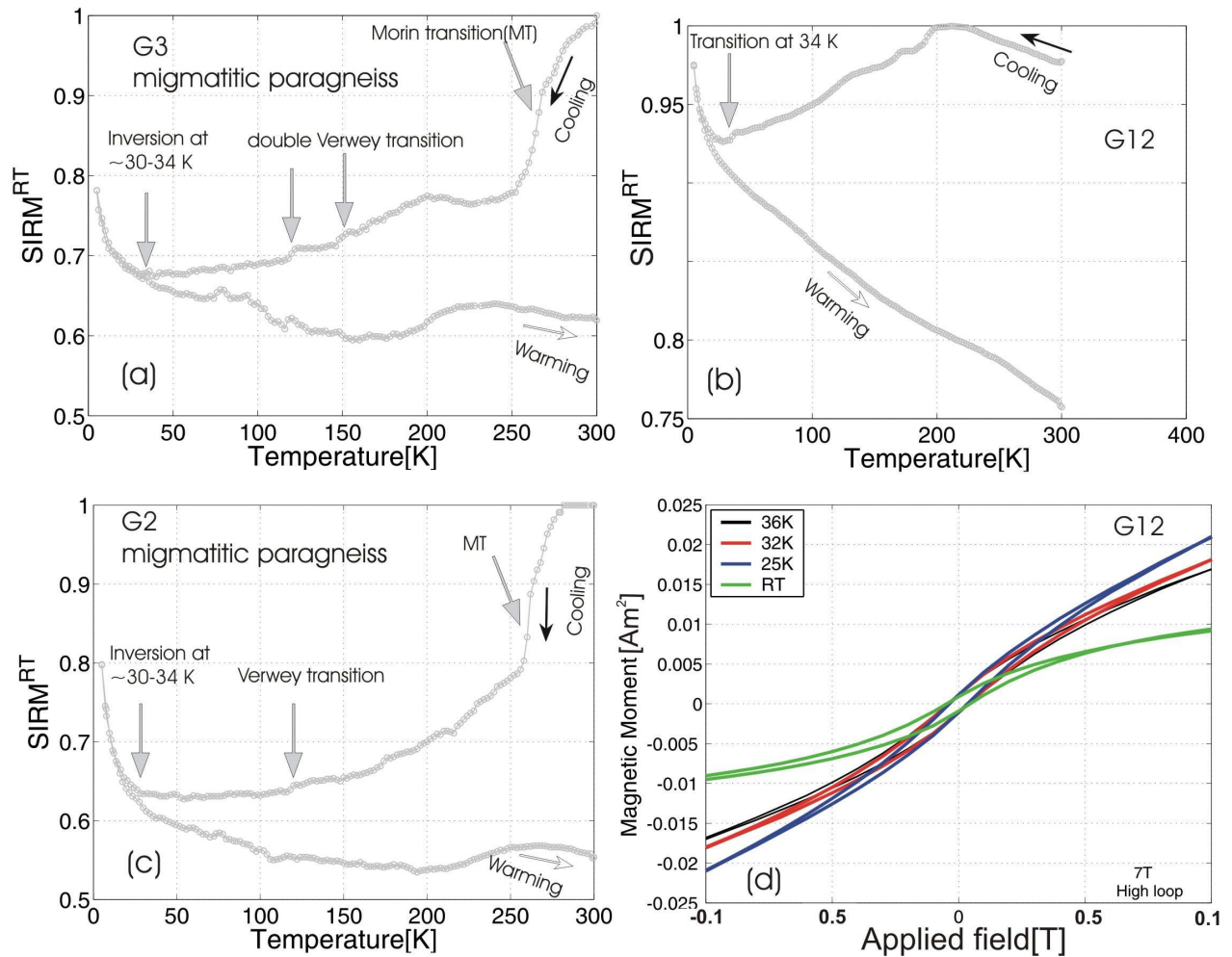


**Fig. 33:** (a, b c): Thermomagnetic runs from 300 to 5 K (field cooling) and back to room temperature (warming in zero-field) monitored in 2.5 K increments. 5 T field at room temperature (SIRM<sup>RT</sup>) was applied prior to cycling. The cycling was performed for samples selected on the basis of ThD- and SIRM<sup>T</sup> results, revealing the dominance of pyrrhotite, partly coexisting with some magnetite. While (a) and (c), thermomagnetic curves for migmatitic paragneiss, share similarities in their magnetic behavior, (b), cycling curve for migmatitic orthogneiss reflect a distinguishable character.

Inversion at ~34 to ~36 K in (a) and (c) is attributed to SD/PSD pyrrhotite grains, probably, increasing up to 30-40 $\mu$ m in (b). ThD curves (e.g. (b) and (e), respectively in Fig. 31) improve these observations. Reflected light microscopy applied for a migmatitic orthogneiss (s. Fig. 35) confirm the presence of larger grains up to 30-40 $\mu$ m.

(d) With a focus on the ferri(o)magnetic phase pyrrhotite, and in order to verify whether a relationship can be established between selected low temperatures and measured fields high field hysteresis measurements were run for a 7 T SIRM, at room temperature as well as at 25-, 32- and 36 K, where 25 is considered as the lower most limit of favorable temperature interval for superparamagnetic fine particles (SPP). 32-, and 36 K, respectively are the intrinsic lower and upper values of the pyrrhotite transition (~34 K). The rectangular shape of the measured open hysteresis loop at RT might approve the presence of low to middle coercive pyrrhotite, probably accompanied by some magnetite and goethite. However, this persisting shape (becoming sharper), with a progressive change toward 25 K, is assumed to be characteristic for the pyrrhotite phase. Similar results (not shown) were obtained for a 2<sup>nd</sup> sample in which pyrrhotite is expected. However, measurements, in analogy, performed for a metacarbonate sample, where pyrrhotite has been identified by its transition reveal the absence of any ferri(o)magnetic phase at 25-, 32- and 36 K (closed straight hysteresis loop). In summary, from the few measurements, the results might be over-interpreted, and further measurements are required for clearance of this case. Note that all curves are not corrected.

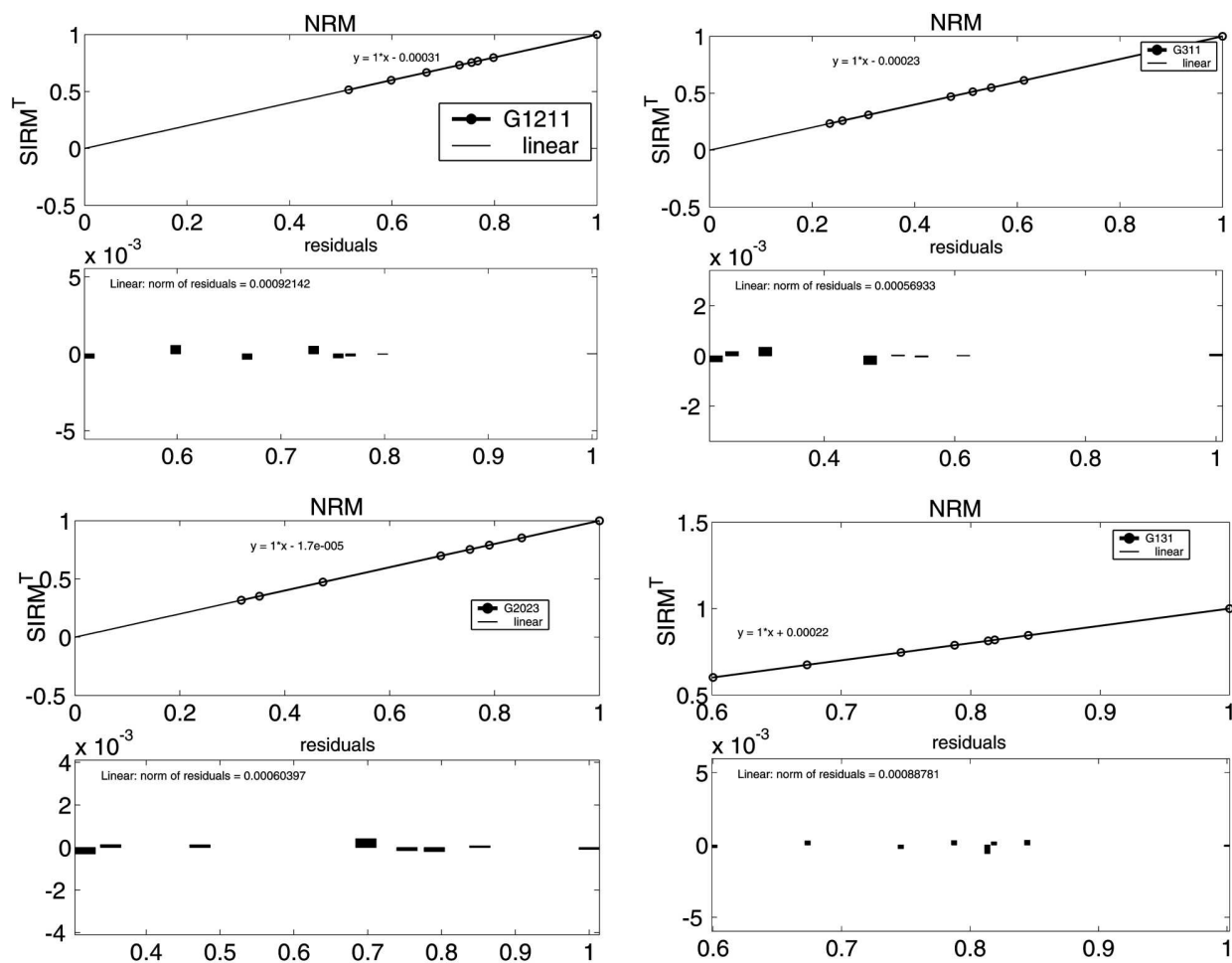


**Fig. 34:** Results of remagnetization experiments (s. for details chapter 2) performed for selected samples from the high-grade metamorphic gneisses of the HHC of Solu Khumbu. The presence of pyrrhotite is approved by its recovery within its unblocking temperature range (250-350°C). The calculated correlation coefficient  $r = 1.00$  for all samples, with a complete recovery between NRM-350°C implies a complete reversible case of pyrrhotite, and might support its record of a thermoremanence as assumed. On the other hand the calculated  $r$  and corresponding norm of residuals might be a qualitative indicator of the existence of a mono-ferro (i) magnetic phase within this temperature interval, being in this case PSD/SD pyrrhotite grains. Comparison with results of measurements performed in analogy to low-grade Tethyan sedimentary series of southern Tibet (s. appendix) reveal differences. Generally, with regard to pyrrhotite the selected samples are mainly (with the exception of one sample) assumed to be representative of a thermo-chemical remanence case. With the exception of two samples, the calculated  $r$  indicate a nearly complete recovery ( $r = 0.98$  in average), additionally, the clearly higher values of norm residuals are interpreted to be indicative for the presence of different grain-sized pyrrhotite. Partial oxidation below 350°C is however not excluded.

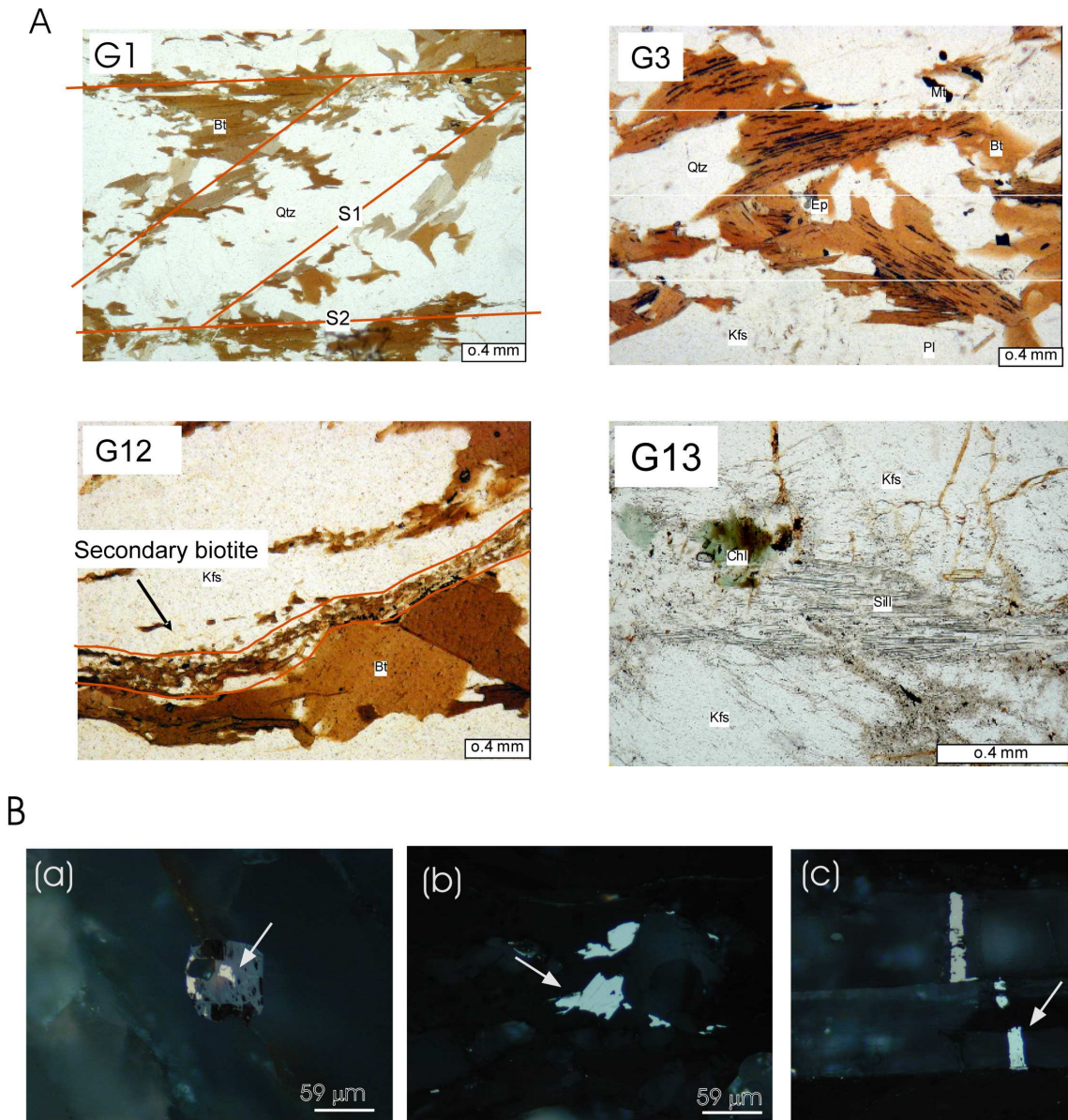


**Fig. 35:** A): Examples of petrographic analyses of selected thin sections (transmitted light microscopy) performed for Namche migmatites (G1, G3 and G12) and Baron paragneisses (G13). Samples were selected according to their ThD results, revealing the dominance of pyrrhotite in the Namche migmatites, but also its coexistence with magnetite in G3. In G13, “secondary” magnetite is dominant. B) In analogy, selected samples for reflected light microscopy (polished samples) indicate the presence of pyrrhotite identified by its high anisotropy included in a plagioclase matrix of a migmatitic orthogneiss (a), and the occurrence of larger grain sized hemo-ilminite (b) and maghematized magnetite (c). PSD/SD grains (below the detection capacity of the conventional method) coexisting with MD phases, are thought to be the recorder of measured stable remanences.

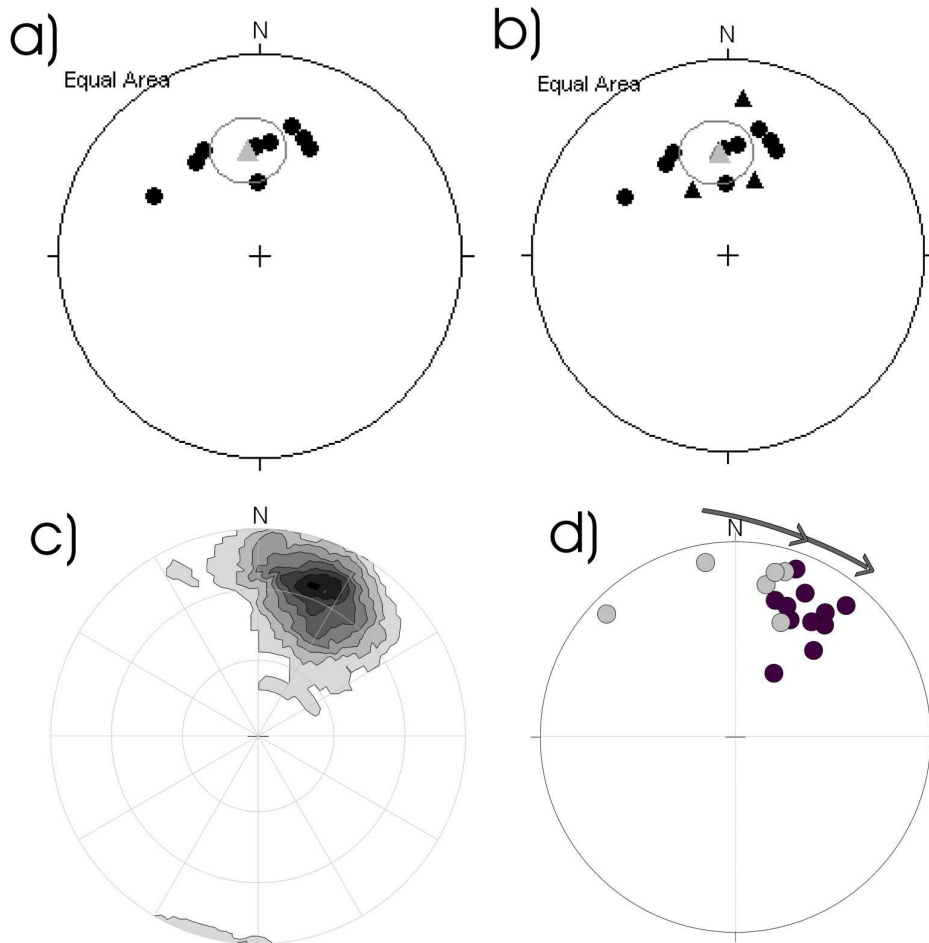


**Fig. 36:**  $ChRM^{pyr}$  (circles) (a),  $ChRM^{pyr}$  (circles) and  $ChRM^{mag}$  (triangles) (b) in situ directions of site means (all positive inclinations) calculated from statistically significant sites ( $k > 10$ ; reverse sites inverted). The overall mean directions are shown (grey triangles) including  $\alpha_{95}$  confidence range. Generally, the site means directions indicate a north-west ward wrenching. A closer view reveal a trend of circular distribution comparable to that observed along the studied east-west transect in southern Tibet. Counter-density stereogram (c) and equal area of in situ remanence directions (d) are representative results of the pilot study from the northern segment. Stable  $ChRM^{pyr}$  directions (black circles) as well as  $ChRM^{mag}$  (grey circles) were isolated for 10 calcgneiss sites. A consistent north-east trend, similar to that observed for Kharta valley is indicated. Remarkable, is that  $ChRM^{pyr}$ - and  $ChRM^{mag}$  directions are reflecting a traceable clockwise path, for instance, interpreted as clear indication for a continuous cooling and a successive magnetization of magnetite and pyrrhotite, respectively, within the upper greenschist facies conditions.

**Tab. 9:** ChRM<sup>pyr</sup> and ChRM<sup>mag</sup> directions mean of individual sites, and overall mean direction (average) of all statistically significant sites (k ≥ 10) in the examined southern segment from the HHC of the Solu Khumbu area.

Site	N	Dg (°)	Ig (°)	kg	a95g (°)	Litho-facies	Carrier of remanence
G1	5	24.5	40.4	13.4	21.7	mp	pyrrhotite
G2	6	200	-37.1	20.9	15	"	"
G3	7	13.4	33.2	14.5	16.4	"	"
G3	4	5.8	19.8	73.5	10.8	"	magnetite
G4	3	146	-42.7	51.2	17.4	"	pyrrhotite
G5	5	203.2	55.4	31.7	13.8	"	"
G10	5	358	59.6	27.3	14.9	"	"
G11	11	358.2	44.2	15.2	12.1	mo	"
G12	8	4.9	42.3	15.7	14.4	"	"
G13	6	198	-56.3	32.6	11.9	bp	magnetite
G18	9	331.8	58.8	14.5	14	"	magnetite
G19	8	332.4	40.3	11.8	16.8	"	pyrrhotite
G20	10	299.6	38.7	11.3	15	"	"
<b>Average1</b>	<b>9</b>	<b>353.8</b>	<b>45.3</b>	<b>15.4</b>	<b>14.4</b>		<b>pyrrhotite</b>
<b>Average2</b>	<b>12</b>	<b>355.6</b>	<b>45.7</b>	<b>14.9</b>	<b>12.2</b>		<b>pyrrhotite/magnetite</b>

Average1: overall sites mean for ChRM<sub>pyr</sub> (site G5 with unexpected positive inclination excluded)

Average2: overall sites mean for ChRM<sub>pyr</sub> and ChRM<sub>mag</sub> (site G5 excluded)

mp: migmatitic paragneiss

mo: migmatitic orthogneiss

bp: Barun paragneiss, south of Lukla, close to the MCT

": ditto

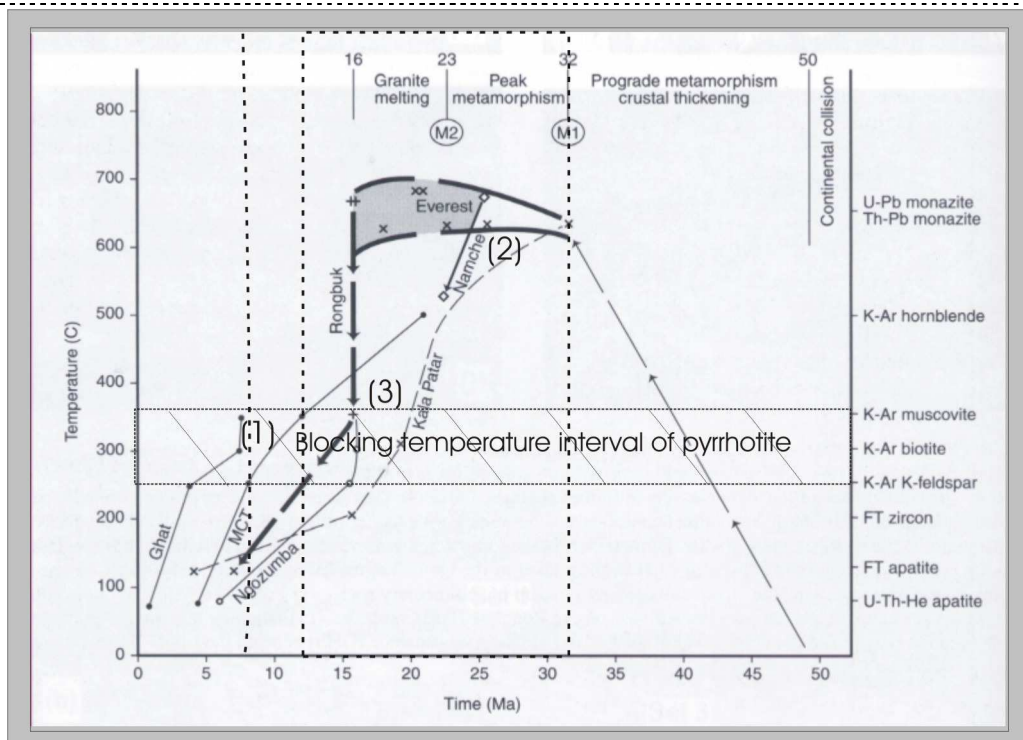


**Fig. 37:** Modified (after Searle et al., 2006) Temperature/Time cooling paths compiled from different data sources for the Everest transect. (1), (2), and (3) are examined sectors within this study. Dashed domain indicate expected closure temperature interval for pyrrhotite. Dashed lines delimitate upper- and lower age limits for the assumed thermoremanence acquired in pyrrhotite.

## References

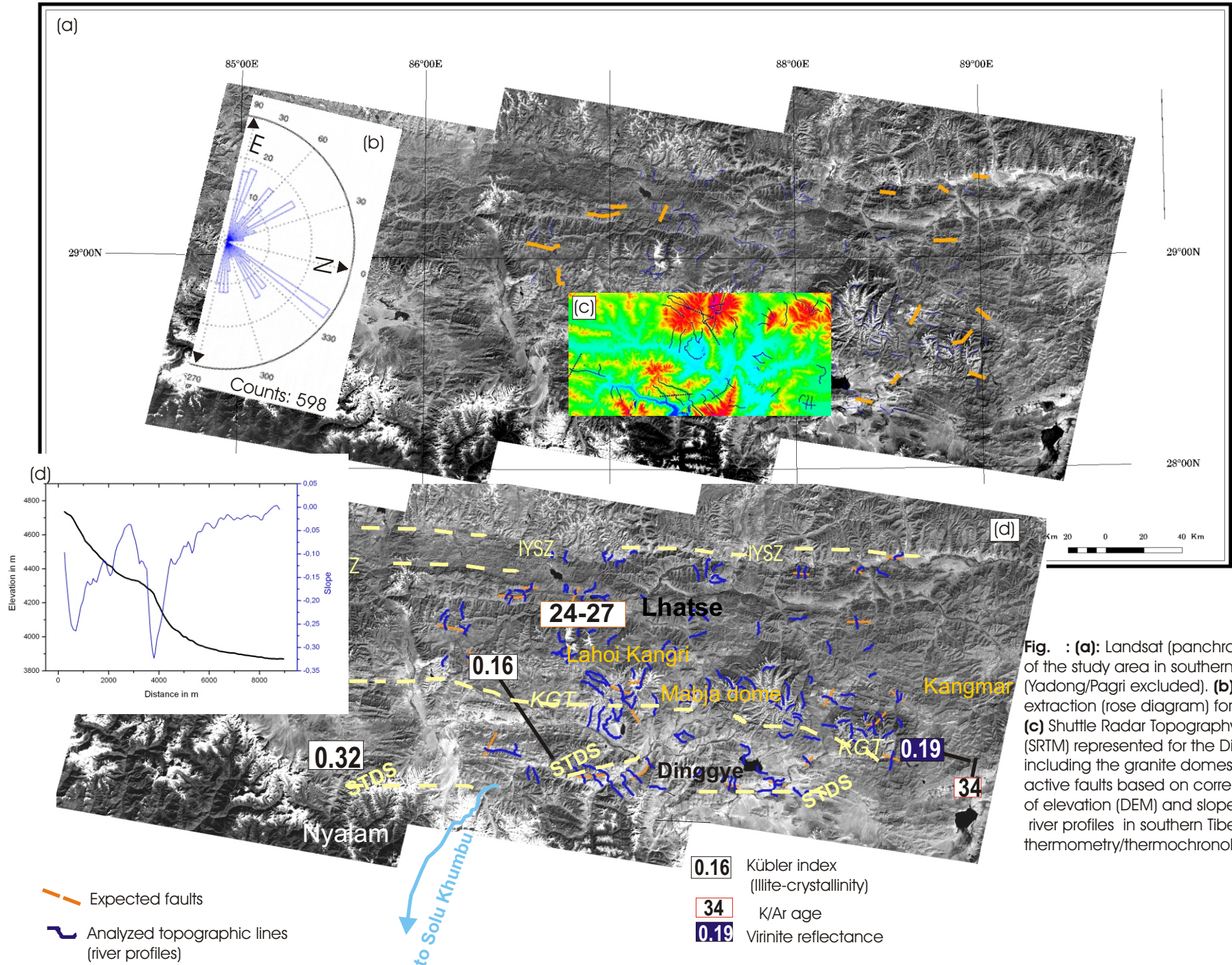
- Acton, G., D., 1999. Apparent Polar Wander of India Since the Cretaceous with Implications for Regional Tectonics and True Polar Wander. *Memoir Geological Society of India* N°. 44
- Appel, E., Müller, R., Widder, R.W., 1991. Palaeomagnetic results from the Tibetan Sedimentary Series of the Manang area (north central Nepal). *Geophys. J. Int.* 104, 255-266.
- Árkai, P., Sassi, F.P., Sassi, R., 1995. Simultaneous measurements of chlorite and illite crystallinity: a more reliable geothermometric tool for monitoring low- to very low-grade metamorphism in metapelites. A case study from Southern Alps (NE. Italy). *European Journal of Mineralogy* 7, 1115-1128.
- Avouac, J-P., and Tapponnier, P., 1993. Kinematic model of active deformation in Asia, *Geophys. Res. Lett.*, 20, 895-898.
- Balogh, K., Dunkl, I., 2005. Argon and fission track dating of Alpine metamorphism and basement exhumation in the Sopron Mts. (Eastern Alps, Hungary): Thermochronology or mineral growth? *Min. Petrol.* 83, 191-218.
- Barshfiel, B., Chen, Z., Liu, Y. and Royden, L., 1997. Tectonics of the Longmen Shan and adjacent regions, central China, *Int. Geol. Rev.*, 37(8), 661-735.
- Beaumont C., Jamieson R.A., Nguyen M.H., Lee B., 2001. Himalayan tectonics explained by extrusion of a low-viscosity crustal channel coupled to focused surface denudation. *Nature* 414, 738-742.
- Besse, J., Courtillot, V., Pozzi, J. P., Westphal, M. and Zhou, Y., 1984. Paleomagnetic estimates of crustal shortening in the Himalayan thrusts and Zangbo suture. *Nature* 311, 621-625
- Brun, J. P., Burg, J. P., and Ming, C. G., 1985. Strain trajectories above the Main Central Thrust (Himalaya) in southern Tibet, *Nature*, 330, 338-390.
- Carosi, R., et al. 1999. Geology of the Higher Himalayan Crystallines in Khumbu Himalaya (Eastern Nepal). *J. Asian Earth Sci.* 17, 785-803.
- Chen, Q., Freymueller, J.T., Wang, Q., Yang, Z., Xu, C., and Liu, J., 2004. A deforming block model for the present day tectonics of Tibet, *J. Geophys. Res.*, 109, B01403, doi:10.1029/2002JB002151.
- Craig, J. K. and Vokes, F. M. 1993. The metamorphism of Pyrite and pyretic ores, an overview. *Mineralogical Magazine* 57, 3-18
- Crouzet, C., Stang, H., Appel, E., Schill, E., Gautam, P., 2001. Detailed analysis of successive pTRMs carried by pyrrhotite in Himalayan metacarbonates: an example from Hidden Valley, Central Nepal. *Geophys. J. Int.* 146, 607-618.
- Crouzet, C., Gautam, P., Schill, E., Appel, E., 2003. Multicomponent magnetization in Western Dolpo (Tethyan Himalaya, Nepal): implications for tectonic motions. *Tectonophysics* 377(1-2), 179-196.
- Crouzet, C., Crouzet, C., Dunkl, I., Paudel, L., Árkai, P., Rainer, T. M., Balogh, K., Appel, E., 2006. Temperature and age constraints on the metamorphism of Tethyan Himalaya in Central Nepal: a multidisciplinary approach. *J. Asian Earth Sci.*, in press.
- Dachs, E., 1990. Geothermobarometry in metasediments of the southern Grossvenediger area (Tauern Window, Austria). *Journal of Metamorphic Geology* 8, 217-230.
- Ding, L., Kapp P., Wan X., 2005. Paleocene-Eocene record of ophiolite obduction and initial India-Asia collision, south central Tibet. *Tectonics*, 24, TC3001, 1-18
- England, P., and Molnar, P., 1997. Active deformation of Asia: From kinematics to dynamics, *Science*, 278, 647-650.
- Enkin, R., 2003. the direction-correction tilt test: An all-purpose tilt/fold test for paleomagnetic studies. *Earth Planet. Sci. Lett.* 212, 151-166.

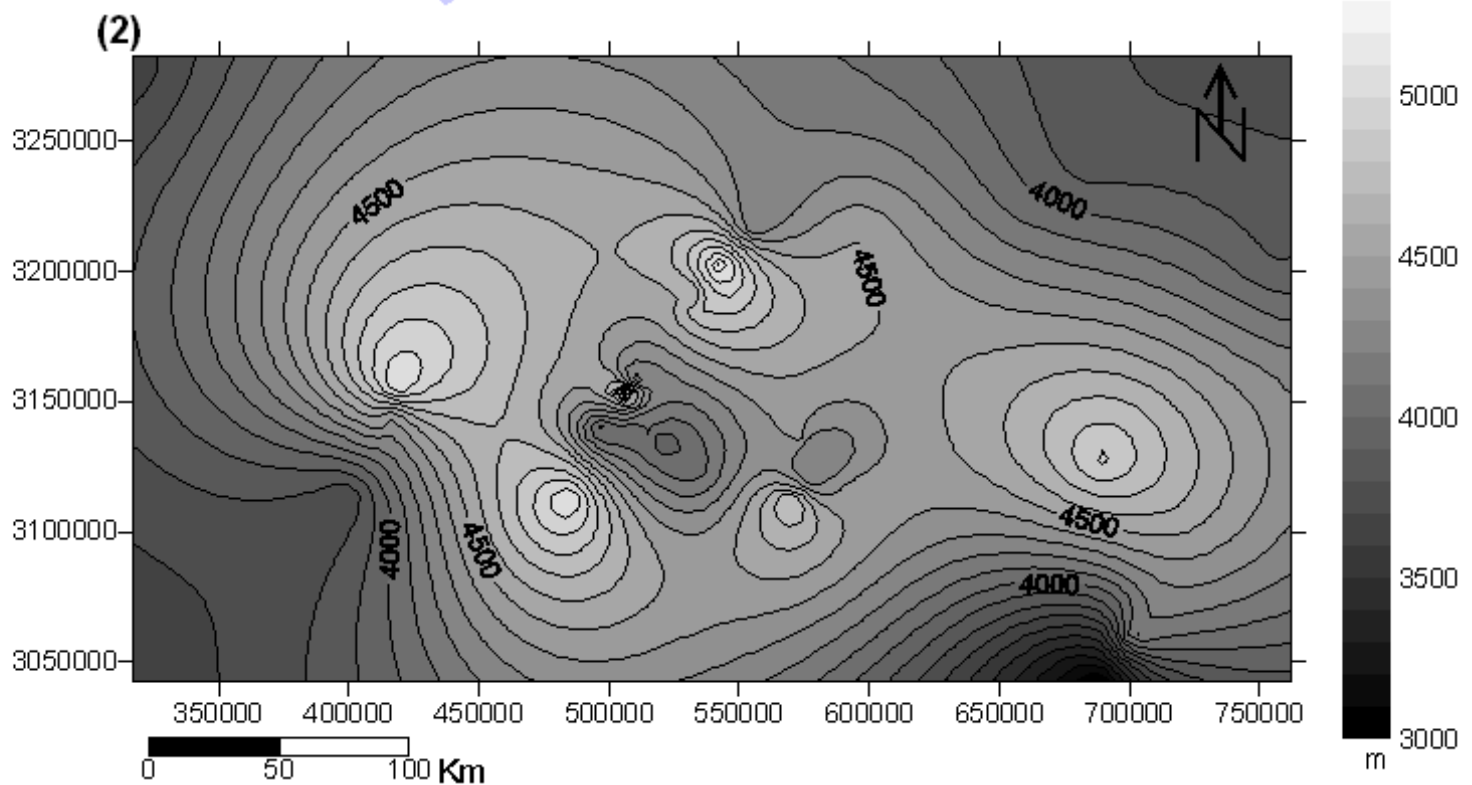
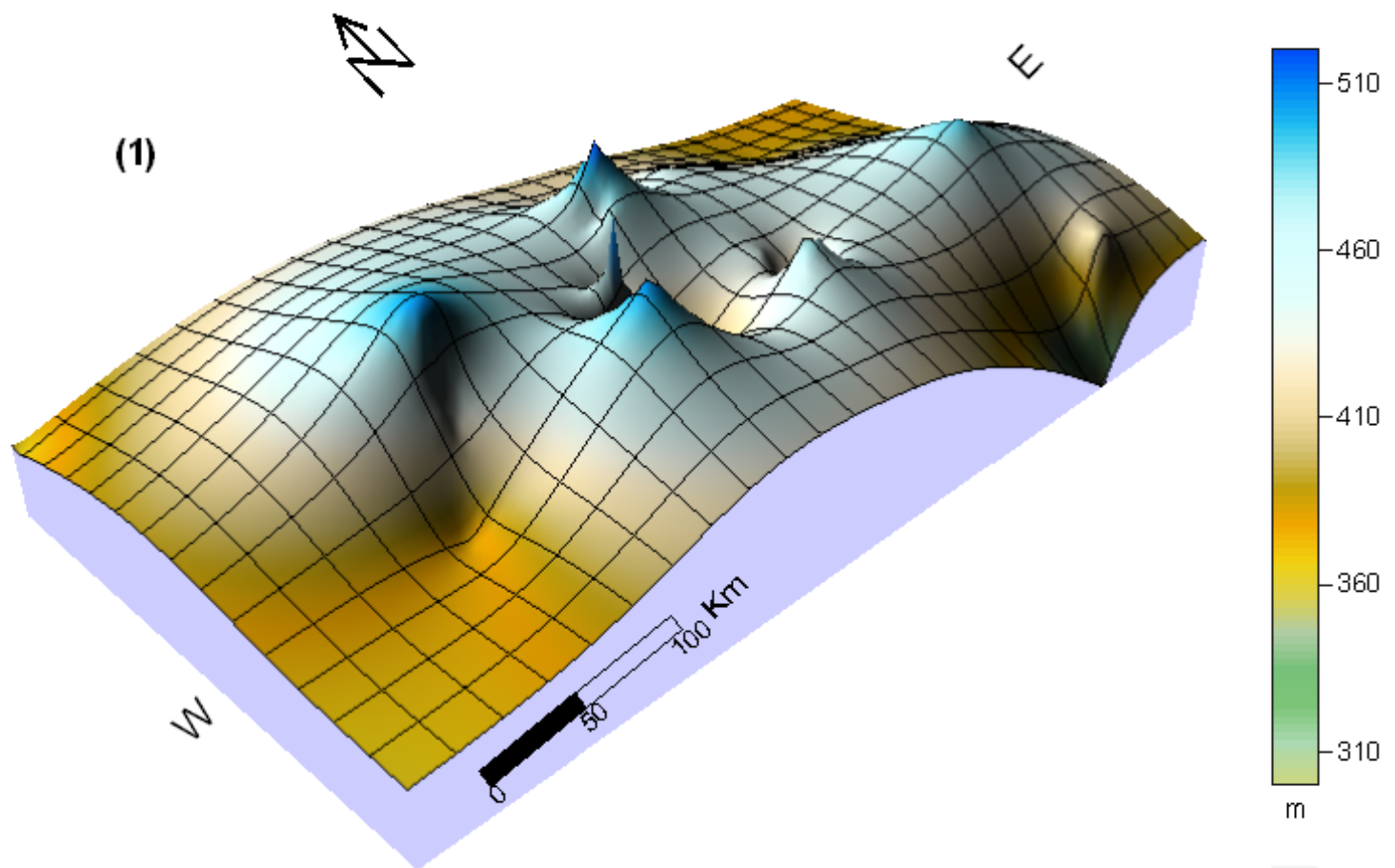
- Fisher, R. A., 1953. Dispersion on a sphere. *Proc. Roy. Soc.* A217, 295-305.
- Flesh, L., Haines, A., and Holt, W., 2001. Dynamics of the India-Eurasia collision zone, *J. Geophys. Res.*, 106, 16,435-16,460.
- Frey M., 1987. Very low grade metamorphism of clastic sedimentary rocks. In: Frey, M. (Eds.), *Low temperature metamorphism*. Blackie, Glasgow, pp. 9-58.
- Gan, W., P. Zhang, Z.-K. Shen, Niu, Z., Wang, M., Wan, Y., Zhou, D., and Cheng, J., 2007. Present-day crustal motion within the Tibetan Plateau inferred from GPS measurements, *J. Geophys. Res.*, 112, B08416, doi:10.1029/2005JB004120.
- Godin, L., Gleeson, T. P., Searle, M. P., Ullrich, T. D. and Parrish, R. R., 2006. Locking of southward extrusion in favour of rapid crustal-scale buckling of the Greater Himalayan sequence, Nar valley, central Nepal in: In. Law, R.D., Searle, M.P. and Godin, L. (eds). *Channel flow, ductile extrusion and exhumation in continental collision zones*. Geological Society, London, Special publications. 268, 91-145.
- Grujic D., Hollister L.S., Parrish R.R., 2002. Himalayan metamorphic sequence as an orogenic channel : insight from Bhutan. *Earth Planet. Sci. Lett.* 198, 177-191.
- Harris N., 2006. The elevation history of the Tibetan Plateau and its implications for the Asian monsoon. *Paleogeography, Paleoclimatology, Paleoecology*, 241, 4-15
- Hodges K.V., 2000. Tectonics of the Himalaya and southern Tibet from two perspectives. *Geol. Soc. Am. Bull.* 112, 324-350.
- Harris N., 2006. The elevation history of the Tibetan Plateau and its implications for the Asian monsoon. *Paleogeography, Paleoclimatology, Paleoecology*, 241, 4-15
- Harrison, T.M. 2006. Did the Himalayan crystalline extrude partially molten from beneath the Tibetan Plateau? In. Law, R.D., Searle, M.P. and Godin, L. (eds). *Channel flow, ductile extrusion and exhumation in continental collision zones*. Geological Society, London, Special publications. 268, 91-145.
- Hodges, K.V., 2000. Tectonics of the Himalaya and southern Tibet from two perspectives. *Geol. Soc. Am. Bull.* 112, 324-350.
- Hubert, A., and Schäfer, R., 2000. *Magnetic domains: The analysis of magnetic microstructures*. Springer
- Jamieson R. A., Beaumont C., Sergei M., Nguyen M. H., 2004. Crustal channel flows: 2. Numerical models with implications for metamorphism in the Himalayan-Tibetan orogen. *J. Geophys. Res.*, 109, B06407, doi:10.1029/2003JB002811, 1-24
- Jessup, M.J., Law, R.D., Searle, M.P. and Hubbard, M.S. Structural evolution and vorticity of flow during extrusion and exhumation of the greater Himalaya slab, Mount Everest Massif, Tibet/Nepal: implications for orogen-scale flow partitioning. In. Law, R.D., Searle, M.P. and Godin, L. (eds). *Channel flow, ductile extrusion and exhumation in continental collision zones*. Geological Society, London, Special publications. 268, 91-145.
- Kirschvink, J. L., 1980. The least-squares line and plane and the analysis of paleomagnetic data, *Geophys. J. R. Astron. Soc.* 62, 699-718.
- Klootwijk, C.T., Conaghan, P., Powell, C., 1985. The Himalayan Arc: large-scale continental subduction, oroclinal bending and back-arc spreading: *Earth Planet. Sci. Lett.* 75, 167-183.
- Klootwijk, C.T, Sharma, M.L., Gergan, J., Shah, S.k., Gupta, B.K., 1986. Rotational overthrusting of the northwestern Himalaya; further paleomagnetic evidence from the Riasi thrust sheet, Jammu foothills, India: *Earth Planet. Sci. Lett.* 80, 375-393.
- Klootwijk, C.T., Gee, J.S., Peirce, J.W., Smith, G.M., 1991. Constraints on the India-Asia convergence: Palaeomagnetic results from the Ninetyeast Ridge, in Weissel, J., Peirce, J., and others, Initial reports, Ocean Drilling Program, Leg 121: College Station, Texas, Ocean Drilling Program, 777-881.

- Kübler, B., 1967. La cristallinité de l'illite et les zones tout à fait supérieures du métamorphisme. In: Etages tectoniques (Colloque de Neuchâtel, 18-21 avril 1966). Neuchâtel, Univ., Inst. Geol. Pages 105-122.
- Kübler, B., Jaboyedoff, M., 2000. Illite crystallinity. *Compte Rendu de l'Académie des Sciences, Paris, Earth Planet. Sci.* 331, 75-89.
- Ménard and Rochette, 1992 Utilisation de réaimentation postmétamorphiques pour une étude de l'évolution tectonique et thermique tardive dans les Alpes occidentales (France). *Bull. Soc. Géol. France*, t. 163, n. 4, 381-392.
- Murphy M. A., An, Y., Kapp, P., Harrison, Ding, L., Guo, J., 2000: Southward propagation of the Karakoram fault system, southwest Tibet Timing and magnitude of slip. *Geology*, 28, 451-454.
- Nelson, K. D., Zhao, W., Brown, L. D., et al., 1996. Partially molten middle crust beneath southern Tibet; synthesis of Project INDEPTH results. *Science*, 274, 1684-1688.
- Lacassine, R., Valli, F., Arnaud, N., Leloup, H. P., Paquette, J. L., Haibing, L., Tapponier, P., Chevalier, M. L., Guillot, s., Maheo, G., Zhiqin, X., 2004. Large-scale geometry, offset and Kinematic evolution of the Karakorum fault, Tibet, *EPSL*, 219, 255-269.
- Lee, J., McClelland, W., Wang, Y., Blythe, A. and McWilliams, M. Oligocene-Miocene middle crustal flow in southern Tibet : geochronology of Mabja Dome. In. Law, R.D., Searle, M.P. and Godin, L. (eds). *Channel flow, ductile extrusion and exhumation in continental collision zones*. Geological Society, London, Special publications. 268, 91-145.
- Pêcher, A., 1991. The contact between the Higher Himalaya Crystallines and the Tibetan Sedimentary Series: Miocene large scale dextral shearing, *Tectonics*, Vol. 10, Nr. 3, 587-598.
- Peltzer, G., and Tapponnier., 1988. Formation and evolution of strike-slip faults rifts, and basins during the India-Asia collision : An experimental approach, *J. Geophys. Res.*, 93, 15,085-15,117.
- Ratschbacher, L., Frish, W., Herrman, U., Strecker, M. 1994. Distributed deformation in southern and western Tibet during and after the India-Asia collision: An experimental approach, *J. Geophys. Res.* 99, 19917-19945
- Replumaz, A., and Tapponnier. , 2003. Reconstruction of the deformed collision zone between India and Asia by backward motion of lithospheric blocks, *J. Geophys. Res.*, 108(B6), 2285, doi : 10.1029/2001JB00661.
- Rochette, P., Scaillet, B., Guillot, S., LeFort, P., Pecher, A., 1994. Magnetic properties of the High Himalayan leucogranites: structural implications. *Earth Planet. Sci. Lett.* 126, 214-234.
- Royden, H., Burchfield, C., King, W., Wang, E., Chen, Z., Shen, F., and Liu, Y., 1997. Surface deformation and lower crustal flow in eastern Tibet, *Science*, 276, 788-790.
- Schill, E., Appel, E., Zeh, O., Singh, V.K., Gautam, P., 2001, Coupling of late-orogenic tectonics and secondary pyrrhotite remanences: Towards a separation of different rotation processes and quantification of rotational underthrusting in the western Himalayas (N-India). *Tectonophysics* 337, 1-21.
- Schill, E., Crouzet, C., Gautam, P., Singh, V.K., Appel, E, 2002. Where did rotational shortening occur in the Himalayas? – Inferences from palaeomagnetic analyses of remagnetisations: *Earth Planet. Sci. Lett.* 203, 45-57.
- Schill, E., Appel, E., Godin, L., Crouzet, C., Gautam, P., Regmi, K.R., 2003. Record of deformations by secondary magnetic remanences and magnetic anisotropy in the Nar/Phu valley (central Nepal). *Tectonophysics* 377(1-2), 197-209.
- Schill, E., Appel, E., Crouzet, C., Gautam, P., Wehland, F., Staiger, M., 2004. Oroclinal bending and regional significant clockwise rotations of the Himalayan arc – constraints from

- secondary pyrrhotite remanences. In: Sussman A.J. and Weil A.B., Orogenic curvature: Integrating paleomagnetic and structural analysis. Geol. Soc. Am. Special Paper 383, 73-85
- Searle, M. P., Godin, L., 2003. The south Tibetan detachment and the Manaslu Leucogranite: a structural reinterpretation and restoration of the Annapurna-Manaslu Himalaya, Nepal, *J. Geol.* 111, 505-523.
- Searle, M. P., Law, R. D. and Jessup, M. J., 2006. Crustal structure, restoration and evolution of the Greater Himalaya in Nepal-South Tibet: implications for channel flow and ductile extrusion in: Channel Flow, Ductile Extrusion and Exhumation in Continental Collision Zones. Geological Society, London, Special Publications, 268, 355-378.
- Shipunov, S. V., 1997. Synfolding magnetization: detection, testing and geological applications. *Geophys. J. Int.*, 130, 405-410.
- Shen, F., Royden, H. L., and Burchfiel, B. C., 2001. Large-scale crustal deformation of the Tibetan Plateau, *J. Geophys. Res.*, 106, 6793-6816
- Shen Z. K., Lü J., Wang M., Bürgmann R., 2005. Contemporary crustal deformation around the southeast borderland of the Tibetan Plateau. *J. Geophys. Res.*, 110, B11409, doi: 10.1029/2004JB003421, 1-17
- Tapponnier, P., Peltzer, G., Le Dan, A.Y., Armijo, R., Cobbold, P., 1982. Propagating extrusion tectonics in Asia: new insights from simple experiments with plasticine. *Geology* 0, 611-616.
- Tapponnier, P., Peltzer, G., Armijo, R., 1986. On the mechanics of the collision between India and Asia, in: Coward, M. P. & Ries, A. C. (Eds.). *Collision tectonics*, Geol. Soc. Spec. Publ. 19, 115-157.
- Tapponnier, P., Xu, Z., Roger, F., Meyer, B., Arnaud, N., Wettlinger, G., and Yang, J., 2001. Oblique stepwise rise and growth of the Tibet Plateau, *Science*, 294, 1671-1677.
- Thatcher, W. 2007. Microplate model for the present day deformation of Tibet. *J. Geophys. Res.*, 112, B01401, doi:10.1029/2005JB004244.
- Unsworth M. J., Jones A. G., Wei W., Marquis G., Gokarn S. G., Spratt J. E. & the INDEPTH-MT team, 2005. Crustal rheology of the Himalaya and southern Tibet inferred from magnetotelluric data. *Nature*, 438, doi:10.1038/nature04154, 78-81
- Waldhör, M., 1999. The small circle reconstruction in paleomagnetism and its application to paleomagnetic data from the Pamir, *Tübinger Geowiss. Arb.* 45, 99p.
- Waldhör, M., Appel, E., Frisch, W., Patzelt, A., 2001. Palaeomagnetic investigations in the Pamirs. *J. Asian Earth Sci.*, 19, 429-451.
- Waldhör, M., Appel, E., 2006. Intersection of remanence small circles: new tools to improve data processing and interpretation in paleomagnetism. *Geophys. J. Int.*, 33-45.
- Wang, Q., et al. 2001. Present day crustal deformation in China constrained by global positioning system measurements, *Science*, 294, 574-577.
- Yin, A., 2006. Cenozoic tectonic evolution of the Himalayan Orogen as constrained by along-strike variation of structural geometry, exhumation history, and foreland sedimentation. *Earth-Science Reviews* 76, 1-131.
- Zhang, J. and Guo, L., 2006. Structure and geochronology of the southern Xainza-Dinggye rift and its relationship to the South Tibetan Detachment system.

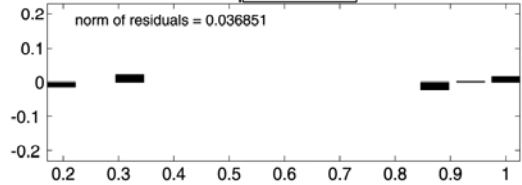
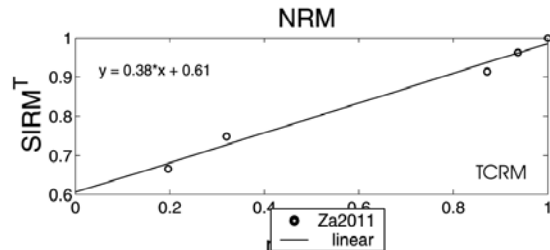
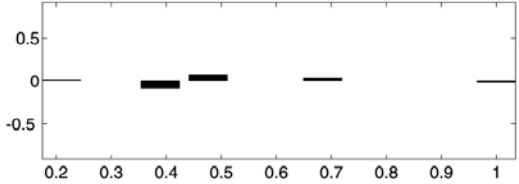
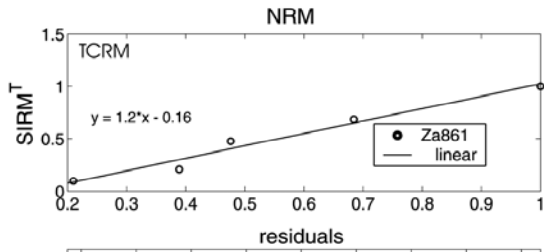
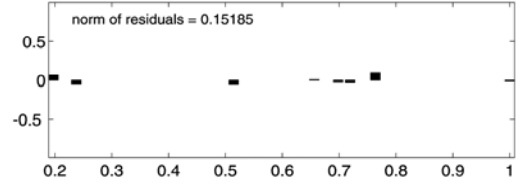
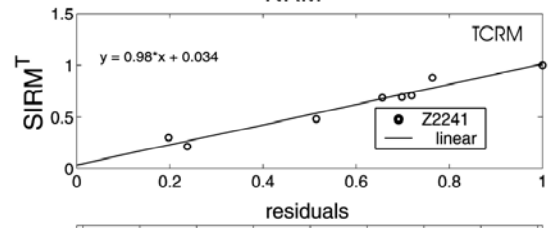
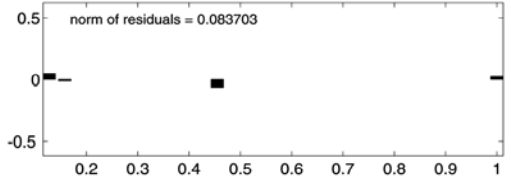
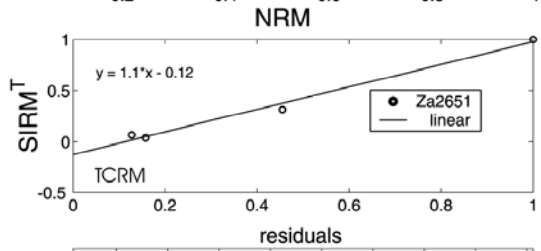
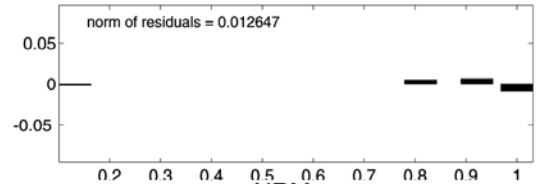
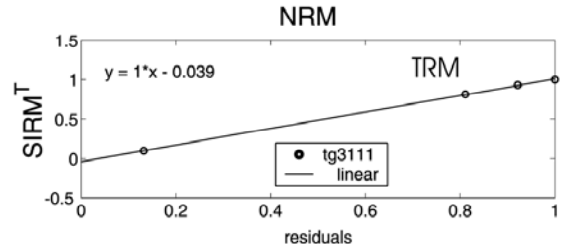
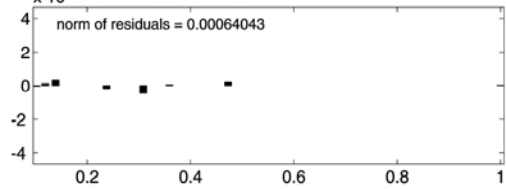
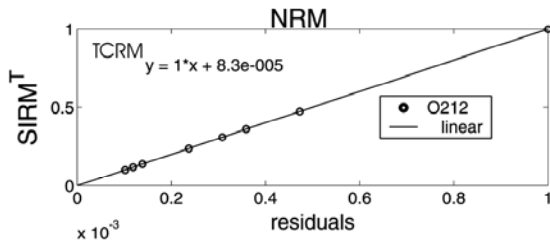
# Appendix

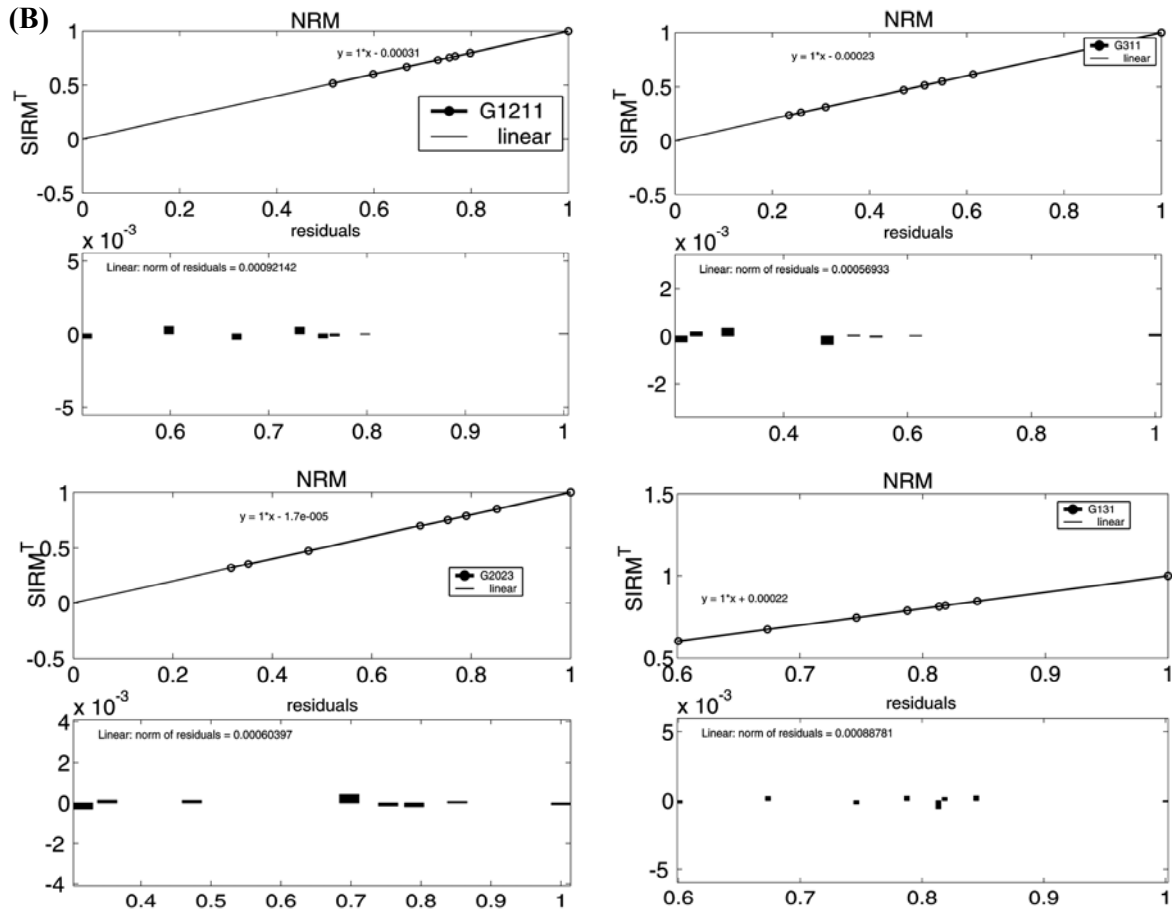




- (1) 3D surface map of the study area between 86 and 89°E in southern Tibet. The map reflects the long wavelength character of the topography, as well as the effect of doming.
- (2) Corresponding contour map.

(A)





(B) Results of remagnetization experiments (s. for details chapter 2) performed for selected samples from the high grade metamorphic gneisses of the HHC of Solu Khumbu. The presence of pyrrhotite is approved by its recovery within its unblocking temperature range (250-350°C). The calculated correlation coefficient  $r = 1.00$  for all samples, with a complete recovery between NRM-350°C implies a complete reversible case of pyrrhotite, and might support its record of a thermoremanence as assumed. On the other hand the calculated  $r$  and corresponding norm of residuals might be a qualitative indicator of the existence of a mono-ferro (i) magnetic phase within this temperature interval, being in this case PSD/SD pyrrhotite grains. Comparison with results of measurements performed in analogy to low grade Tethyan sedimentary series of southern Tibet (A) reveal differences. Generally, with regard to pyrrhotite the selected samples are mainly (with the exception of one sample) assumed to be representative of a thermochemical remanence case. With the exception of two samples, the calculated  $r$  indicate a nearly complete recovery ( $r = 0.98$  in average), additionally, the clearly higher values of norm residuals are interpreted to be indicative for the presence of different grain-sized pyrrhotite. Partial oxidation below 350°C is however not excluded.

## Summary of sampling sectors and corresponding analyzed sites in southern Tibet

Site	Latitude (deg., min)	Longitude (deg., min)	Geological units	Site	Latitude (deg., min)	Longitude (deg., min)	Geol. units
<b>Nyalam Section</b>				<b>Dinggye area</b>			
O1	28.37948	86.11275	Ordovician	ZA8	28.06301	87.98063	Ordovician
O2	28.38228	86.10967	Ordovician	ZA9	28.06257	87.98032	Ordovician
C3	28.39483	86.11722	Carboniferous	ZA10	28.16187	87.97382	Devonian
C4	28.39491	86.11427	Carboniferous	ZA11	28.17142	87.94701	Devonian
T5	28.43673	86.13778	Triassic	ZA12	28.17505	87.87438	Ordovician
T6	28.43882	86.13861	Triassic	ZA13	28.17517	87.86923	Ordovician
T7	28.44067	86.14445	Triassic	ZA14	28.13753	87.71072	Ordovician
T8	28.44071	86.14445	Triassic	ZA15	28.13838	87.70957	Devonian
T9	28.44195	86.14523	Triassic	ZA16	28.23995	87.73983	Ordovician
Ny41	28.37858	86.11811	Ordovician	ZA17	28.07563	87.42578	Ordovician
Ny42	28.42133	86.13658	Devonian	ZA18	28.10598	87.70113	Ordovician
<b>Kharta valley</b>				ZA19	28.10878	87.69991	Ordovician
T10	28.54541	87.08481	Triassic	ZA20	28.10905	87.70183	Ordovician
J11	28.47017	87.02965	Jurassique	ZA21	28.31383	87.85852	Devonian
P12	28.45302	87.01041	Permian	ZA22	28.32433	87.85038	Devonian
O13	28.35247	87.18562	Ordovician	ZA23	28.32978	87.77697	Devonian
O14	28.35373	87.18247	Ordovician	ZA24	28.33425	87.77908	Devonian
D15	28.35952	87.17295	Devonian	ZA25	28.30901	87.89671	Devonian
C16	28.37661	87.16057	Carboniferous	ZA26	28.24678	87.81668	Ordovician
C17	28.37882	87.15717	Carboniferous	ZA27	28.24463	87.81998	Ordovician
P18	28.37132	86.94683	Permian	<b>Yadong/Pari area</b>			
P19	28.37631	86.94763	Permian	Yd1	27.61688	89.04271	Ordovician
P20	28.39813	86.97057	Triassic	Yd2	27.61508	89.04162	Ordovician
TG28	28.35648	87.17975	Ordovician	Yd3	27.63913	89.03827	Ordovician
TG29	28.35572	87.18065	Ordovician	Yd4	27.64087	89.04015	Ordovician
TG30	28.35012	87.20025	Ordovician	Yd5	27.62461	88.93771	Ordovician
TG31	28.35133	87.19128	Ordovician	Yd6	27.38504	88.56969	Ordovician
TG32	28.35167	87.18595	Ordovician	Yd7	27.67158	88.95523	Ordovician
RB33	28.27881	86.81017	Ordovician	<b>Area between Tingri and Lhatse</b>			
RB34	28.27697	86.72598	Ordovician	L21	28.82871	87.33503	Triassic
RB35	28.28358	86.80595	Ordovician	L22	28.83197	87.33407	Triassic
RB36	28.28107	86.80388	Ordovician	L23	29.06631	87.55313	Triassic
RB37	28.28251	86.81231	Ordovician	L24	29.06968	87.55707	Triassic
RB38	28.37132	86.94683	Permian	L25	29.07808	87.56281	Triassic
RB39	28.39107	86.96528	Triassic	L26	29.11032	87.53472	Triassic
RB40	28.39957	86.97158	Triassic	L27	29.11101	87.54703	Triassic
				L28	29.11101	87.54703	Triassic
				L30	28.73617	87.22245	Triassic
				L31	28.81038	87.28298	Triassic
				L32	29.07821	87.56283	Triassic
				L33	28.81748	87.32375	Triassic